

PAUL SCHERRER INSTITUT



PSI Bericht Nr. 96-10
April 1996
ISSN 1019-0643

Nuclear Energy and Safety Research Department

Evaluation of the Smolensk-3 Shutdown System

Final report

Phase II and III:
Steady State and Transient Analysis

E. Knoglinger, et al.

Paul Scherrer Institut
CH - 5232 Villigen PSI
Telefon 056 310 21 11
Telefax 056 310 21 99

Evaluation of the Smolensk-3 Shutdown System

Final report

Phase II and III: Steady State and Transient Analysis

**E. Knoglinger, Paul Scherrer Institut
E. Burlakov, A. Krayushkin, A. Kubarev, RRC-Kurchatow Institut
I. Stenbok, A. Ionov, M. Rozhdestvensky, all RDIPE**

April 1996

ABSTRACT

This report describes phase II and phase III of a study jointly performed by the Research and Development Institute for Power Engineering (RDIPE), the Russian Research Centre Kurchatov Institute (RRC-KI) and the Paul Scherrer Institut (PSI). The purpose of the study was to evaluate the shutdown system of the Smolensk Nuclear Power Plant Unit-3 (SMOLENSK-3).

The shutdown system of SMOLENSK-3 was evaluated based on 3-dimensional analyses of the shutdown reactivity at hot zero power, and cold zero power xenon free core conditions. 3-dimensional transient analyses were performed of the LOCA in the main cooling circuit (MCC) and in the cooling circuit of the control and protection system (CPS), for which also the loss of coolant in single channels was investigated. The analyses also covered the erroneous withdrawal of single control rods.

The results of the study show that the shutdown system comprising 24 fast acting rods of SDS-1 (fast shutdown system) and 187 rods of SDS-2 can cope with any accident analysed.

However, SDS-1 alone cannot suppress a power excursion during the loss of coolant in the cooling channels of the control rods. Therefore, this system does not comply with the basic principles for shutdown system requirements in force in the West.

It has to be realized that the analyses presented are best-estimate and preliminary in nature. Yet the results of the loss of coolant in single CPS channels appear to have surfaced a new safety issue which needs proper attention. The lack of SDS-1 to be able to cope with the CPS -LOCA already has been identified as a concern previously by PSI and IAEA.

In view of the fact that occurrences involving voiding of individual CPS channels already have happened in several RBMK and considering the safety significance of such events it appears absolutely mandatory that further detailed analyses be performed in a systematic way to cover all potential reactivity initiated accidents related to failures in the CPS circuit including air ingress into the system.

This work was performed under contract with the "Eidgenössische Department für Auswärtige Angelegenheiten" (EDA)

CONTENTS

ABSTRACT	ii
EXECUTIVE SUMMARY	1
1. INTRODUCTION	7
2. THE SMOLENSK-3 SHUTDOWN SYSTEM	7
3. OBJECTIVES OF THE BILATERAL PROGRAM	8
4. ARROTTA IMPLEMENTATION AND VALIDATION	11
4.1 ARROTTA validation based on experiments performed at the critical facility of RRC-KI	11
4.2 Analysis of the SMOLENSK-3 start up experiment.	15
4.2.1 Analysis of the initial core	15
4.2.2 Analyses of an interim core	16
4.2.2.1 Comparison of measured and calculated reactivities	16
4.3 ARROTTA analyses at full power	28
4.3.1 Xenon distribution	28
4.3.2 ARROTTA Xenon transient	29
4.3.3 ARROTTA nodalization studies	32
4.3.4 Void coefficient at full power	32
4.4 Status of ARROTTA adaptation for RBMK analyses	42
5. STEADY-STATE ANALYSIS OF SMOLENSK-3	43
5.1. Criticality at full power	43
5.2 Fuel temperature, void and power distribution at full power	47
5.3 Void reactivity at full power	47
5.4 Shutdown reactivity at hot zero power	58
5.5 Shutdown reactivity at cold zero power	59
5.6 Maximum allowable operative reactivity margin (ORM)	60
5.6.1 Compensating the ORM by fully inserted control rods.	60
5.6.2 Compensating the ORM by partly inserted rods.	62
6. TRANSIENT ANALYSIS OF SMOLENSK -3	65
6.1 LOCA analysis of MCC (ultimate design base accident)	65
6.1.1 Reactor shutdown by SDS-1 plus SDS-2	67
6.1.2 No actuation of shutdown and ECCS system.	67
6.2 LOCA analysis of CPS circuit	76
6.2.1 Shutdown by SDS-1 plus SDS-2	77
6.2.2 Shutdown by SDS-1 only	84
6.3 Erroneous control rod withdrawal accident (ECRWA)	87
6.4 Transient ARROTTA analysis	96
6.4.1 The loss of coolant in the CPS system.	97
6.4.2 The loss of coolant in a single CPS channel	97
APPENDIX 1	105
APPENDIX 2	114
APPENDIX 3	118
APPENDIX 4	119

Executive summary

The shutdown system of the SMOLENSK Nuclear Power Plant (NPP) Unit-3 was evaluated in cooperation with the RRC Kurchatov Institute (RRC-KI) and the Research and Development Institute of Power Engineering (RDIPE) in Moscow. The objectives of the cooperation were to investigate the adequacy of RBMK shutdown systems with regard to shutdown effectiveness and shutdown rate and to compare the results of the respective calculations performed by the individual partners using their own computational techniques. It was not the intention to perform a comprehensive, representative safety analysis for the plant. The project was structured in three phases as shown in the project outline presented below:

Phase I: Code implementation and testing

1. Implement the QUABOX/CUBBOX-HYCA computer code (QCH) neutronic part at PSI.
2. Execute QCH sample problems obtained from GRS.
3. Execute RBMK Chernobyl Benchmark
 - a) Macro Cell containing a typical arrangement of 12 by 12 assemblies
 - b) 3-D Chernobyl-3, full three dimensional core model.
4. Perform HZP, CZP calculations as in sections 8 and 9 below, using Chernobyl-3 data and Smolensk-3 fresh core data.
5. Implement and test QCH thermal hydraulic options for RBMK configuration (12x12). This task will also include a stability test run on the Macro-cell defined under task 3.
6. Implementation of special subroutine in QCH for initial data feeding. Provide initial data for Smolensk-3 critical experiments.

Phase II: Steady state analysis of Smolensk-3

The calculations will be performed for an equilibrium core with an ORM of 43 -48 rods, 97 additional absorbers, 578 fuel assemblies with an initial enrichment of 2 % U-235 and 986 fuel assemblies with an initial enrichment of 2,4 % U-235.

7. Calculate 3-D criticality at hot full power (HFP) using SADCO and STEPAN.
 - 7.1 Provide PSI with precise data for 3-D core configuration, CR position, follower position, absorbers positions, BU-distributions, and inlet flow and enthalpy and the geometry and material composition for core components
 - 7.2 Calculate core k eff, 3-D power, void and temperature distribution.
 - 7.3 Calculate the reactivity coefficient of the water density in the fuel channels.

Calculate 3-D criticality at hot zero power (HZP), equilibrium Xenon.

8. Calculate subcriticality for the following conditions:
 - a) BAZ-mode (all CRs inserted)
 - b) all the CRs except for 24 Fast CRs inserted
 - c) Fast CRs (there is no mode of operation where the Fast CRs only would be used to shut the reactor down) inserted

The calculations will be performed in accordance with the conditions defined in table 1.

Task	Hot Zero Power X_e^∞	Water in Fuel Channels	Water in CPS channels
9.2	BAZ-mode	+	+
8.3	BAZ-mode	+	-
8.4	BAZ-24 Fast CRs	+	+
8.5	BAZ-24 Fast CRs	+	-
8.6	24 Fast CRs	+	+
8.7	24 Fast CRs	+	-

Table 1: Matrix for the analyses of the hot zero power cases (Equilibrium burn-up; ORM = 45; 97 Additional Absorbers; fuel mix)

9. Calculate 3-D criticality at cold zero power (CZP) with no Xenon.

9.1 Calculate subcriticality for the following conditions:

- a) BAZ-mode (all CRs inserted)
- b) all the CRs except for 24 Fast CRs inserted.

The calculations will be performed in accordance with the conditions defined in table 2.

Task	Cold Zero Power $X_e^\infty = 0$	Water in Fuel Channels	Water in CPS channels
9.2	BAZ-mode	+	+
9.3	BAZ-mode	+	-
9.4	BAZ-24 Fast CRs	+	+
9.5	BAZ-24 Fast CRs	+	-

Table 2: Matrix for the analyses of the cold hot zero power cases (Equilibrium burn-up; ORM = 45; 97 additional absorbers; fuel mix)

10. Calculate the maximum ORM for which the reactor can be safety shutdown (ARI) to cold clean (no Xe) conditions.

11. Provide a cross section library for the QCH code for the Smolensk-3 reactor for the full range of parameters of interest. The parameters of interest for the fuel assemblies are BU, α , T_f , T_m , and X_g . The parameters for the CPS channels are T_m , α and the presence or absence of water in the CPS channels.

12. Interface to QCH

12.1 Develop and provide an interface program capable of processing macro cross-sections and preparing a QCH cross-section input library.

12.2 Compare the generated cross-section libraries with the PSI data.

Phase III: Transient analysis of Smolensk-3

13. Transient analysis of Smolensk-3 NPP to verify compliance of the shutdown systems with the KT standards using the TRIADA, DINA and STEPAN codes.

13.1 LOCA of MCC

› 13.2 LOCA of CPS circuit.

Scenarios and initial conditions for the transient analyses will be defined jointly prior to the respective calculations.

14. Prepare a final report

In addition to the work defined in the project outline the implementation and validation of ARROTTA - a three dimensional transient neutronics core code with thermal hydraulic feed back - was included in the program and steady state and transient analyses were performed using this code and Russian computer programs. Also the analysis of the erroneous control rod withdrawal accident and the investigation of the loss of coolant in single CPS channels were added to the original scope of work.

The investigations were limited to the steady state analysis of the Smolensk-3 core, to the analysis of the shutdown reactivity at hot zero and at cold zero power and to a best estimate transient analysis of the most severe reactivity initiated accidents e.g. the loss of coolant accidents in both, the main circulation circuit (MCC) and the cooling circuit of the protection and control system (CPS) and the erroneous control rod withdrawal accident. The analyses were performed under realistic assumptions, no attempt was made to include worst case conditions or to evaluate the uncertainties of the calculational results. The major results of the joint program are listed below:

- ARROTTA has been successfully implemented and modified for RBMK application. The code extensively validated for LWR steady state and transient analysis has been verified for RBMK core analysis by recalculating critical experiments performed at the RRC-KI critical facility and measurements taken during the start up test program for Smolensk-3.
- The code is able to predict reactivity, power distribution and void reactivity effects at full and zero power within acceptable limits. The discrepancies between the calculated and measured radial and axial power distributions observed in the analysis of the interim core loading during the start up testing of Smolensk-3 need further investigations.
- A model for the calculation of graphite temperature distributions has to be included. Further ARROTTA modifications are required to provide a user friendly tool for RBMK transient analyses.
- The results of the Russian codes SADCO and STEPAN compare quite well. Discrepancies of the calculated graphite temperatures need further investigations.

- The discrepancies between the calculated and measured power and flux distributions manifest in all computer codes used in the analyses (including ARROTTA) appear to be quite high.
- Both, RDIPE and the RRC-KI use flux reconstruction methods in order to reduce these discrepancies. These methods and their applicability to transient analyses need further investigations.
- The void reactivity coefficient of the main cooling circuit in Smolensk-3 is less than 1\$ at full power.
- The void reactivity (reactivity insertion due to voiding the channels from 0 % to 100 % void) of the CPS cooling channels is still 4-5 \$.
- The shutdown system including all control rods except the fast acting rods is able to provide the required shutdown margin of 2 % specified in the Russian regulations for cold zero power conditions.
- The shutdown system comprising all the control rods including the fast acting shutdown rods is able to cope with any of the transients investigated under this study.
- The fast acting shutdown rods alone cannot suppress a power excursion during the CPS LOCA
- The loss of coolant in single CPS channels needs further investigations. Similarly additional analyses are required for the investigations of voiding the channels by air ingress.
- Due to the low void coefficient at full power there is no signal available for reactor shutdown based on neutron power or period during the MCC-LOCA.

The shortcomings of the control and protection system will be eliminated by the reactor designer by implementing an additional diverse shutdown system in all RBMK. This system will utilize the present 24 fast acting shutdown rods in combination with a liquid poison system as an additional mean to shut the reactor down from any operational or accidental condition and to provide long term subcriticality. The reactor scram system (first shutdown system) will utilize the remaining rods to shut the reactor down quickly enough to cope with any accident and to maintain long term subcriticality. The new systems have been reported to be installed in Sosnoby Bor in 1997.

1. Introduction

During a topical meeting on RBMK shutdown systems organized by the IAEA and hosted by the PSI in Switzerland in December 1993, the implementation of the basic principles of shutdown system requirements in the design of the SMOLENSK-NPP Unit 3 was reviewed by OECD experts, Russian regulators and designers, and representatives from the IAEA [1].

The purpose of the meeting was to define compatibility of the two shutdown systems available in the SMOLENSK-NPP Unit 3 with the international requirements on independence, diversity, shutdown effectiveness and hold-down capability.

During the meeting, the Russian designers and regulators, and the experts from the OECD countries agreed that the two systems cannot be considered as fully independent and diverse even though the rod design and rod cooling are different, there are no displacers on the fast shutdown rods and the speed of rod insertion is different.

In the aftermath of this meeting, the PSI entered into an agreement of co-operation with the RDIPE, the Russian chief designer of RBMK reactors, and the Kurchatov Institute (RRC-KI) to jointly evaluate the existing shutdown systems and to investigate the feasibility of an additional diverse shutdown system based on liquid poison injection.

2. The SMOLENSK-3 shutdown system

As a result of the design modifications implemented by RDIPE in all RBMK-reactors following the Chernobyl accident, there are two shutdown systems available in SMOLENSK-3 today. The fast acting emergency protection system, called the BAZ system and later referred to as shutdown system 1 (SDS-1), and the emergency protection system, called the AZ-1 system and referred to as shutdown system 2 (SDS-2).

The post-Chernobyl modifications of the RBMK shutdown systems implemented by RDIPE to improve shutdown effectiveness and reactivity hold-down capability include:

- the implementation of SDS-1, comprising 24 fast shutdown rods;
- the reduction of the insertion time of the 155 control rods of SDS-2 to about 12s;
- the integration of 32 part-length rods entering the core from the bottom into the SDS-2;
- the modification of the control rod design to eliminate the positive scram effect – a major contributor to the Chernobyl accident.

The shutdown reactivity provided by the entirety of the control rods of SDS-1 plus SDS-2 is now about -12\$ in the hot zero power, equilibrium xenon condition .

Both the fast shutdown rods and the rest of the control rods are uniformly distributed throughout the reactor core.

The rods are cooled by the gravity-driven, low-pressure, low-temperature cooling circuit of the control and protection system (CPS) which is completely separated from the main coolant circuit (MCC) as shown in Fig. 1.

Whereas the fast shutdown rods of SDS-1 are fully withdrawn under normal operating conditions and only used for reactor shutdown, the control rods of SDS-2 are also used for reactivity control, power shaping and local and global power control. A schematic of the design of the different types of control rods presently in use in RBMK reactors is shown in Fig. 2.

In this report the SMOLENSK-3 shutdown system is evaluated based on the assumption that there are two systems available for reactor shutdown, SDS-1 and SDS-2. However, the authors want to point out, that in the West, there is common consensus that there is only one system which provides two different modes of operation, the BAZ mode and the AZ-1 mode. In both modes, the entirety of the available control rods (211 in SMOLENSK-3) simultaneously actuated by the same signals is used for reactor shutdown. In the BAZ mode, the 24 fast shutdown rods are inserted within 2s, but only within 7s in the AZ-1 mode. A mode of reactor shutdown based on the fast shutdown rods alone does not exist.

It is acknowledged in the West that the present system is able to cope with any operational or incidental occurrence to be considered in the design of the plant. However, an additional independent and diverse shutdown system is recommended to fully comply with international codes and standards.

For a more comprehensive and detailed description of the SMOLENSK-3 shutdown system, the reader is referred to [1] which also presents a detailed discussion of the shortcomings of the present system.

3. Objectives of the bilateral program

The joint program focused on two projects:

- the evaluation of the SMOLENSK-3 shutdown system;
- the investigation of liquid poison as a mean for additional diverse reactor shutdown.

The objectives of the program were to jointly evaluate the shutdown effectiveness and the reactivity hold-down capability of the two respective systems SDS-1 and SDS-2, and to evaluate the feasibility of liquid poison injection as an additional diverse shutdown system. This report describes the work performed under the first project only.

The project was structured in three major tasks:

- code implementation and validation;
- 3-dimensional steady-state analysis;
- 3-dimensional transient analysis.

Four different 3-dimensional computer codes were used for the analyses. SADCO and TRIADA, both codes developed by RDIPE, STEPAN developed by RRC-KI and ARROTTA, a 3-dimensional reactor core space-time neutron kinetics and thermal hydraulics code [2] in use at PSI exclusively for RBMK analysis. Code descriptions and information on the experimental verification of the STEPAN code are given in the appendices of this report.

Fig. 1

RBMK core cross section

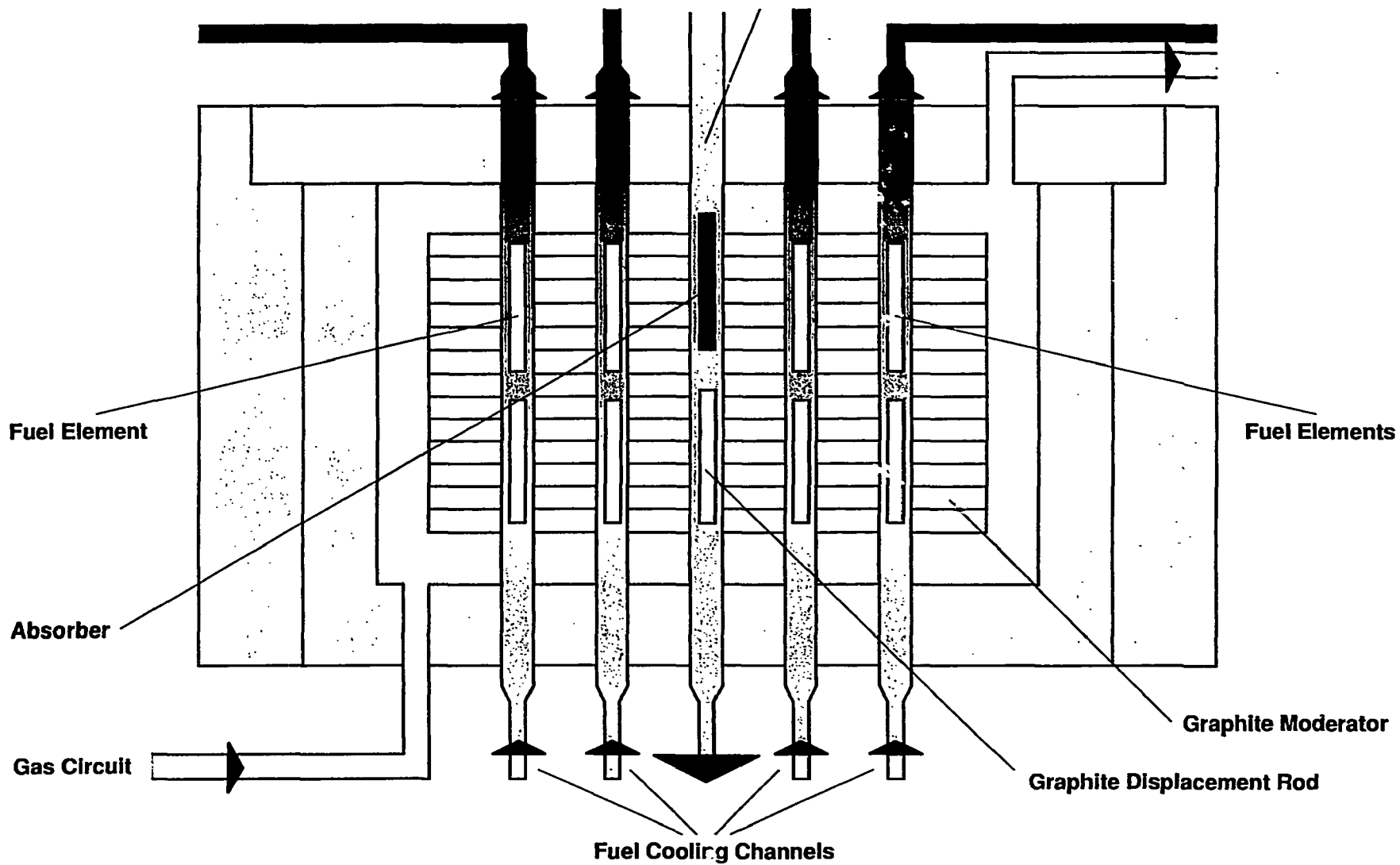
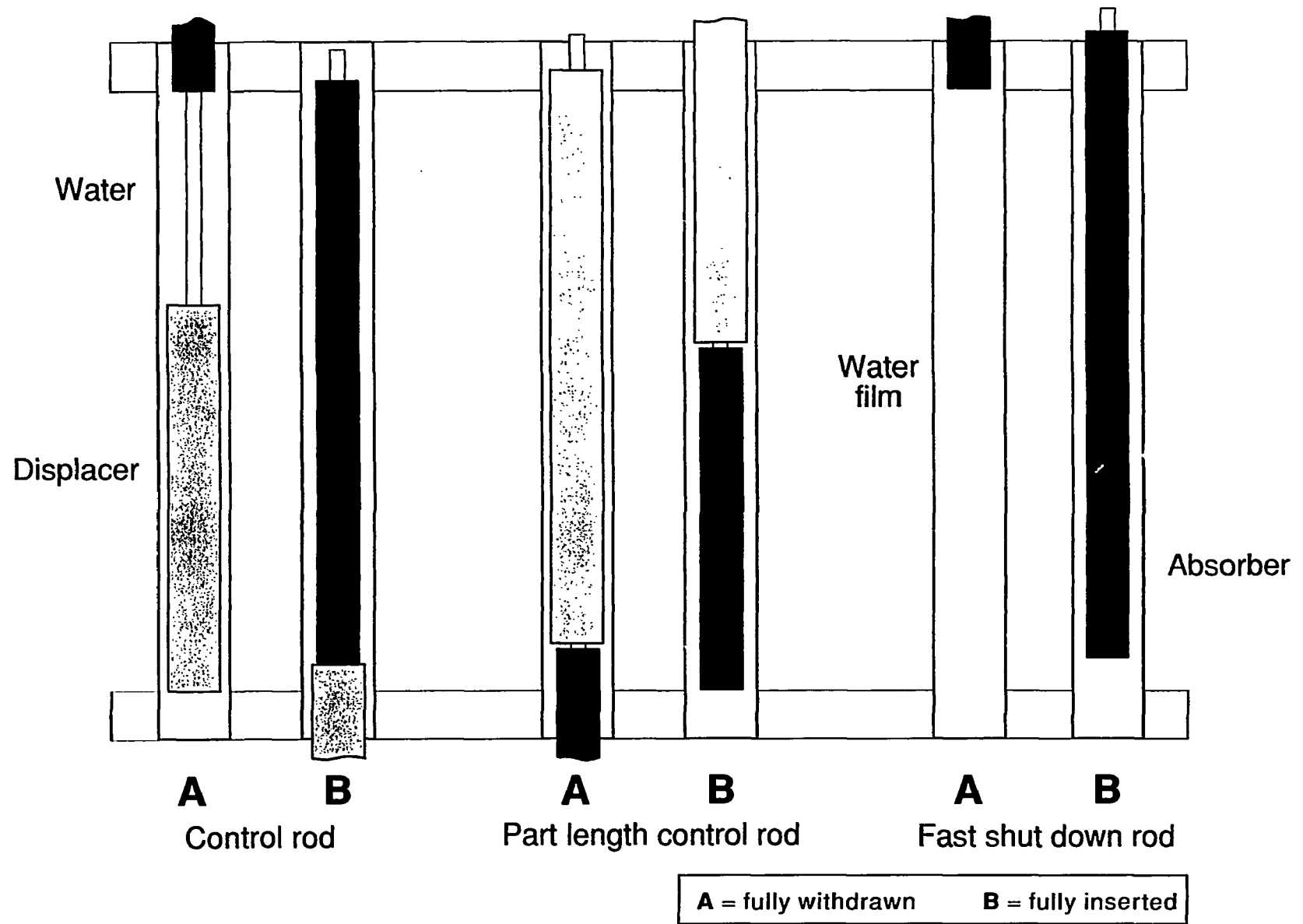


Fig. 2 Schematic of the present control rod designs



4. ARROTTA implementation and validation

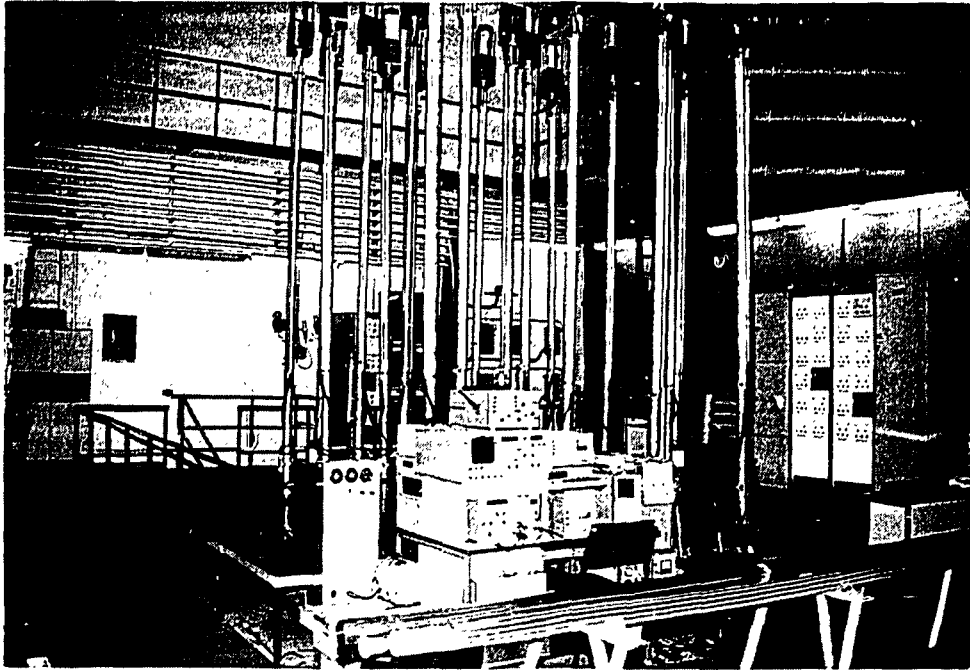
In phase I of the project the implementation of QUABOX CUBBOX [4], a three dimensional transient neutronics computer code with thermal hydraulic feedback developed by the German GRS was described in great detail [3]. In parallel to this work ARROTTA was implemented at PSI since a new systems code RETRAN-3D using ARROTTA as three dimensional transient neutronics core code became available. It is planned to use RETRAN- 3D in PSI's future RBMK work since presently only an experimental version of the code is available and a users license was only acquired after the work under the bilateral agreement was completed.

Considerable effort was devoted to the validation of ARROTTA to verify its applicability to RBMK cores. This validation was based on the evaluation of cold critical experiments previously performed at the critical facility of the RRC-KI, and on zero-power measurements taken during start-up of the SMOLENSK-3 nuclear power plant. At full-power, spatially-dependent burn-up conditions, 3-D ARROTTA analyses were performed for SMOLENSK-1 and SMOLENSK-3, for which plant the void reactivity coefficient was also analyzed and compared with the measured values. For all the ARROTTA analyses the RRC-KI cross section libraries were used just as in the STEPAN code.

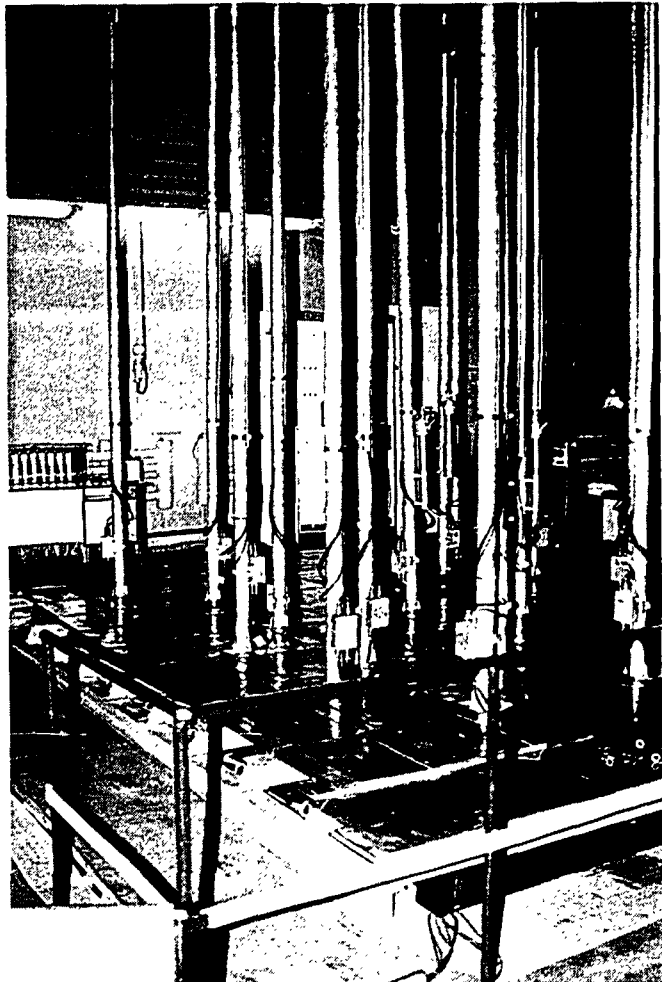
4.1 ARROTTA validation based on experiments performed at the critical facility of RRC-KI

The experiments were performed on the graphite RBMK critical facility at room temperature and atmospheric pressure. The graphite stack of the assembly comprises 324 graphite blocks arranged in an 18 x 18 quadratic array. Its overall dimensions are 450 x 450 x 410 cm. There are 324 vertical bores penetrating the graphite block and housing the channel tubes. The channel pitch is 25 cm just as in the RBMK core. The graphite effective density (taking into account the gaps within the stack) is equal to $1.70 \pm 0.01 \text{ g/cm}^3$. The diameter of the channel tubes is 88 mm, their wall thickness is 4 mm. The material is the aluminum alloy CAB-6. The assembly is designed to accommodate as built RBMK fuel assemblies (half length) and control rods.

For the experiments two critical assemblies were used. The first comprises 21 fresh dry fuel assemblies (FA) with an enrichment of 2% U-235, surrounded by 12 fully withdrawn dry control rods. The second assembly includes 192 FA with an enrichment of 2 % U-235, 28 dry control rods, 32 additional absorbers (AA) and 4 empty fuel channels. For both assemblies k_{eff} , radial and axial flux distributions were measured. The loading pattern of assembly 1 is shown in Figure 3, and the corresponding radial flux distributions are shown in Figure 4. For comparison also the values calculated by ARROTTA are shown. The average deviation between the calculated and the measured values is 4.3%.



RRC KI critical facility



MCR dry,out		MCR dry,out		MCR dry,out		MCR dry,out
				FA-2% dry	FA-2% dry	
MCR dry,out	FA-2% dry	FA-2% dry	FA-2% dry	FA-2% dry	FA-2% dry	MCR dry,out
	FA-2% dry	FA-2% dry	FA-2% dry	FA-2% dry	FA-2% dry	
MCR dry,out	FA-2% dry	FA-2% dry	FA-2% dry	FA-2% dry	FA-2% dry	MCR dry,out
	FA-2% dry	FA-2% dry	FA-2% dry	FA-2% dry	FA-2% dry	
MCR dry,out		MCR dry,out		MCR dry,out		MCR dry,out



- the location of the axial flux measurement

Fig. 3 Array of critical assembly 1 showing fuel loading and control rod positions

0.862 - ARROTTA calculations

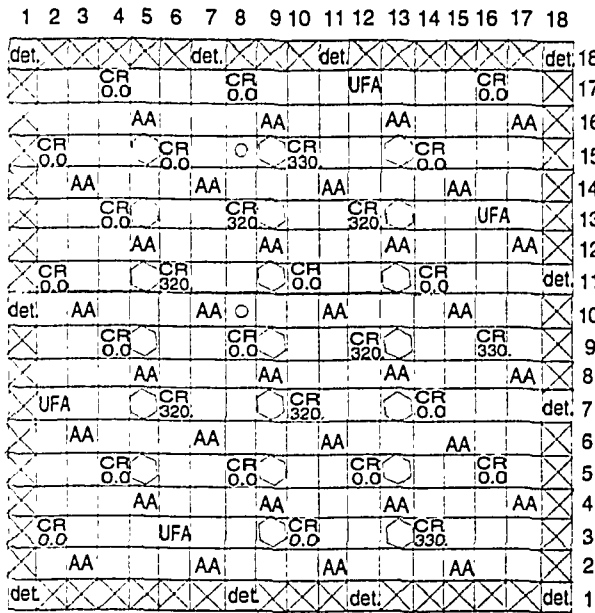
0.864 - measured value

The map of radial flux distribution and control rod position

MCR 1.85m		MCR 0.0 m		MCR 0.0 m		MCR 1.85m
				0.862 0.864	0.671 0.722	
MCR 0.0 m	0.841 0.836	1.079 1.025	1.090 1.135	1.097 1.059	0.888 0.909	MCR 0.0 m
	0.939 0.942	1.187 1.131	1.306 1.246	1.244 1.189	0.993 1.012	
MCR 0.0 m	0.899 0.921	1.137 1.110	1.245 1.207	1.160 1.140	0.933 0.969	MCR 0.0 m
	0.720 0.790	0.930 0.957	1.019 1.043	0.943 0.976	0.738 0.816	
MCR 1.85m		MCR 0.0 m		MCR 0.0 m		MCR 1.85m

Fig. 4 Radial flux distribution of assembly 1

The Assembly 2 representation



- AA - additional absorber
- det. - detector
- CR 0.0 - fully withdrawn dry control rod
- UFA - empty fuel channel
- CR 330 - inserted dry control rod
- - fuel assembly
- ⊗ - reflector
- ⊠ - location of radial flux measurement
- ⊡ - location of axial flux measurement

Fig. 5 Array of critical assembly 2

	5	6	7	8	9	10	11	12	13	
15	0.842 0.768				0.557 0.543				0.728 0.629	
14										
13	1.009 0.928				0.808 0.798				0.836 0.767	
12										
11	0.934 0.911				1.416 1.420				1.185 1.155	
10										
9	1.172 1.187				1.499 1.539				1.008 1.007	
8										
7	0.944 0.937				1.081 1.189				1.272 1.266	
6										
5	1.030 1.032				CR* 1.088 1.8m 1.300				1.181 1.201	
4										
3					0.836 0.850				0.560 0.582	

0.842 - ARROTTA calculation
0.768 - measured value

CR* - positions of other control rods are the same as at fig.5
1.8m

Fig. 6 Radial flux distribution of assembly 2

The calculated $k_{eff} = 1.007537$ and compares quite well with the measured value of 1.0017. The deviation is 0.58%.

The arrangement of the second assembly is shown in Figure 5. Criticality was achieved by partly inserting control rods as indicated in the Figure. The measured k_{eff} of the assembly was $k_{eff} = 1.0019$, the corresponding ARROTTA value is $k_{eff} = 0.9985$, the deviation being 0.34%. The radial flux distribution is shown in Figure 6. The average deviation between the measured and the calculated values is $\Delta=6.8\%$. The axial flux distributions of both assemblies are shown in Table 1.

Table 1: Axial flux distribution, comparison of ARROTTA results with measurements (relative units).

Detector location	Assembly 1		Assembly 2			
Top=0 mm	Central core position		Core position 10-8		Core position 15-8	
mm	measured	calculated	measured	calculated	measured	calculated
180	0.450	0.468	0.504	0.533	0.452	0.485
540	0.770	0.780	0.817	0.884	0.807	0.880
900	1.080	1.060	1.112	1.110	1.146	1.121
1260	1.300	1.270	1.338	1.278	1.361	1.298
1620	1.400	1.391	1.404	1.395	1.432	1.420
1980	1.420	1.406	1.419	1.383	1.401	1.408
2340	1.290	1.303	1.286	1.207	1.266	1.224
2700	1.090	1.082	1.032	1.008	1.044	1.016
3060	0.760	0.763	0.713	0.756	0.704	0.748
3420	0.440	0.478	0.399	0.447	0.387	0.400

The location of the measurements are marked in Figures 3 and 6. The average deviation between the measured and the calculated values are 2% for assembly 1 and 4.45% in assembly 2.

4.2 Analysis of the SMOLENSK-3 start up experiment.

Out of the start up experiments performed at SMOLENSK-3 [5] in 1989 two configurations were selected for the validation calculations, the initial core and an interim core:

4.2.1 Analysis of the initial core

In the initial core 1381 fuel assemblies were loaded with an enrichment of 2% U-235. There were 234 additional absorbers and 46 empty fuel channels filled with water. Criticality was achieved with 28 control rods fully withdrawn, one control rod was inserted to 1.6 m from the top of the core. In addition to the measurements performed at zero power and with critical control rod positions two measurements were taken with the 28 control rods fully inserted and with the 28 control rods plus the 24 fast shutdown rods fully inserted.

4.2.1.1 Comparison of measured and calculated reactivities

The results of the criticality analyses are shown in Table 2. For comparison also STEPAN results (lower numbers ARROTTA values) are given.

Table 2: k eff values of initial core, comparison of ARROTTA and STEPAN results with measurements

Control rod positions	k eff	Reactivity (β_{eff})		Error (%)
	calculation	calculation	measurement	
critical position	0.9965081	-	-	0.35
	(1.00282)	-	-	0.28
28 CR fully inserted	0.9832016	1.79	1.76 \pm 6%	12.5
	0.991564	1.65		
28 CR plus 24 FASS fully inserted	0.968172	4.29	4.0 \pm 6%	7.2
	0.97798	3.7		7.5

The errors of the reactivity measurements were estimated by RDIPE to have been 6%.

The effective delayed neutron fraction for fresh fuel enriched to 2% U-235 and used in the reactivity calculation was $\beta_{eff} = 0.00685$.

4.2.1.2 Comparison of measured and calculated flux distributions.

The flux measurements were taken by means of compact fission chambers in 32 radial positions. All chambers were located in the same axial plane at 4.5 m from the bottom of the core. For the initial core loading the results of the measurements and the ARROTTA and STEPAN results are shown in Figures 7-8. The average deviation between ARROTTA and the measured radial flux distribution is $\Delta=25\%$, which appears rather high but compares well with the error of the STEPAN calculations ($\Delta=22\%$).

4.2.2 Analyses of an interim core

In a second step an interim core loading was investigated with 1371 fresh fuel assemblies enriched to 2% U-235, 234 additional absorbers, 46 empty fuel channels filled with water, and 10 empty fuel channels without water. To achieve criticality 32 control rods were fully withdrawn and one control rod was inserted to 2.5 m from the top of the core. As in the case of the initial core loading in addition to the measurements taken at critical zero power conditions, two measurements were taken with the 32 control rods fully inserted and with the 32 control rods plus the fast acting shutdown rods fully inserted. The measurements were done for voided and unvoided channel conditions. Measurements of flux distributions were also performed for this core configuration.

4.2.2.1 Comparison of measured and calculated reactivities

The results of the ARROTTA criticality analysis are presented in Table 3 together with the corresponding results of the STEPAN calculations (lower numbers).

Table 3: k eff values of interim core, comparison of ARROTTA and STEPAN results with measurements

Control rod positions	k eff	Reactivity (β_{eff})		Error (%)
		calculation	experiment	
Critical positions	0.9968184			0.32
	1.00255			0.26
32 CR fully inserted	0.9823162	2.16	1.92 \pm 6%	12.5
	0.990112	1.83		4.7
32 CR plus 24 FASS fully inserted	0.967774	4.39	4.1 \pm 6%	7.0

4.2.2.1 Comparison measured vs. calculated flux distributions

For the interim core loading the radial flux distribution is shown in the Figures 9-10. The average value of the calculated error is 33% for ARROTTA and 25% for the STEPAN analysis. The average axial flux distributions shown in Figure 11 were obtained by averaging the 63 thermal flux values for each axial node in both, the measurements and the analyses.

Initial core loading

192 - ARROTTA calculation

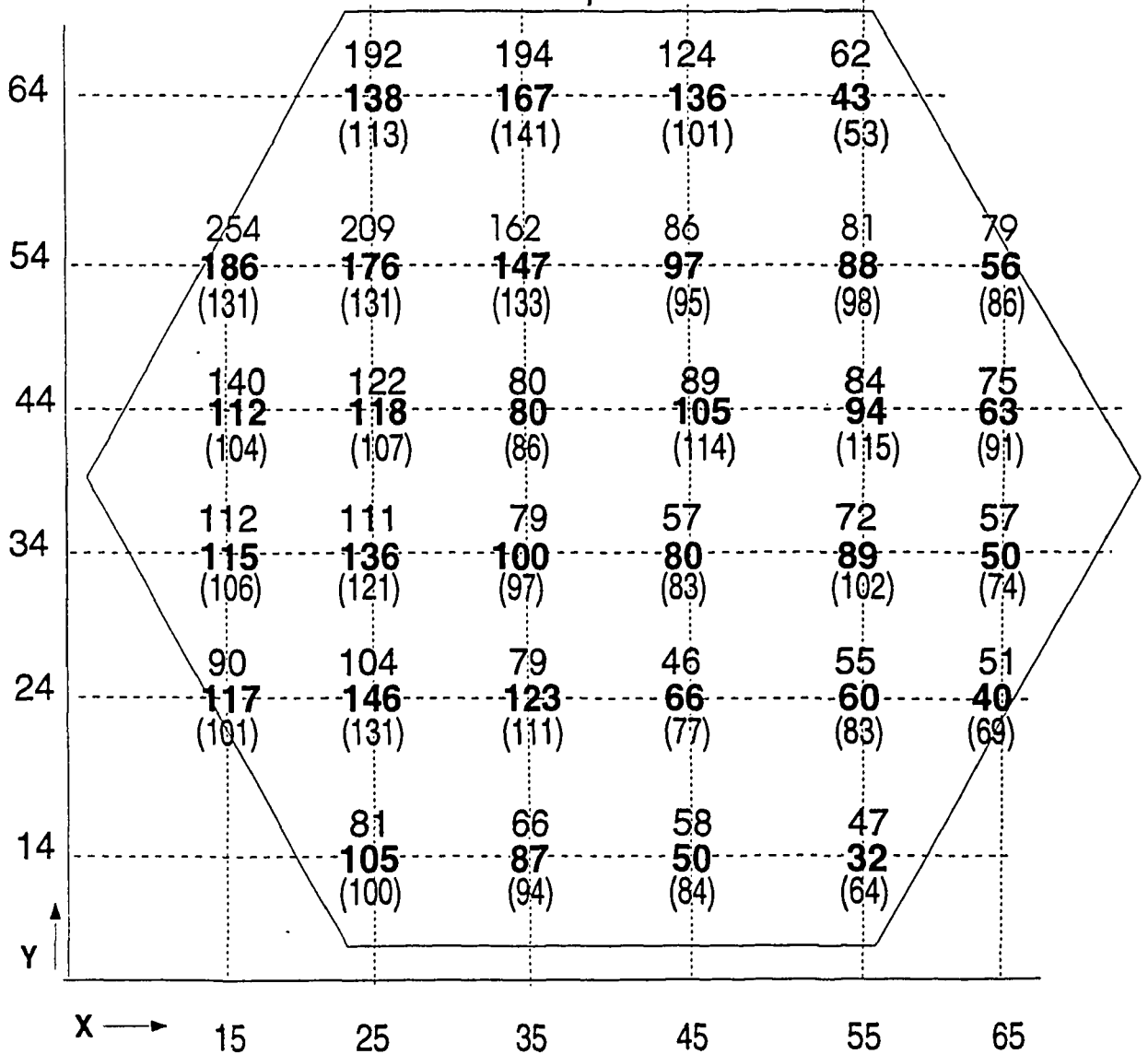
138 - measured value(113) - **STEPAN** calculation*The map of the core*

Fig. 7

Radial flux distribution of initial core loading

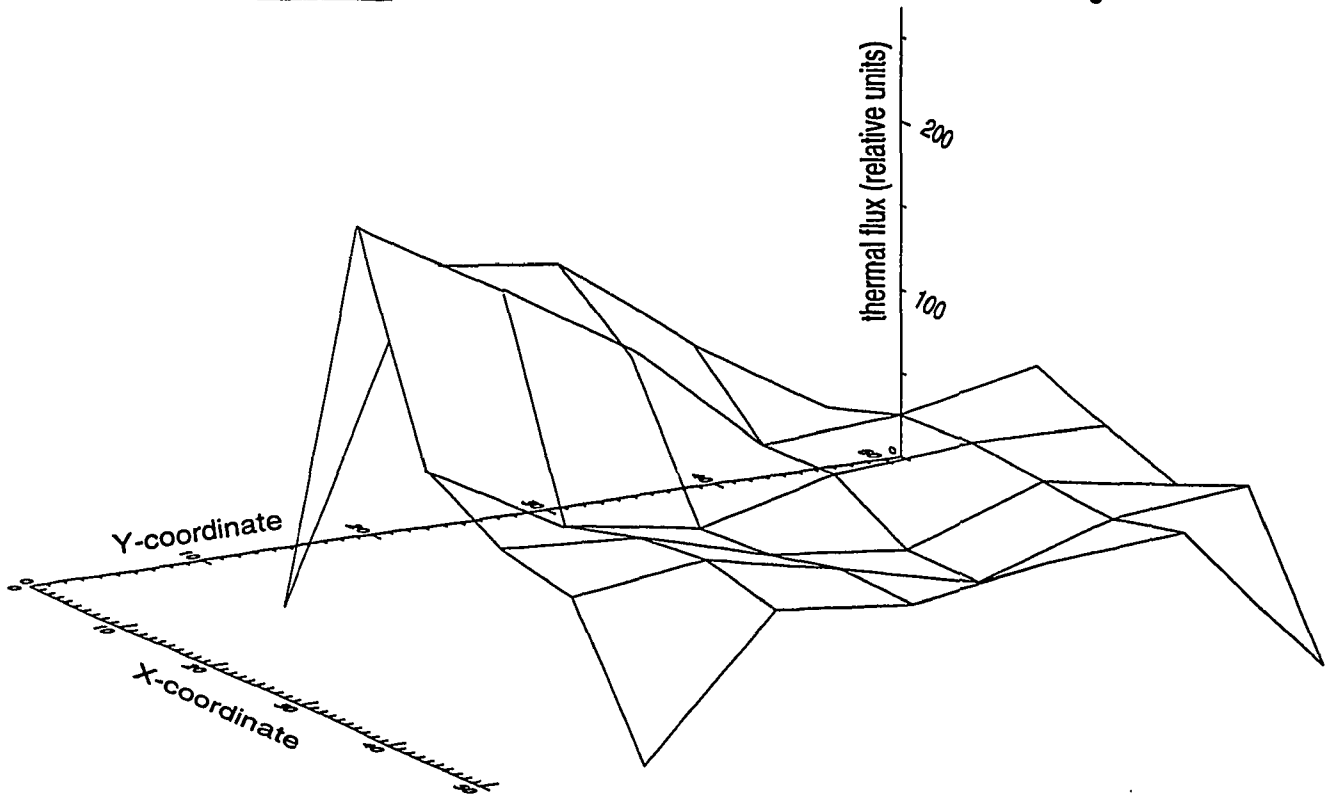
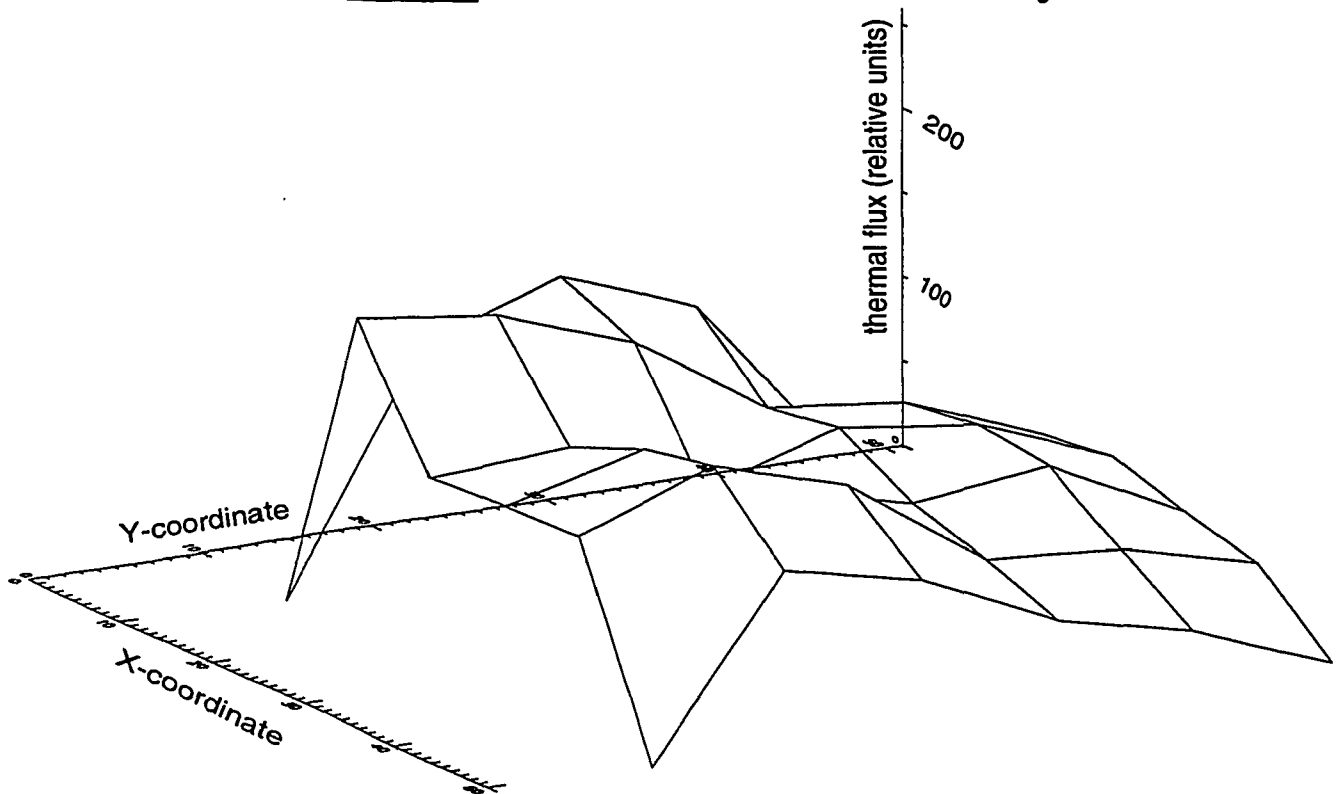
ARROTTA calculation thermal flux distribution of initial core loadingMeasured thermal flux distribution of initial core loading

Fig. 8 3-D map of radial flux distribution of initial core loading

Radial thermal flux distribution of interim core loading

128 - **ARROTTA** calculation
 132 - measured value
 (100) - **STEPAN** calculation

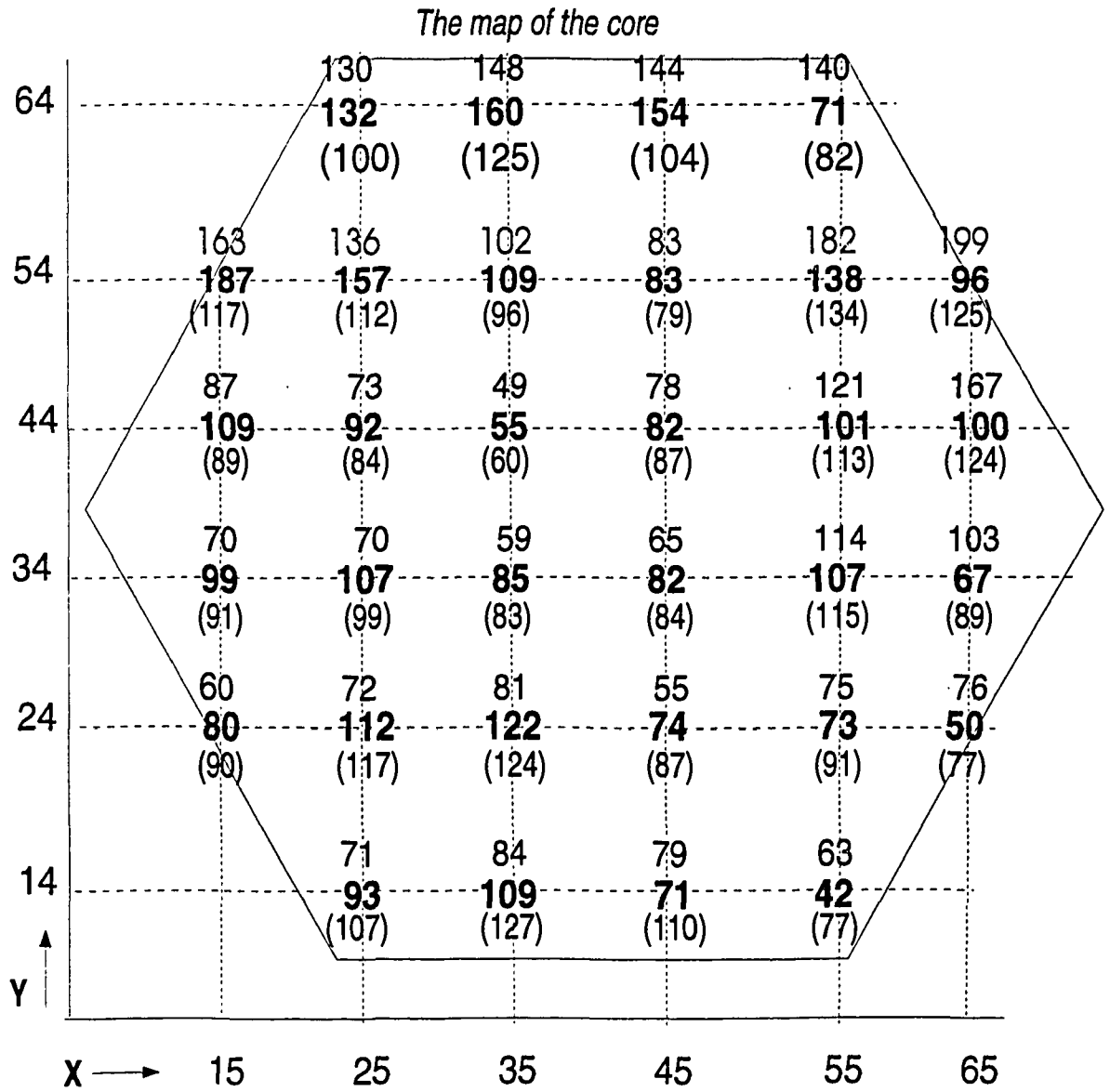
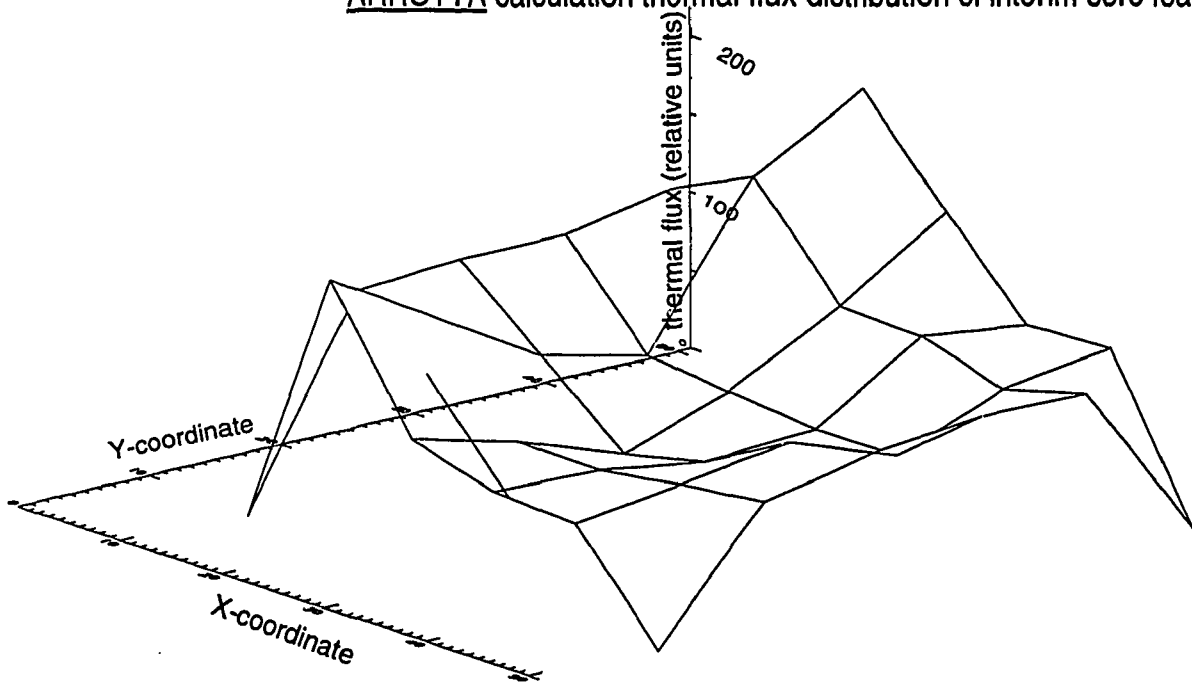


Fig. 9 Radial flux distribution for interim core loading

ARROTTA calculation thermal flux distribution of interim core loading



Measured thermal flux distribution of interim core loading

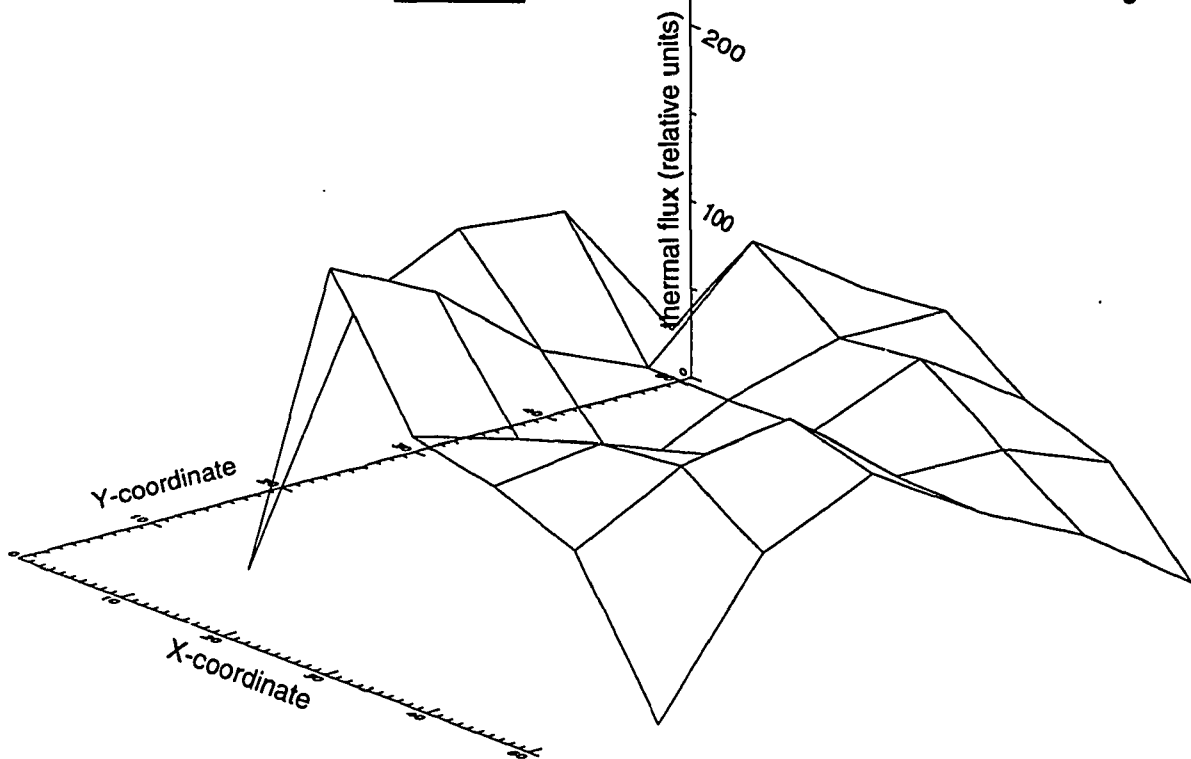


Fig. 10 3-D map of radial flux distribution of interim core loading

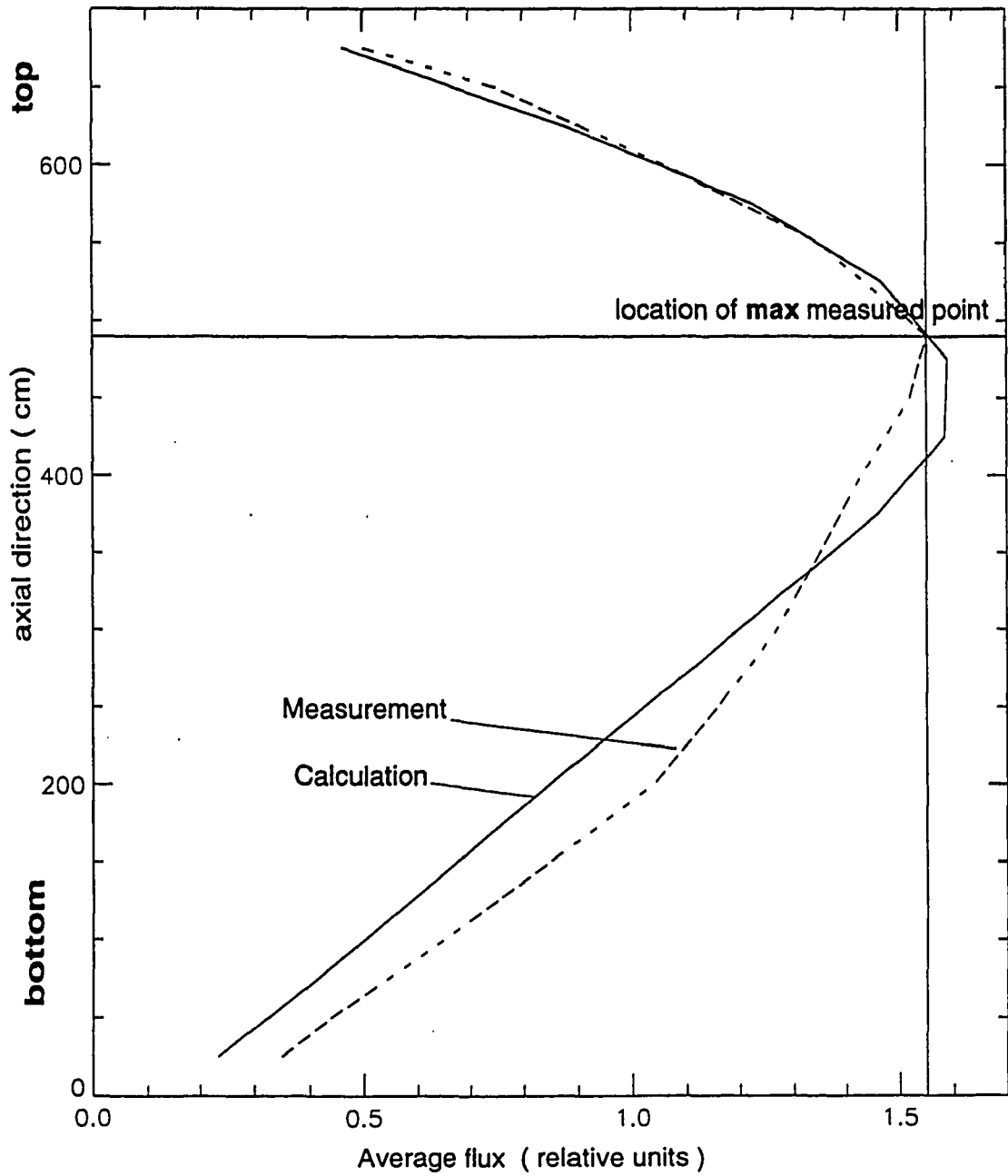


Fig. 11 Average axial flux distribution of interim core loading

4.2.2.3 Comparison of measured and calculated void reactivities of the main cooling circuit (MCC) and the cooling circuit of the control and protection system (CPS)

The void reactivities of the main cooling circuit and the cooling circuit of the CPS were determined only for the interim core loading. Both, reactivities and flux distributions were measured. The measurements were taken for the voided MCC, the voided CPS, and for the voided MCC and CPS.

Three different control rod positions were considered:

- critical rod positions;
- 58 control rods fully inserted;
- 58 control rods plus 24 fast acting shutdown rods fully inserted.

Both, ARROTTA and STEPAN calculations were performed for the comparison. The results are given in Table 4 and Figure 12.

Note that the maximum error of the ARROTTA criticality analysis for the voided core channels is 10.3%. The corresponding value of STEPAN 16.1%. The discrepancy between the ARROTTA radial flux distribution and the measurements is even worse, namely 43%. Here the STEPAN analysis shows a much better agreement with the measurement, the error being only 15%.

MCC without water.

34 - ARROTTA calculation

36 - measured value

(34) - STEPAN calculation

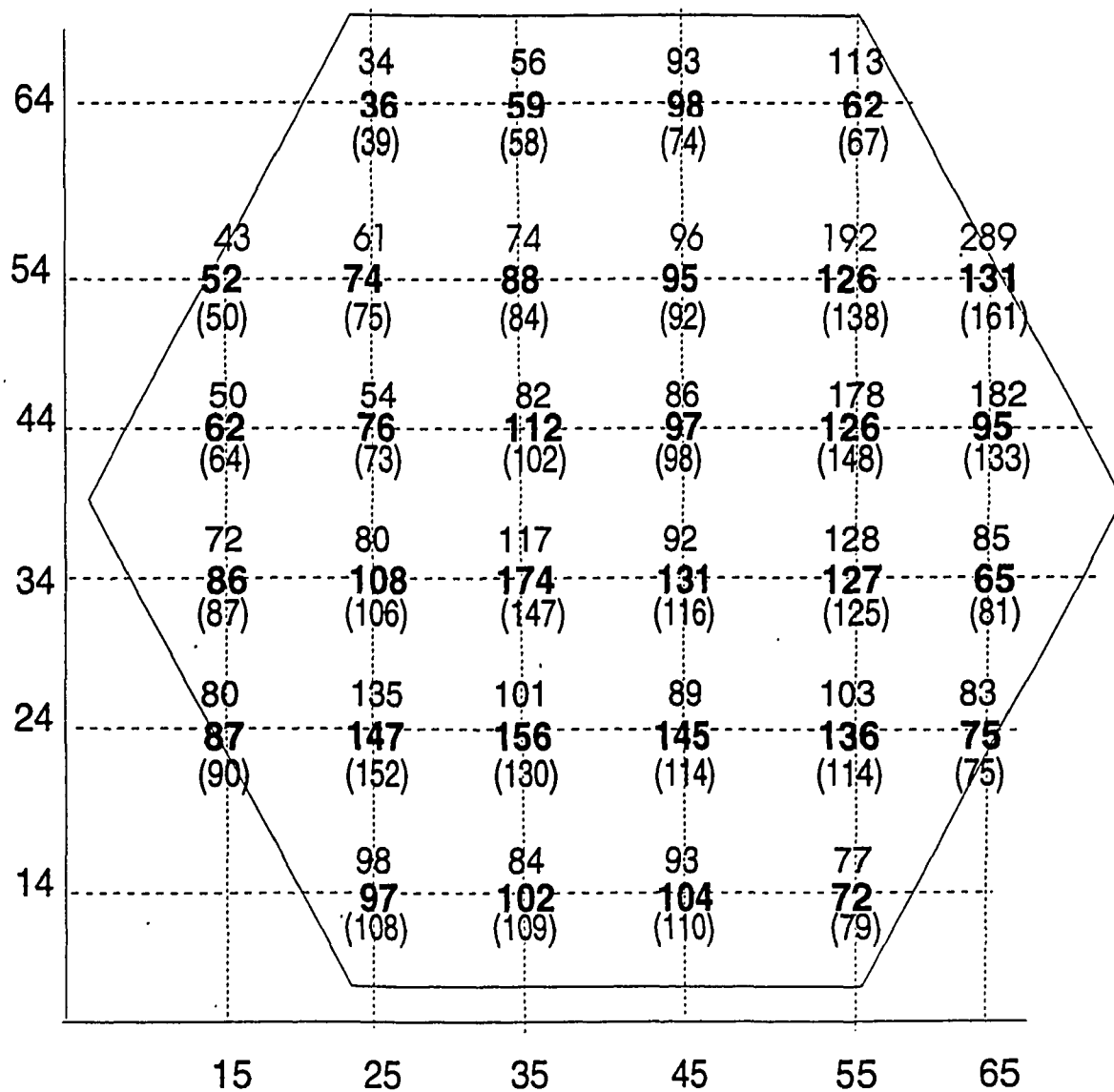
The map of the core

Fig. 12 Radial flux distribution of interim core, no water in the fuel channels

Table 4: k_{eff} values of interim core with voided MCC, comparison of ARROTTA and STEPAN results with measurements

Control rod positions	k_{eff}	Reactivity (β_{eff})		Error (%)
		calculation	measurement	
Critical position	0.9925738			0.74
	0.993702			0.63
58 CR fully inserted	0.9583984	5.24	5.6 ± 0.34	6.4
	0.96306	4.7		16.1
58 CR plus 24 FASS rods fully inserted	0.9409744	8.07	9.0 ± 0.54	10.3
	0.943385	7.84		12.9

Also for the case of the voided CPS circuit three measurements were taken for different control rod positions:

- critical control rod positions;
- 30 control rods fully inserted;
- 30 control rods plus 24 fast acting shutdown rods fully inserted.

The results of the ARROTTA and STEPAN analyses are presented in Table 5 and Figure 13 and compared with the measurements.

Table 5: k_{eff} values of interim core with voided CPS circuit, comparison of ARROTTA and STEPAN results with measurements

Control rod position	k_{eff}	Reactivity (β)		Error (%)
		calculation	measurement	
critical position	0.9961028			0.39
	1.00512			0.51
30 CR fully inserted	0.9770537	2.86	2.7 ± 0.2	5.9
	0.987557	2.58		4.4
30 CR plus 24 FASS rods fully inserted	0.9621839	5.17	5.0 ± 0.3	3.4
	0.973525	4.71		5.8

As in the case of the voided main cooling circuit, the error of the calculated reactivities is the lowest at critical control rod positions. The flux measurements shown in Figure 13 were taken for the critical control rod position. The deviation between the measured and the calculated values are extremely high for both, the ARROTTA (53%) and STEPAN (51%) results. Further investigations are required to clarify the discrepancies observed, which might also at least partly be caused by the instrumentation used.

CPS without water.

150 - ARROTTA calculation

180 - measured value

(90) - STEPAN calculation

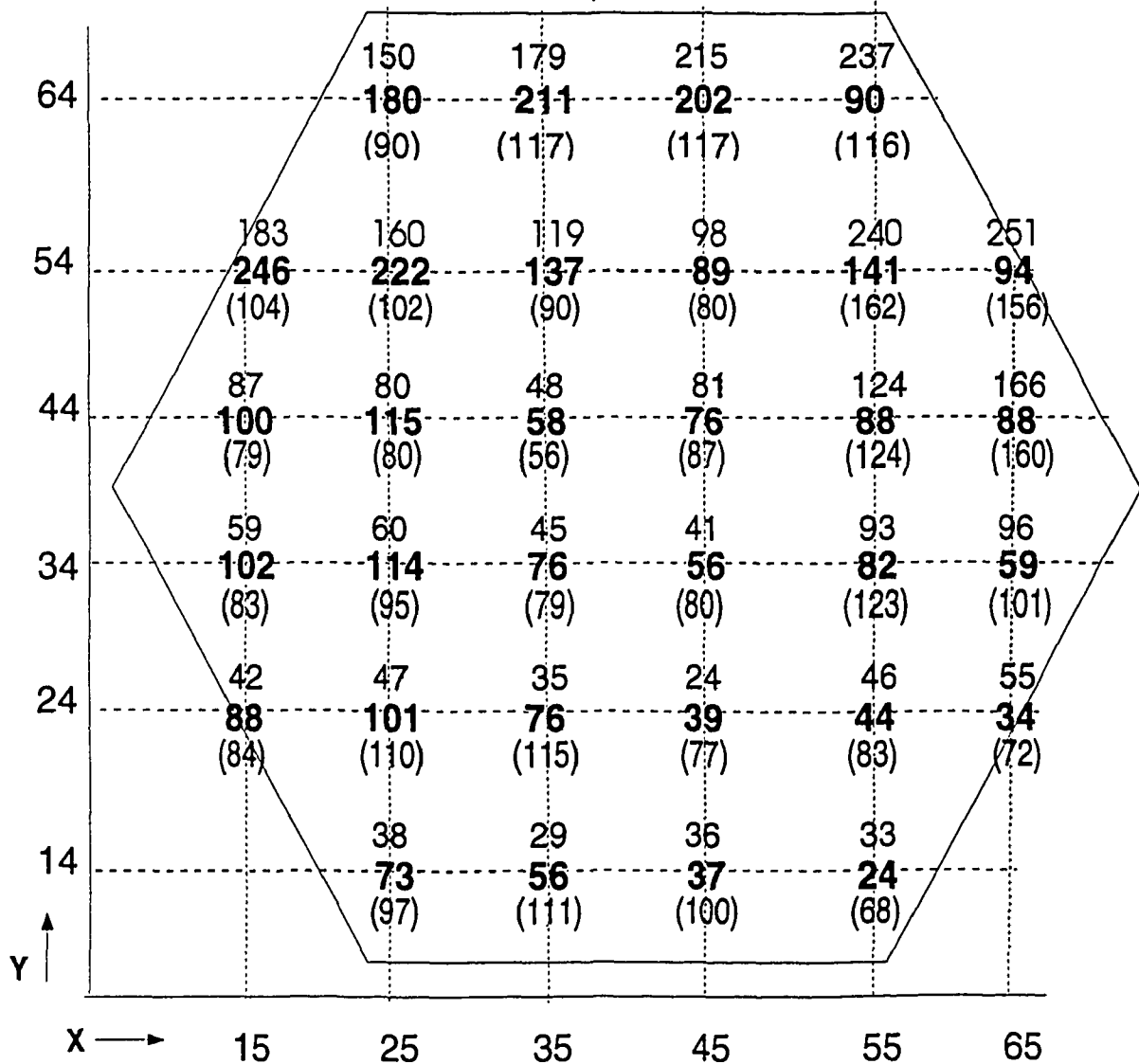
The map of the core

Fig. 13 Radial flux distribution of interim core, no water in the CPS channels

CPS and MCC without water.

39 - ARROTTA calculation
26 - measured value
 (37) - STEPAN calculation

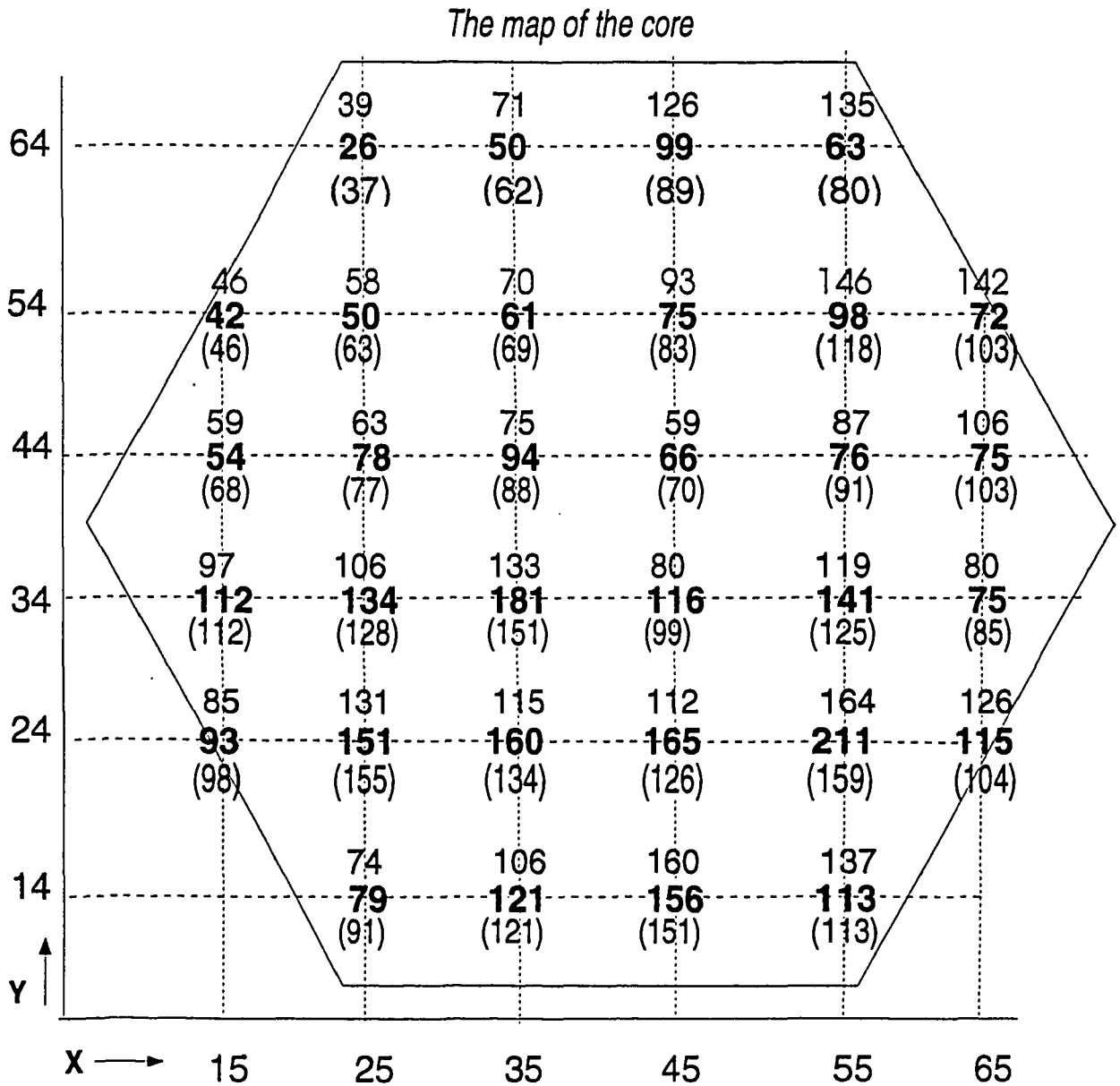


Fig. 14 Radial flux distribution of interim core, no water in fuel and CPS channels

Table 6: k eff values for interim core for voided MCC and CPS, comparison of ARROTTA and STEPAN with measurements.

Control rod position	k eff	Reactivity (β)		Error (%)
		calculation	measurement	
Critical position	0.9909916			0.90
	0.994794			0.52
51 CR fully inserted	0.9527498	5.91	6.4 \pm 6%	7.7
	0.957309	5.75		10.2
51 CR plus 24 FASS rods fully inserted	0.9349625	8.83	9.8 \pm 6%	9.9
	0.936752	9,09		7.2

Finally the experiments performed addressed the question of the core behavior under conditions when the whole core including the CPS channels was voided. The agreement between the measured criticality values and the analyses is comparable with the previous case. The results are shown in Table 6 and Figure 14.

Conclusions

In summary, the error of the reactivity analyses on the average was found to be approximately 8% for both codes. For critical rod positions this error is less than 1 %. The average error of the calculated flux distribution is about 37% for ARROTTA and around 27% for STEPAN. In both cases the discrepancies between the analyses and the measurements are unexpectedly high and need further investigation. Beyond the reason given above the potential cause for this observation might be found in the utilization of reprocessed uranium in 400 fuel assemblies loaded in the core prior to the measurements. These assemblies were treated just as regular assemblies in the analyses. This assumption is also supported by the comparatively good agreement found in the critical experiments performed at the Kurchatov critical facility.

4.3 ARROTTA analyses at full power

In order to be able to analyze the core at full power it was necessary to investigate the ability of ARROTTA to predict the spatial distribution of the xenon concentration in the core and to perform a nodalization study to find an optimum number of axial nodes required to adequately predict spatial power distributions when the thermal hydraulic feed back mechanisms come into play.

4.3.1 Xenon distribution

Two ways of calculating the xenon concentrations at full power were investigated:

- the usual ARROTTA approach which calculates power and xenon concentrations iteratively, using cross sections as a function of the absolute value of the respective xenon concentrations in each node (ARROTTA model);
- the ARROTTA approach for the calculation of the xenon distribution combined with the RRC-KI library, based on cross sections which are a function of an average reference xenon concentration.

To simplify the problem the three dimensional analyses were performed assuming a uniform xenon distribution. As is shown in Table 7 the two methods are equivalent, since the results are in

reasonable good agreement. The straight forward ARROTTA model was used for all further calculations and it was concluded that also STEPAN based on the RRC-KI library would adequately predict xenon and xenon distributions.

Table 7: k eff and power peaking calculated by ARROTTA, uniform xenon concentration.

Xenon model	k eff	Δ k eff (%)	radial peaking factor (-)	axial peaking factor (-)
Straight forward ARROTTA	0.9982	- 0.18	2.11	1.3
ARROTTA combined with RRC-KI library	1.0036	+ 0.36	2.19	1.3

In order to investigate the impact of spatially distributed xenon on the integral core parameters, reactivity and power distribution were calculated for uniform and non uniform xenon distributions. The results are presented in Table 8.

Table 8: k eff and power peaking for different xenon distributions at full power

NPP	Xenon condition	k eff (-)	radial peaking factor (-)	axial peaking factor (-)
SMOLENSK-3	uniform distribution	1.0008	1.82	1.26
	real distribution	0.9936	1.65	1.18
SMOLENSK-1	uniform distribution	1.0036	2.19	1.28
	real distribution	0.9951	1.96	1.20

The results are also shown in Figure 15. For comparison also STEPAN results are presented in this Figure. The discrepancies between the results of the two codes might be explained by the fact that the present ARROTTA version used for this analysis does not have the capability to calculate space dependent graphite temperatures.

4.3.2 ARROTTA Xenon transient

To test the ARROTTA Xenon Transient option a power ramp was calculated reducing the reactor power from 100 % to 50 % within two hours as shown in Figure 16. The calculations were performed for three different time steps: 1 hour, 30 minutes and 10 minutes. The results are strongly depending on the time step as shown in Figure 17 and 18, suggesting a time step maximum of no more than 30 minutes. Since it is difficult for the user to estimate in advance how big the time step for a specific problem has to be, the code was modified in the meantime to provide an automatic time step control.

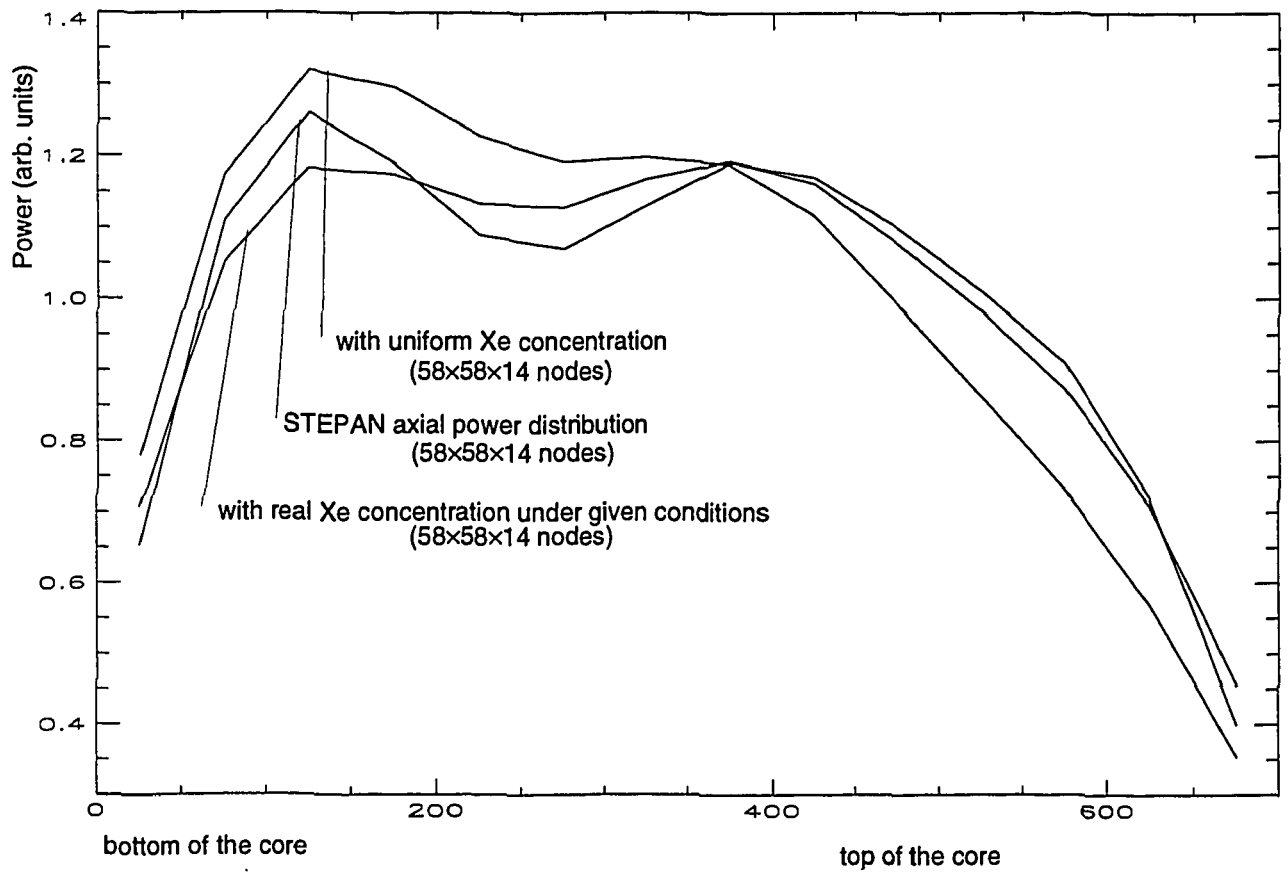


Fig. 15 Radially averaged axial power distribution of SMOLENSK-3 (Dec. 28, 1993)

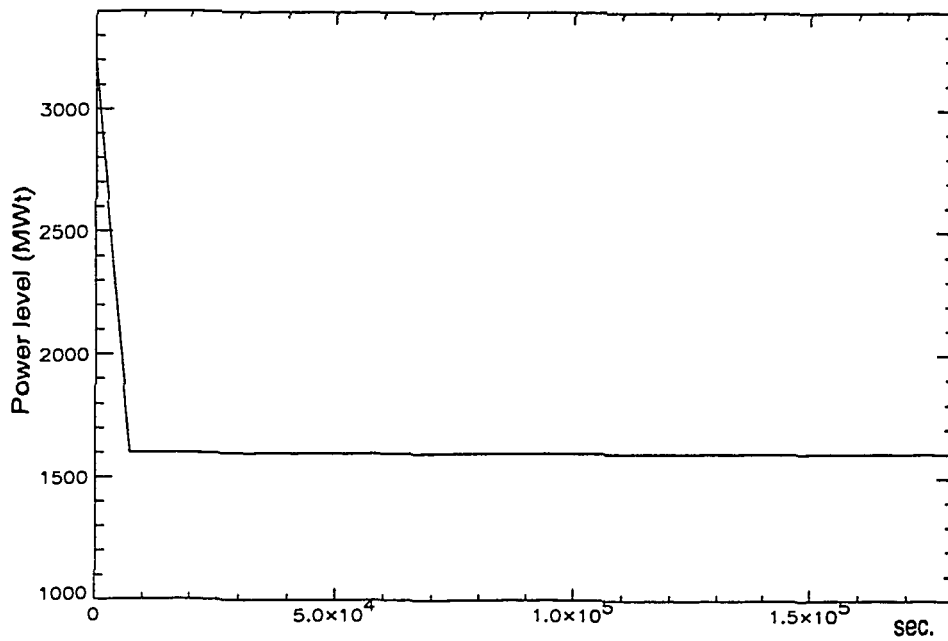


Fig. 16 ARROTTA Xenon Transient, power vs. time

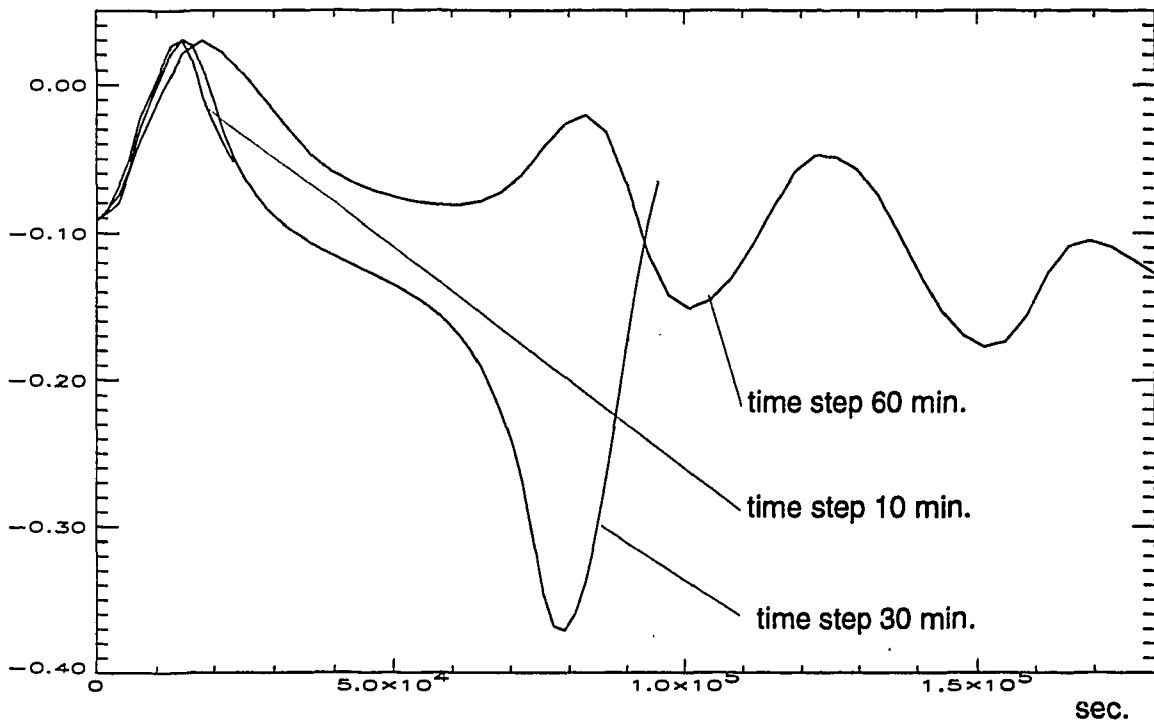


Fig. 17 ARROTTA Xenon Transient, axial offset vs. time for different time steps

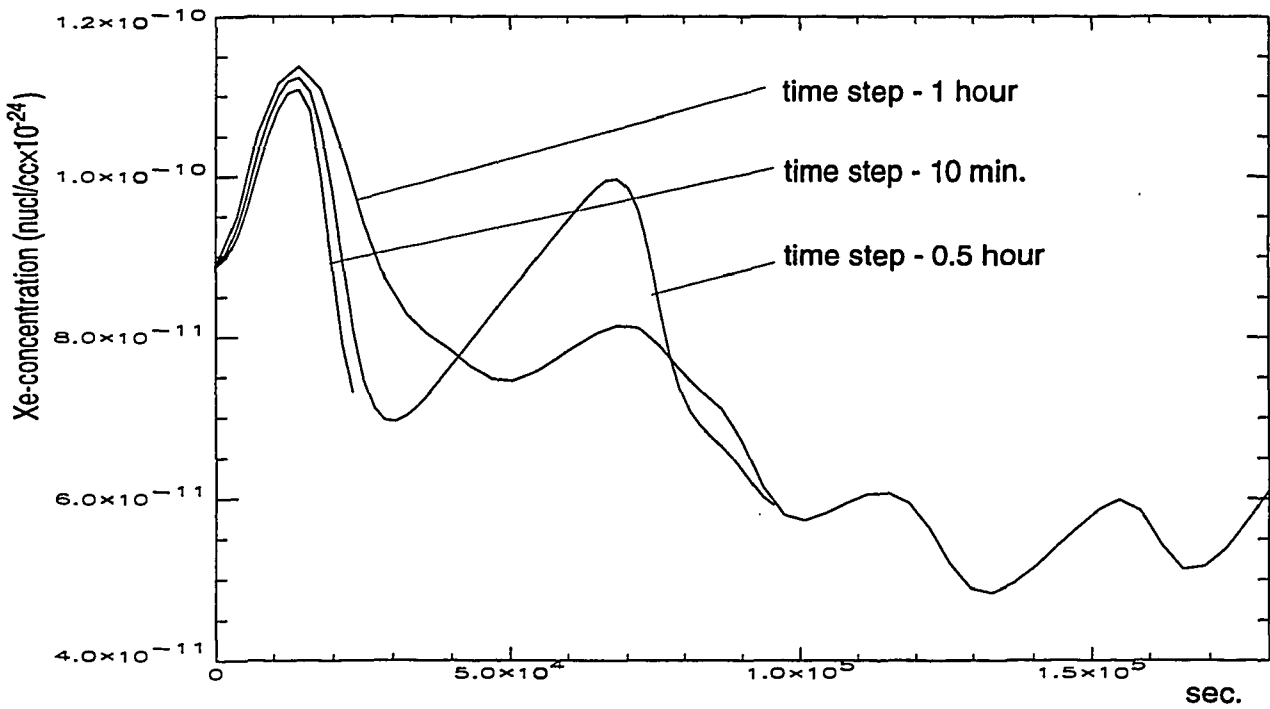


Fig. 18 ARROTTA Xenon Transient, average xenon concentration vs. time for different time steps

4.3.3 ARROTTA nodalization studies

To investigate the sensitivity of ARROTTA towards nodalization, three dimensional analyses were performed for different numbers of axial and radial nodes. The results are given in Table 9. Nodalization does not appear to strongly influence the results. A number of 14 axial nodes in the core region was felt to be acceptable for future work. In radial direction the selected number was 50.

Table 9: k eff and power peaking at full power for different nodalization schemes.

Nodalization	k eff (-)	radial peaking factor (-)	axial peaking factor (-)	location of max. axial peak (cm from bottom)
58 x 58 x 14	0.9936	1.65	1.18	375
54 x 54 x 14	0.9938	1.65	1.18	375
52 x 52 x 14	0.9938	1.65	1.19	375
50 x 50 x 14	0.9938	1.67	1.19	375
50 x 50 x 10	0.9940	1.63	1.16	375
50 x 50 x 12	0.9939	1.67	1.18	379
50 x 50 x 20	0.9937	1.67	1.19	402
50 x 50 x 22	0.9936	1.67	1.19	414
52 x 52 x 20	0.9937	1.66	1.19	402
52 x 52 x 12	0.9939	1.63	1.18	379
58 x 58 x 12	0.9936	1.64	1.17	379

For the final radial 50 x 50 nodalization scheme the core cross section averaged axial power distribution is graphically presented in Figure 19.

The ARROTTA radial power distribution is shown in Figure 20 and 21. For comparison the STEPAN results for the same core conditions are shown in Figure 22 and 23 before the so called flux reconstruction and afterwards Figure 24 and 25. The flux reconstruction is a method in use at RRC-KI to improve the agreement of the STEPAN calculations with the in core instrumentation readings. It forces the fluxes to assume the values of these readings by modifying the fission cross sections in the thermal region. The method is very briefly described in appendix A to this report but needs further evaluation.

4.3.4 Void coefficient at full power

Similar to the procedure in use to experimentally determine the void reactivity coefficient in RBMK the inlet temperature of the coolant was perturbed to calculate the void reactivity coefficient at full power. The ARROTTA results for the void coefficients of SMOLENSK-3 and SMOLENSK-1 at full power and with the control rods being in critical positions are 0.32 \$ and 0.731 \$ respectively. They compare quite well with the measured values of 0.3 \$ and 0.8 \$. The corresponding STEPAN results are 0.52 \$ and 1.03 \$. Axial power distribution and perturbed void fraction used in the analysis of the void coefficient for SMOLENSK-3 are presented in Fig. 26.

In addition to the void reactivity coefficient, also the void reactivity function was calculated for full power and with the control rods in critical positions. The eigenvalues of this configuration were calculated for different inlet temperatures and correlated with the average core void fraction. The results are shown in Figure 27. It is obvious that the void coefficient may be generated from this plot as a function of the average void fraction in the core.

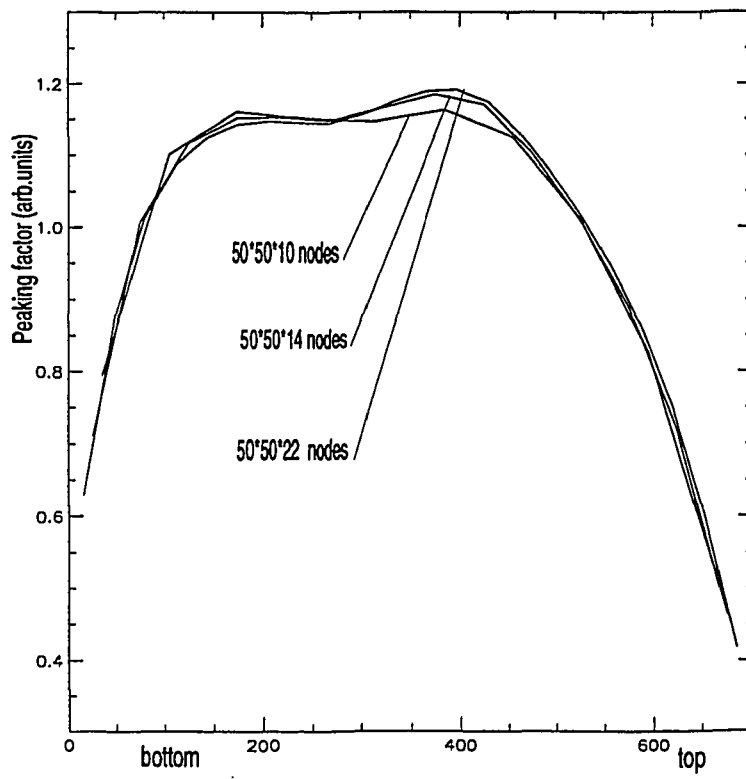


Fig. 19 Radially averaged axial power distribution for different axial nodalizations

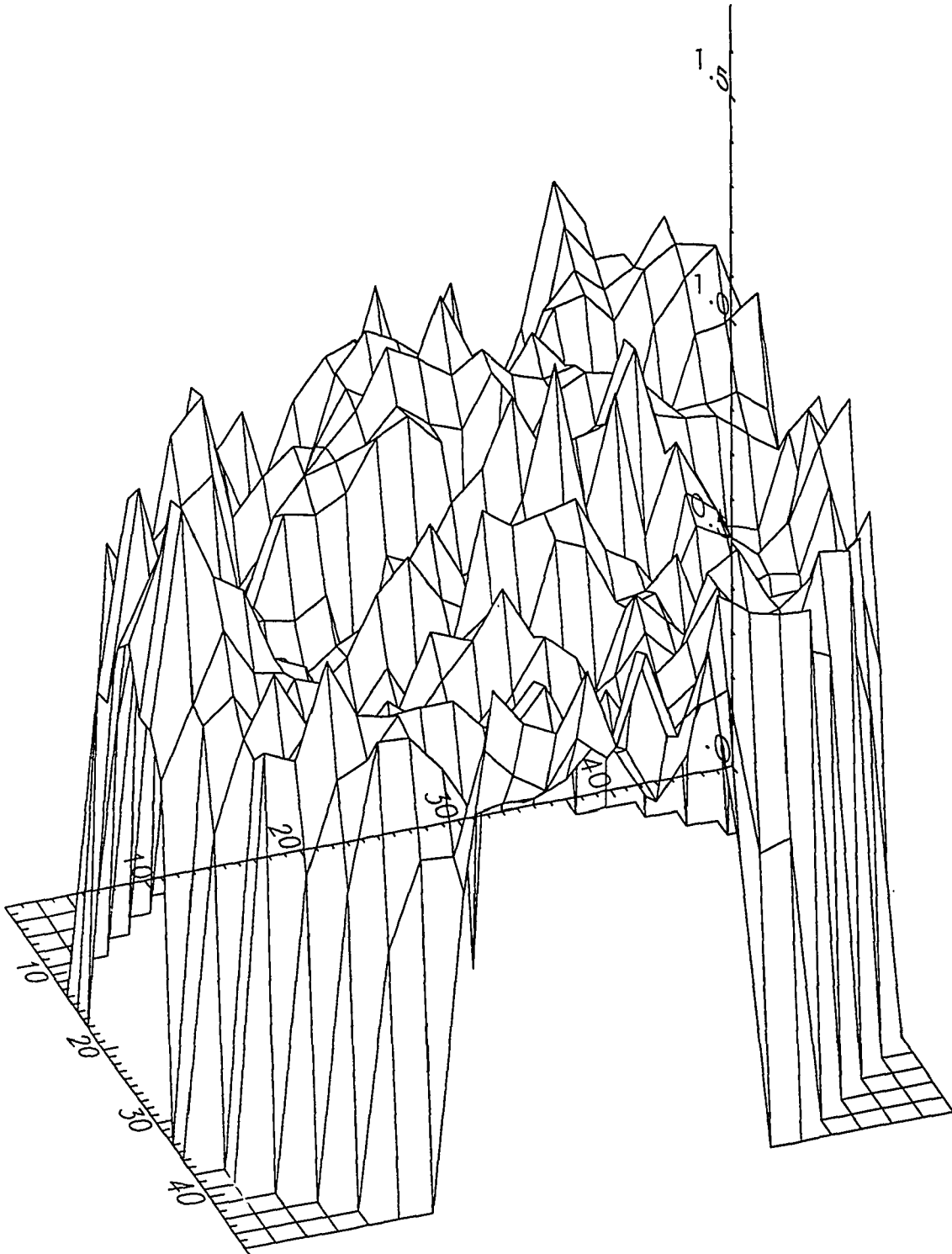


Fig. 20 ARROTTA radial power distribution for SMOLENSK-3 (Dec. 28, 1993)

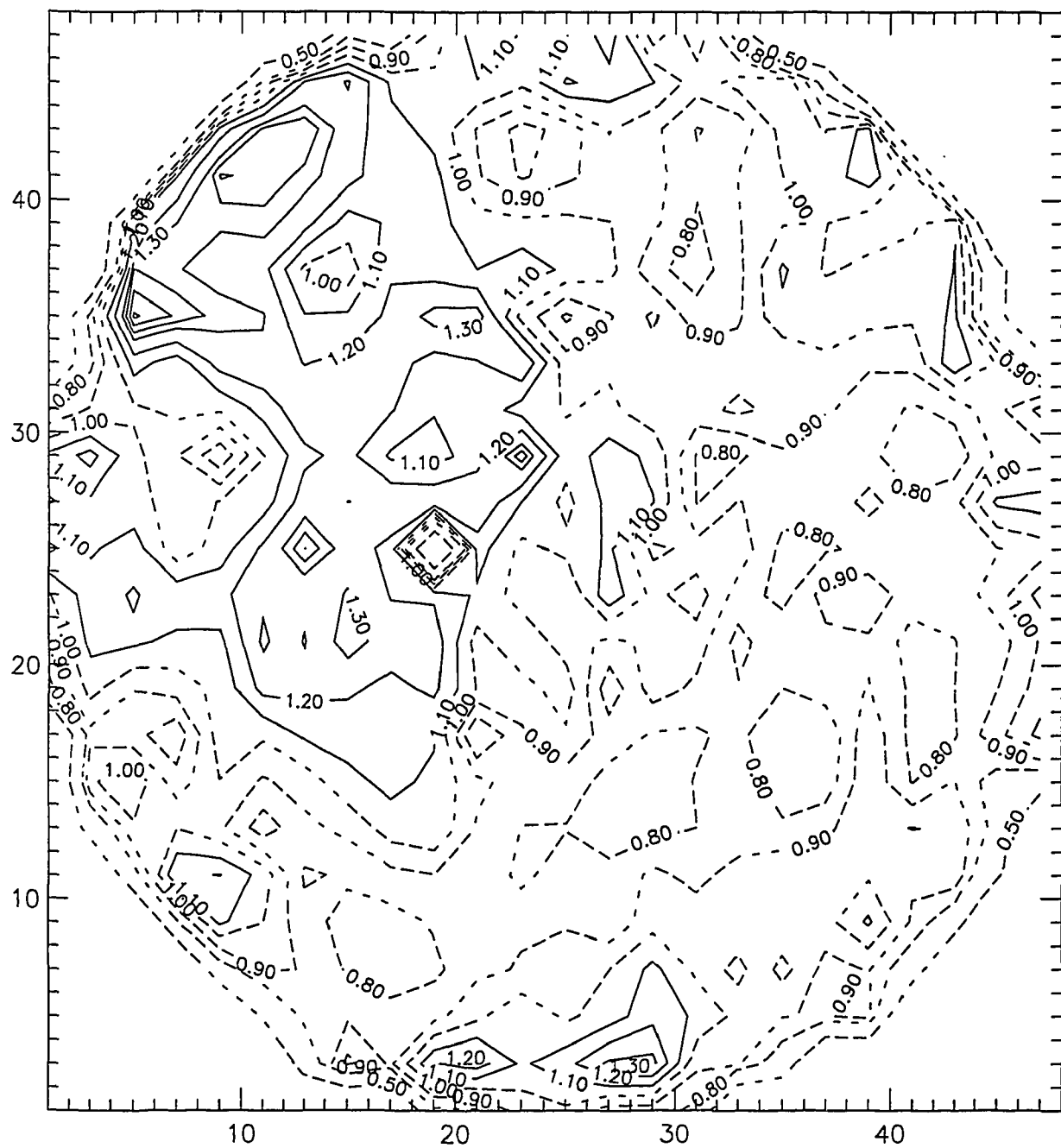


Fig. 21 Two dimensional map of ARROTTA radial power distribution of SMOLENSK-3 (Dec. 28, 1993)

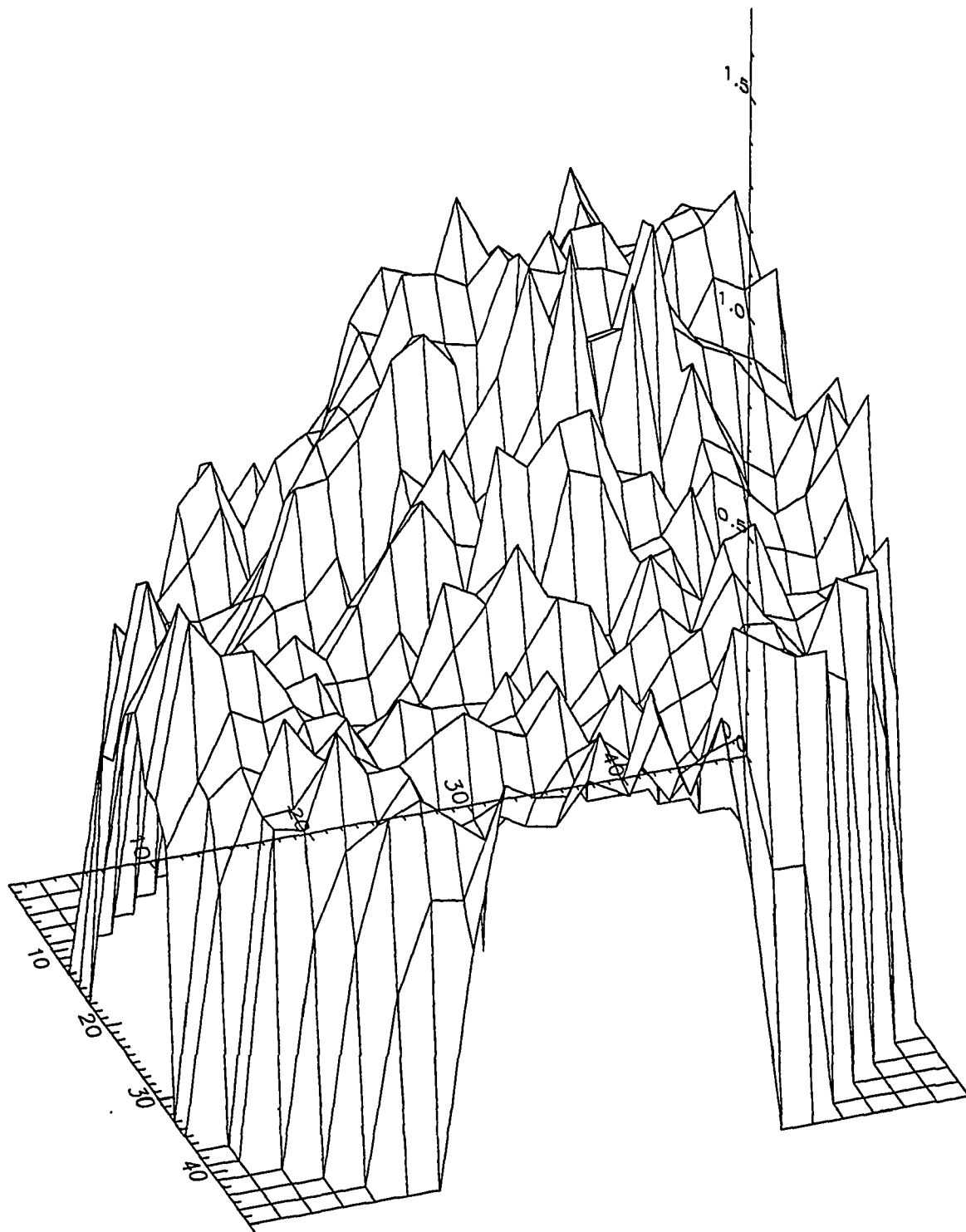


Fig. 22 STEPAN radial power distribution of SMOLENSK-3 (Dec. 28, 1993) before flux reconstruction



Fig. 23 Two dimensional map of STEPAN radial power distribution of SMOLENSK-3 (Dec. 28, 1993) before flux reconstruction

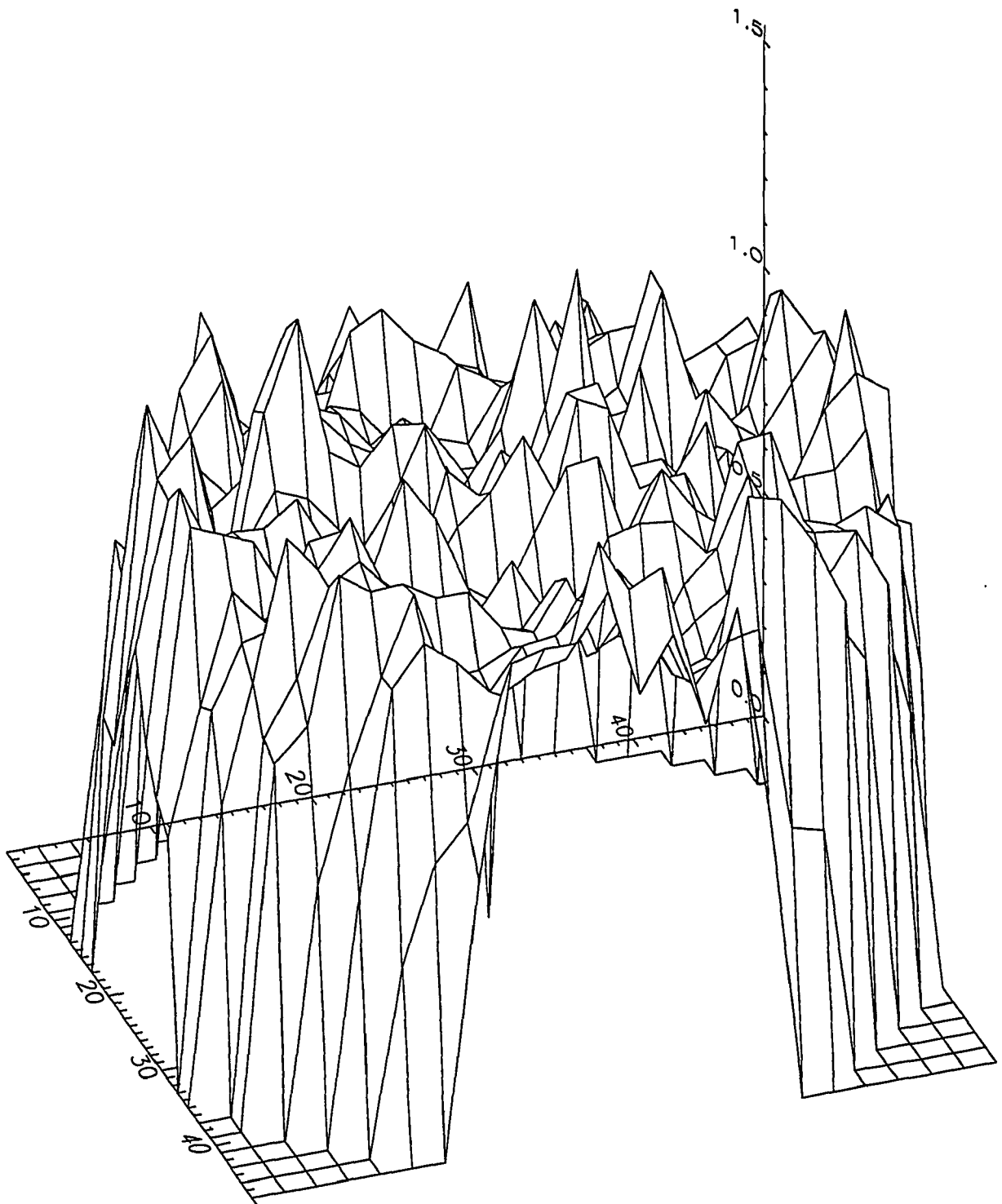


Fig. 24 STEPAN radial power distribution of SMOLENSK-3 (Dec. 28, 1993) after flux reconstruction

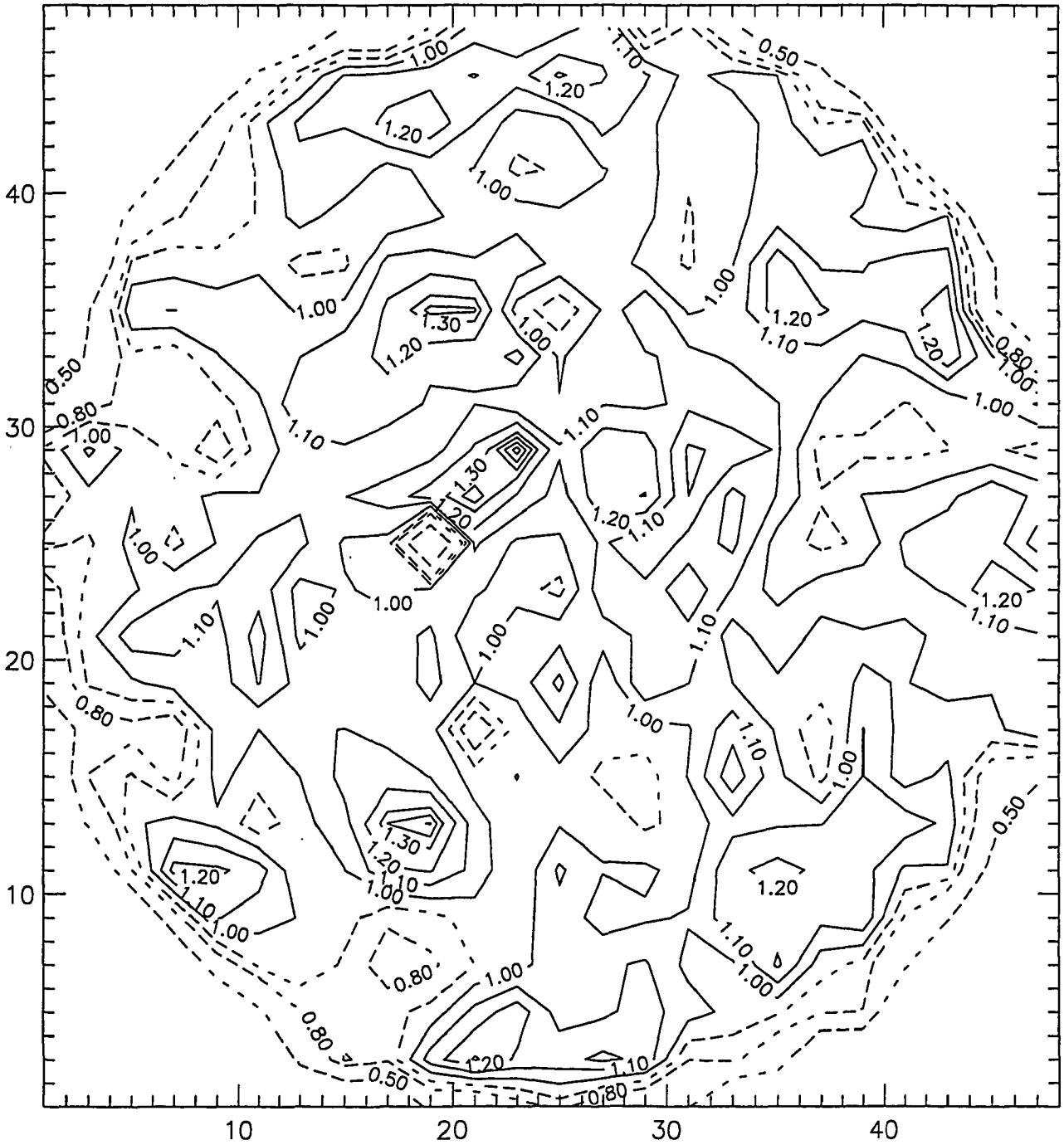


Fig. 25 Two dimensional map of STEPAN radial power distribution of SMOLENSK-3 (Dec. 28, 1993) after flux reconstruction

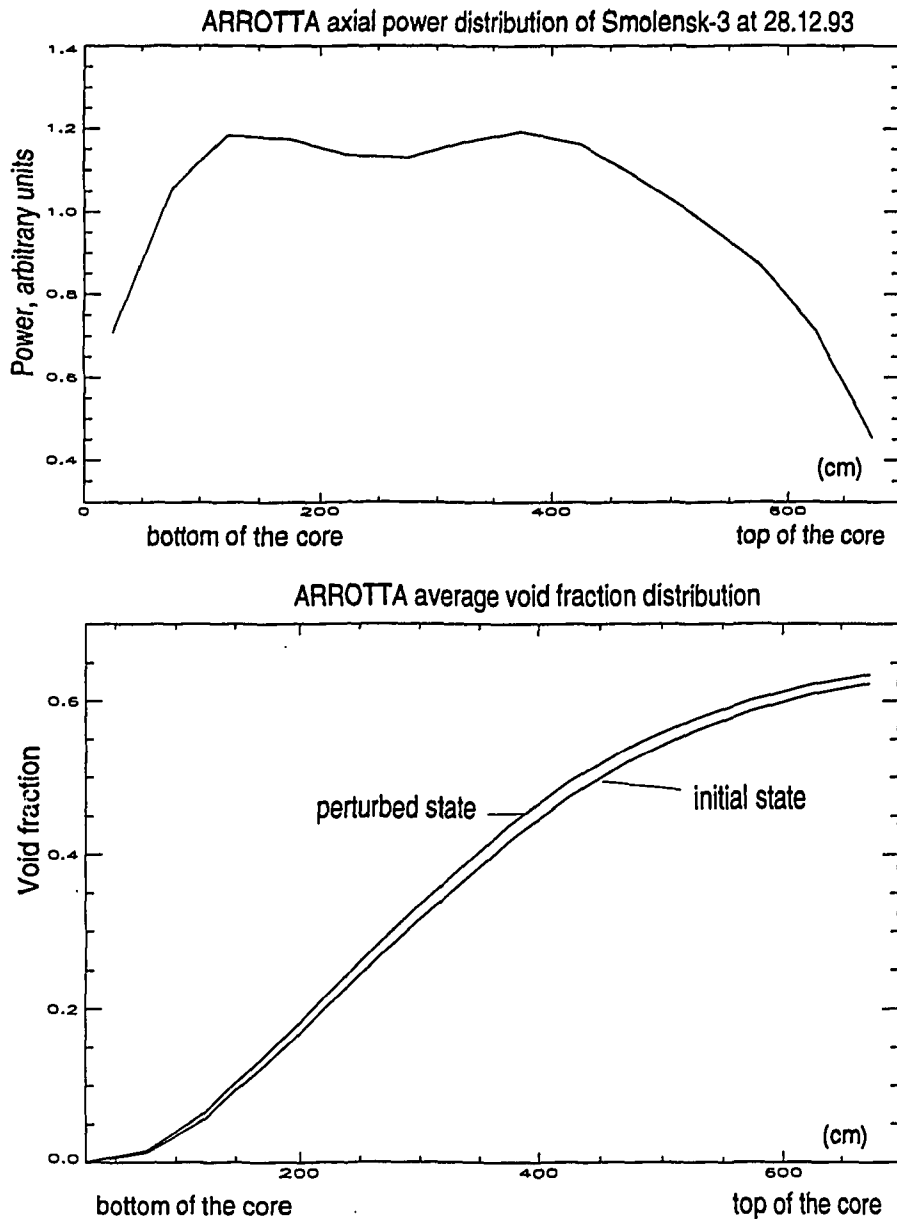


Fig. 26 ARROTTA axial power distribution and void fraction before and after perturbation of inlet coolant temperature

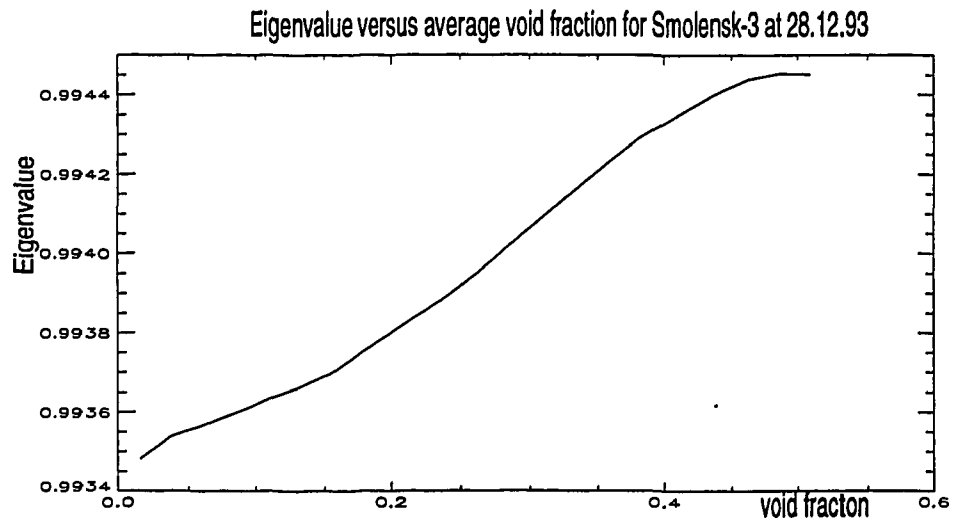


Fig. 27 Void reactivity function, eigenvalue vs. average core void fraction

4.4 Status of ARROTTA adaptation for RBMK analyses

During the project work ARROTTA has to be adapted for the application of the code to RBMK steady state and transient analyses. The major modifications performed include models for individual movements of the RBMK control rods and the calculation of the steady state and transient graphite temperatures.

The present version of ARROTTA is using the library of the Kurchatov Institut and TRECON which provides the interface between ARROTTA and this library. Further modifications are required to eliminate the need to directly access the source deck in some applications.

The present status of the required code modifications is listed below.

Modification	Status of implementation
Time step correction for xenon transients	completed
Control rod movement option for RBMK	completed
Graphite temperature steady state	not working
Graphite temperature transient	not available
Freeze option for xenon concentration	not completed
„Freeze all“ options to by pass thermal hydraulic calculation	available for transients
Freeze graphite temperature option	not available
Loss of water in single or groups of CPS channels	completed
Increase dimensions up to 15 MB	completed
Boron option to be passed to TRECON routine	completed
Simultaneous kinetics and xenon problem	not available
Ability to run kinetics after xenon problem	not available
Avoid „100% void problem“ by bypassing some of the thermal hydraulics	not available
Problem of flux reconstructing or ADF	not available

5. STEADY-STATE ANALYSIS OF SMOLENSK-3

In order to evaluate the SMOLENSK-3 steady state core characteristics three dimensional analyses of the following core parameters were performed:

- criticality, power density, fuel temperature, and void distribution at full power;
- void reactivity coefficient at full power;
- shutdown reactivities at hot zero power;
- shutdown reactivities at cold zero power.

The analyses primarily were done using the Russian codes SADCO and STEPAN. In some cases also ARROTTA analyses were performed.

5.1. Criticality at full power

The SCALA system data of the 28.12.93 were the input data used for the calculations and three dimensional neutronic-calculations with thermalhydraulic feedback available in SADCO and STEPAN were performed. The main reactor parameters used in the analysis are given below:

Thermal power, MW	2877
Operational reactivity margin, manual rods	45.4
Core loading:	
Number of fuel assemblies (FA) with 2.4% enrichment	1156
Number of FA with 2% enrichment	405
Average fuel burn up, MWD/kg	9.78
Average 2,4 % fuel burn up, MWD/kg	8,34
Average 2% fuel burn up, MWD/kg	13.9
Number of additional absorbers	97
Number of channels without FA	3

The core loading pattern and the radial fuel burn up distribution used are shown in Fig. 28 and 29. The axial burn up distribution is shown in Fig. 30. The first set of calculations was carried out for reactor operating conditions at 2877 MW or 90% of nominal power. The following SADCO/STEPAN results were obtained:

k eff	0.9982/0.9989
Maximum radial peaking factor,	1.49/1.53
Maximum axial peaking factor	1.19/1.26
Average core void fraction, ϕ	0.302/0.339, 0.328 ¹²
Average coolant density, γ (g/cc)	0.508/0.513, 0.513
Average fuel temperature, K	911/963
Average graphite temperature, K	692/737
Effective fraction of the delayed neutrons, β_{eff}	0.0058/0.0059
Void reactivity coefficient, (β_{eff})	0.2 \pm 0.1/0.47

¹ STEPAN results were obtained for left and right half of the core

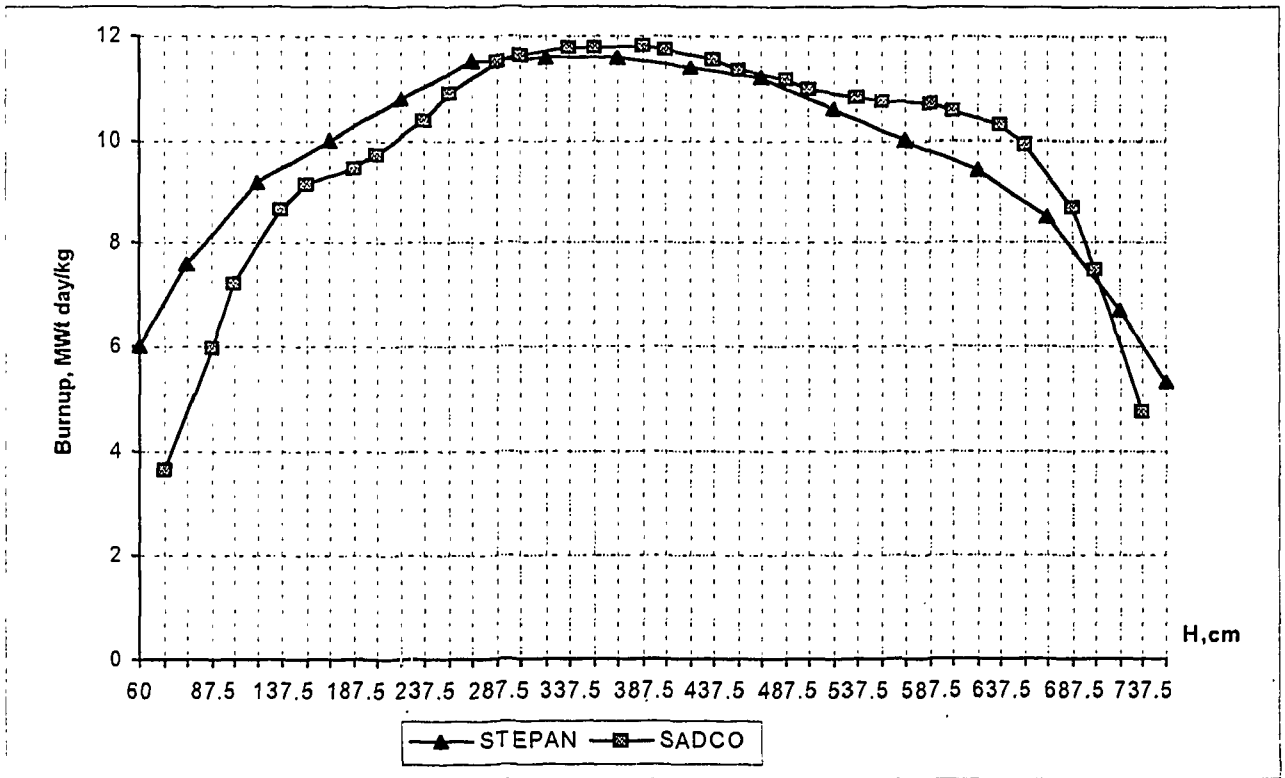


Fig. 30 Average axial burn up distribution (bottom of the core at 7 m)

5.2 Fuel temperature, void and power distribution at full power

A two dimensional map of the average fuel channel powers is shown in Fig. 31. The average axial power distribution calculated by ARROTTA and STEPAN is shown in Fig. 32. The axial distribution of power density, water density, fuel temperature, and graphite temperature for some selected channels is shown in Fig 33 - 48.

5.3 Void reactivity at full power

The calculated value of the void reactivity which is defined as the reactivity change caused by voiding the main circulation circuit from full power void conditions to zero void is $\Delta\rho_{mcc} = 0.13/0.60 \beta_{eff}$.

CONCLUSIONS

The agreement between k_{eff} predictions made by SADCO and STEPAN is in the range of 0.5% with some exceptions where the discrepancies are in the order of 1%. For the time being such agreement may be considered as satisfactory. The differences of the axial power distributions calculated by the two codes and presented for 4 fuel channels are explained by the different axial burn up profiles used in the two analyses (Fig. 30; 33-36) This is also the cause for the differences of the axial distributions of both water density and fuel temperature (Fig. 37-40; 41-44). The discrepancy of the graphite temperatures calculated by STEPAN and SADCO needs an additional investigation. Both codes use simplified models for the calculations of graphite temperatures and use different distributions for the heat sources involved.

A comparison of the radial power distributions calculated by SADCO and STEPAN was conducted. The fields were reconstructed according to the readings of the in core sensors. For this reconstruction 130 channels were chosen. These channels don't coincide with the channels of the regular radial detectors. 102 channels are in the central region of the core, 28 channels are located on the periphery including two border rows of channels. The average deviation between the calculational results and the instrumentation readings is 6.6%. The standard deviation is 5.9% for the 102 channels in the central region. The maximum deviation is 17.7% in channel 54-32. Higher deviations are obtained for the peripheral regions with a standard deviation of 9.3%, and a maximum deviation of 31.3% (channel 67-46). The power of the peripheral channels is under predicted by STEPAN as compared to SADCO.

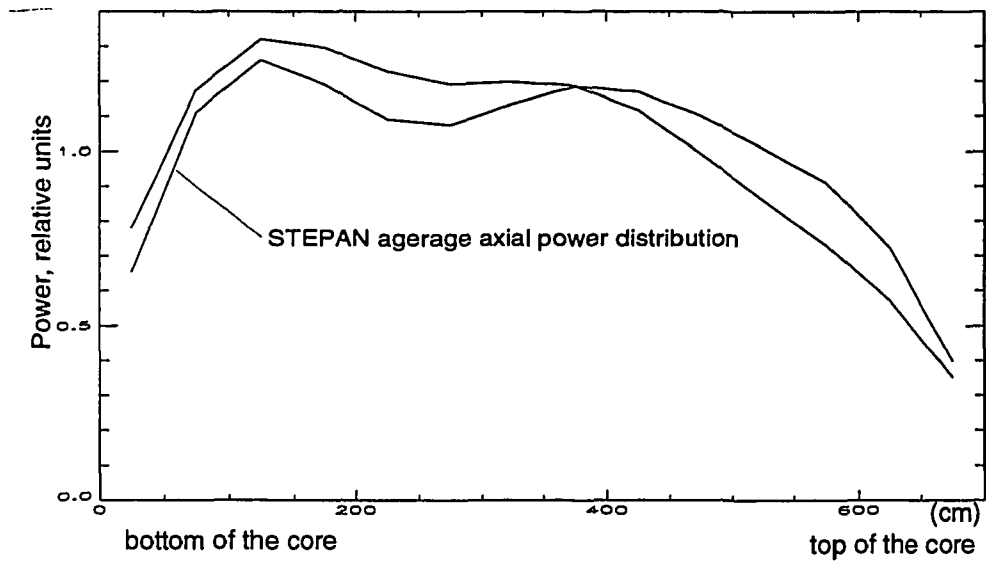


Fig. 32 Comparison of ARROTTA and STEPAN average axial power distribution of SMOLENSK-3 at full power

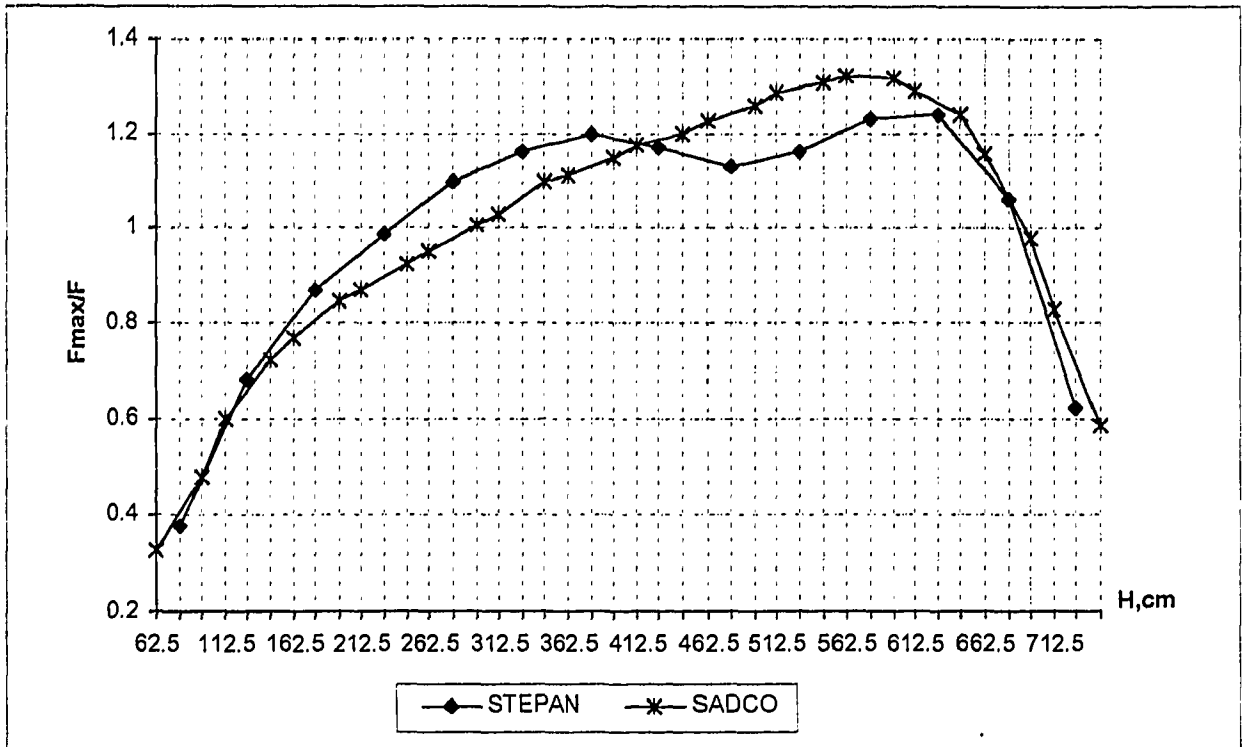


Fig. 33 Axial power distribution (core position 40-42; bottom of the core at 7 m)

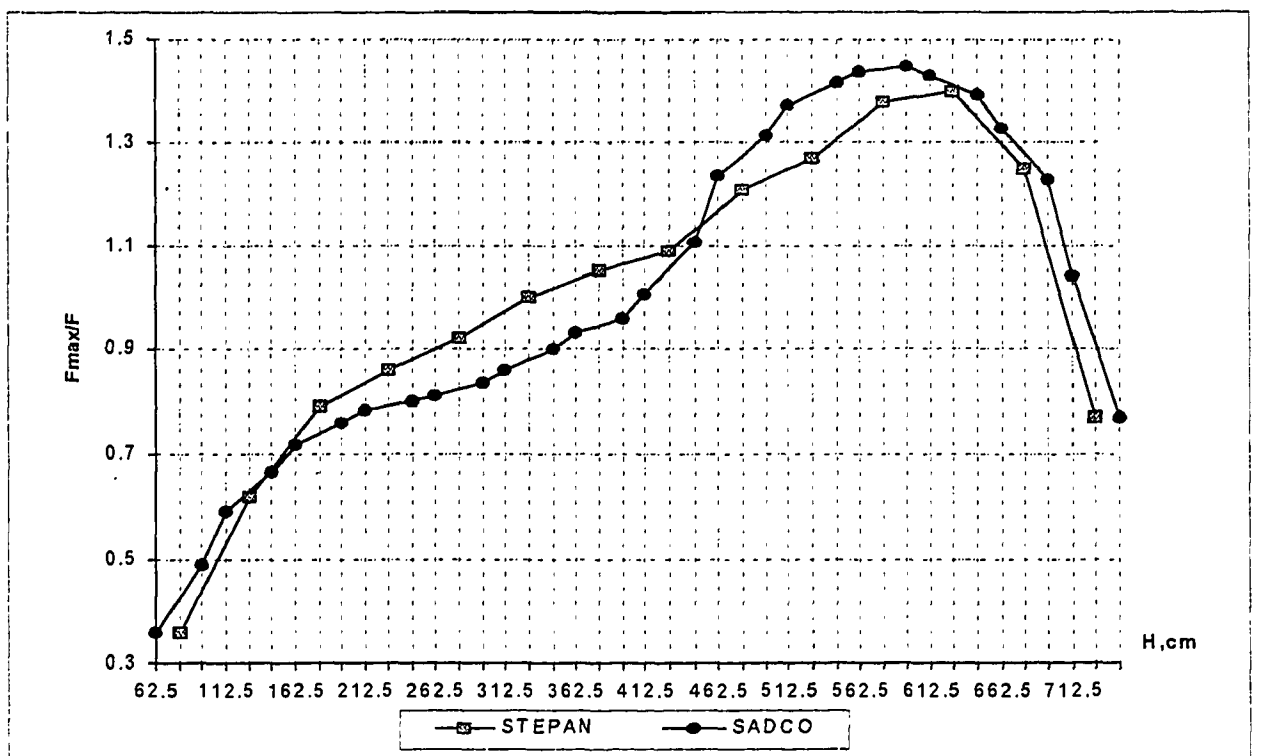


Fig. 34 Axial power distribution (core position 24-46; bottom of the core at 7 m)

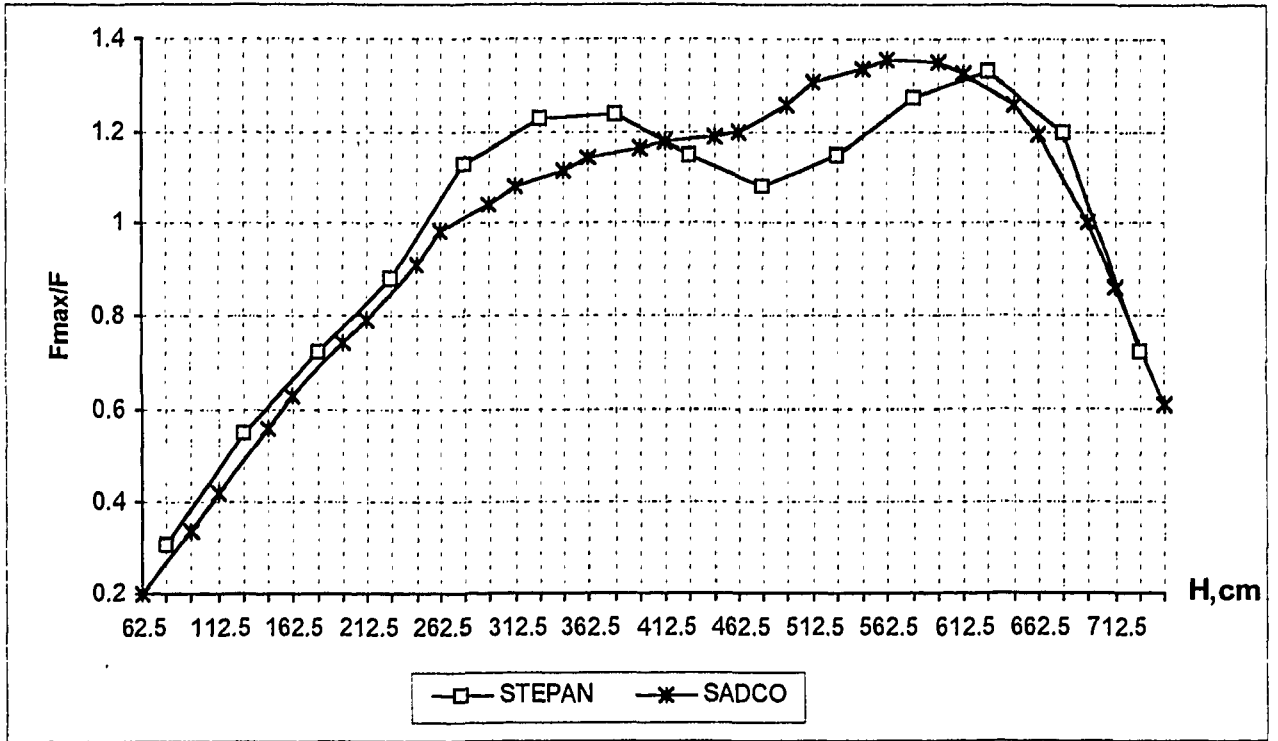


Fig. 35 Axial power distribution (core position 35-35; bottom of the core at 7 m)

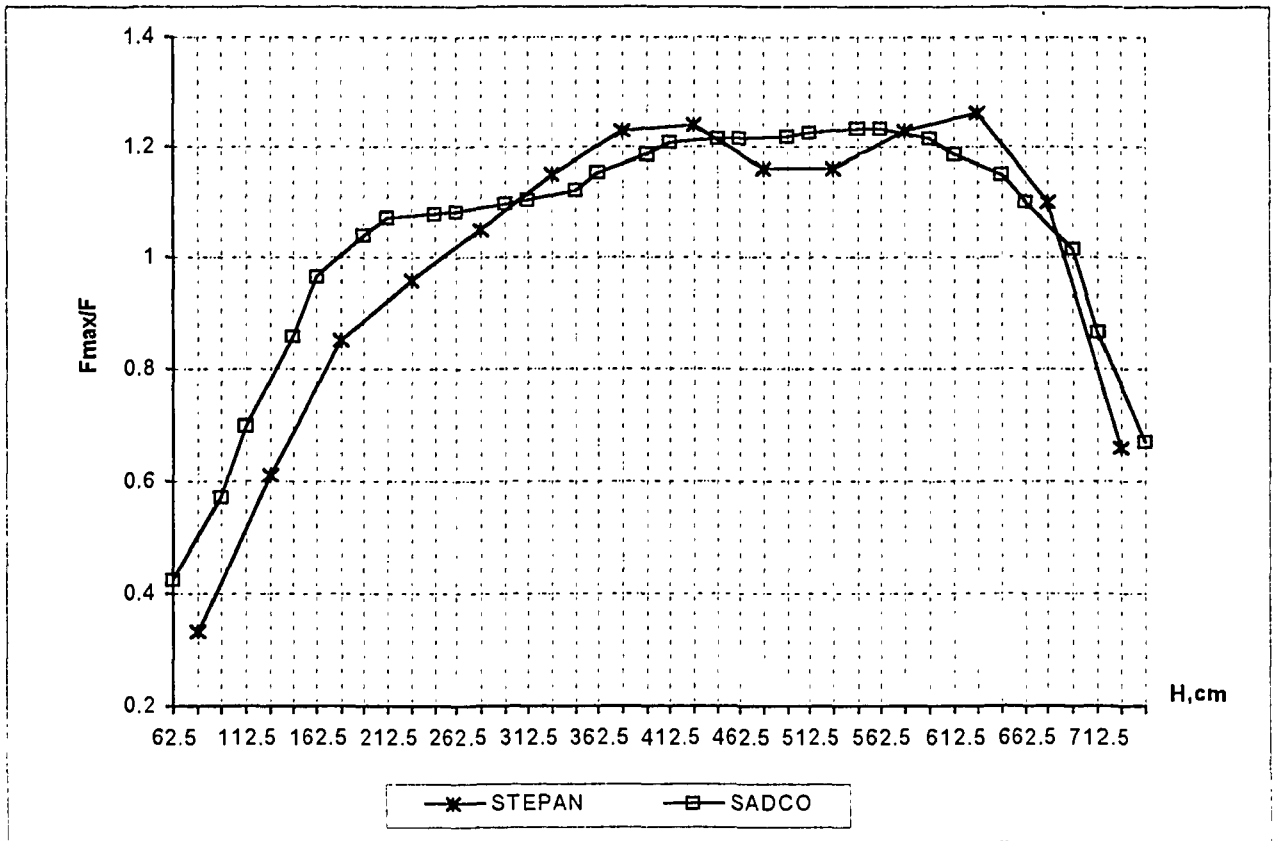


Fig. 36 Axial power distribution (core position 45-31; bottom of the core at 7 m)

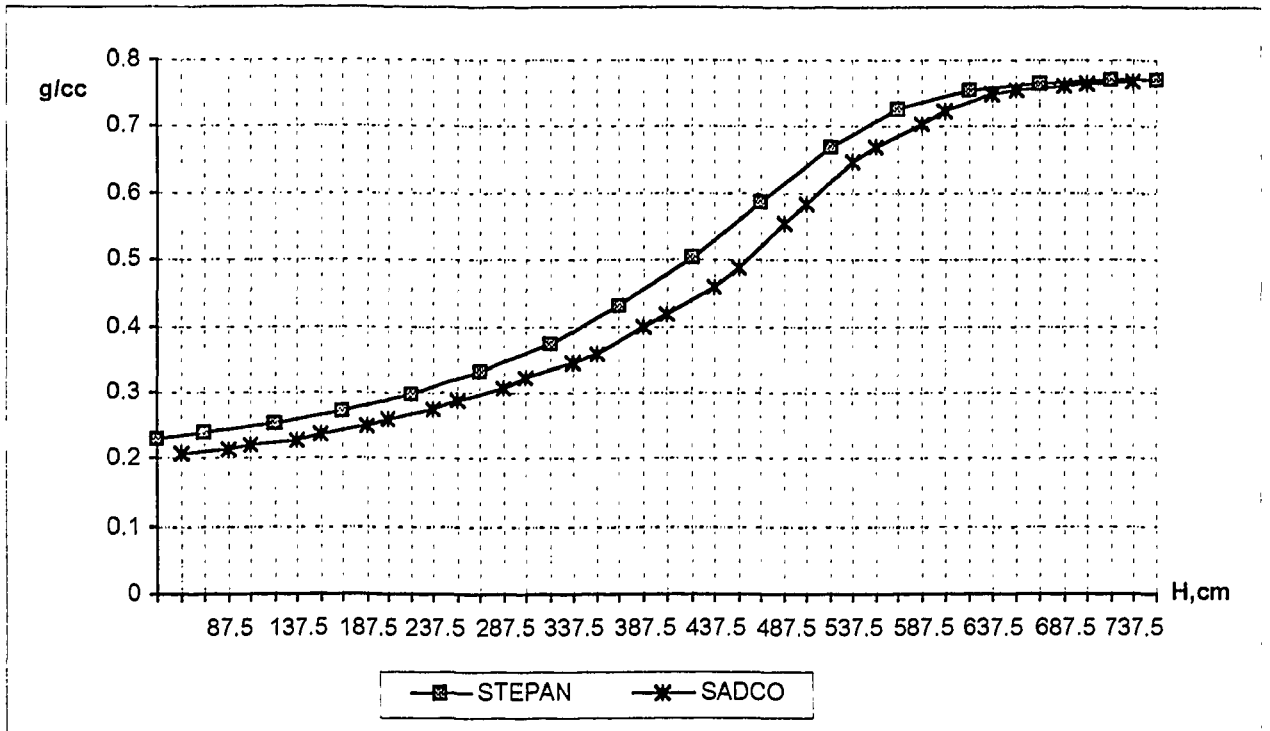


Fig. 37 Axial water density distribution (core position 40-42; bottom of the core at 7 m)

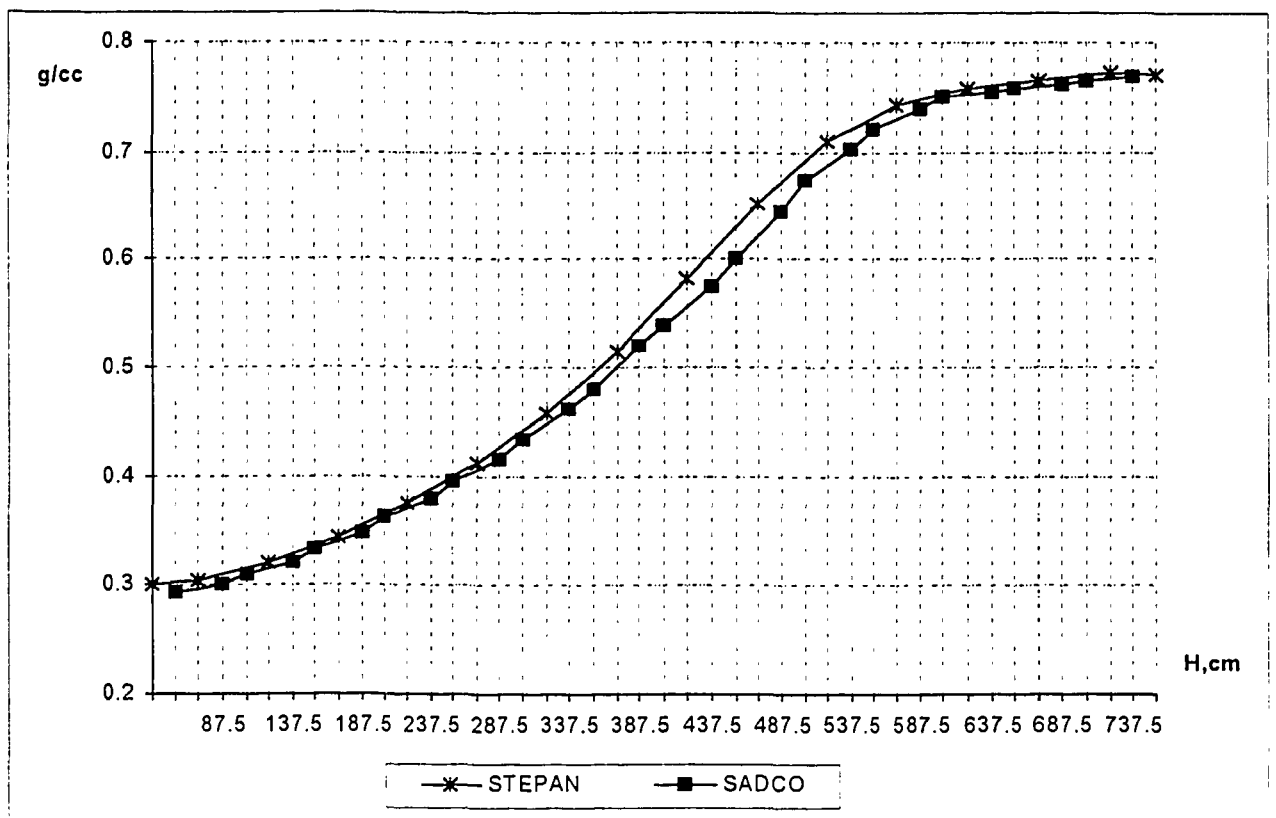


Fig. 38 Axial water density distribution (core position 24-46; bottom of the core at 7 m)

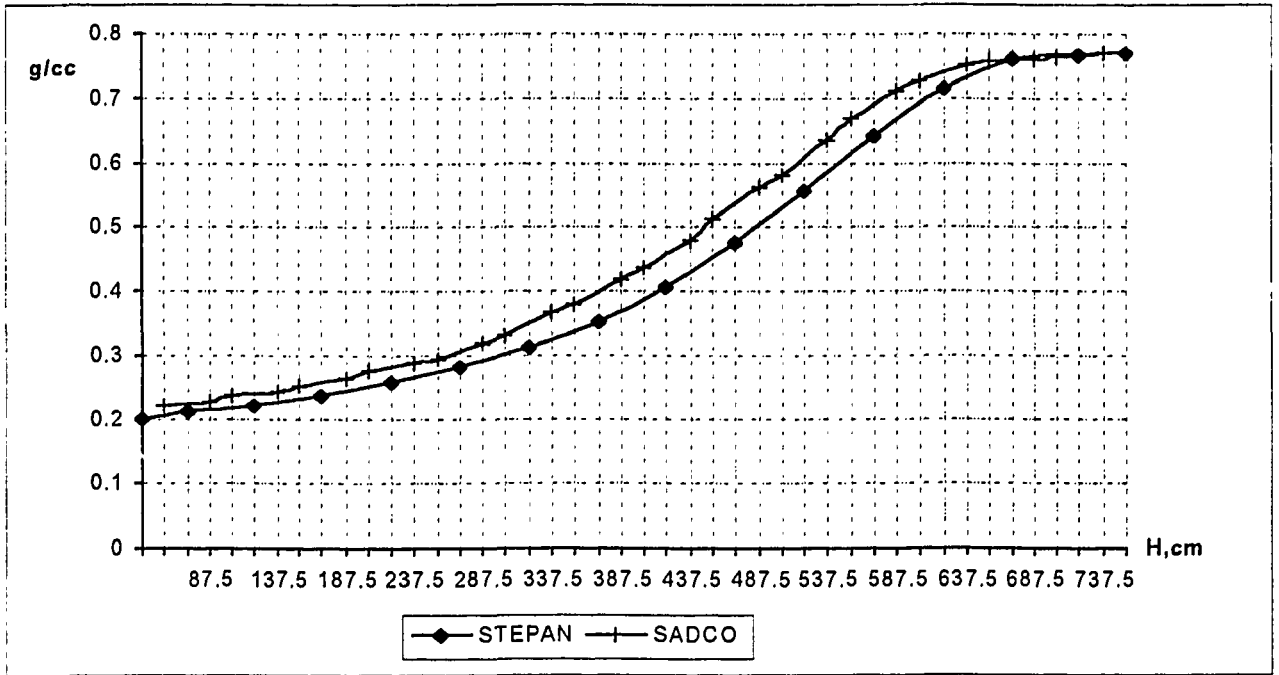


Fig. 39 Axial water density distribution (core position 35-35; (bottom of the core at 7 m)

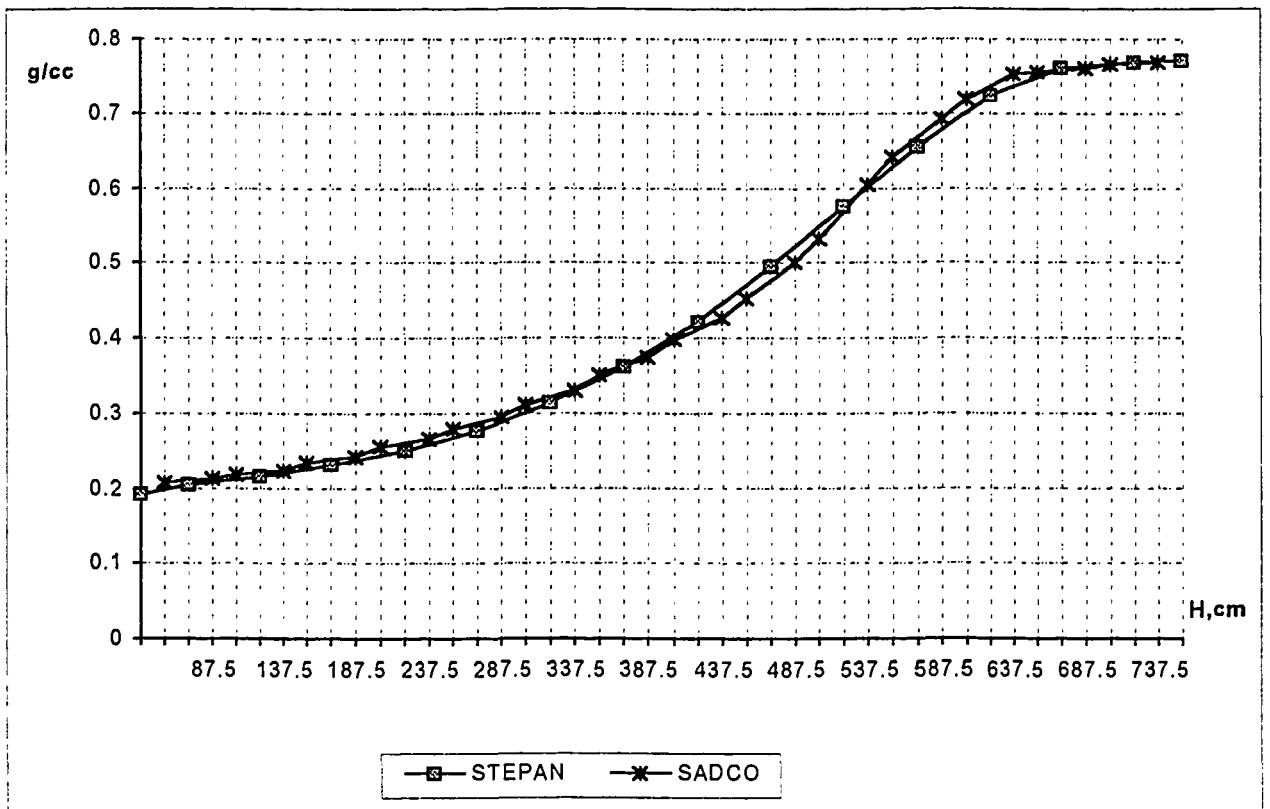


Fig. 40 Axial water density distribution (core position 45-31; bottom of the core at 7 m)

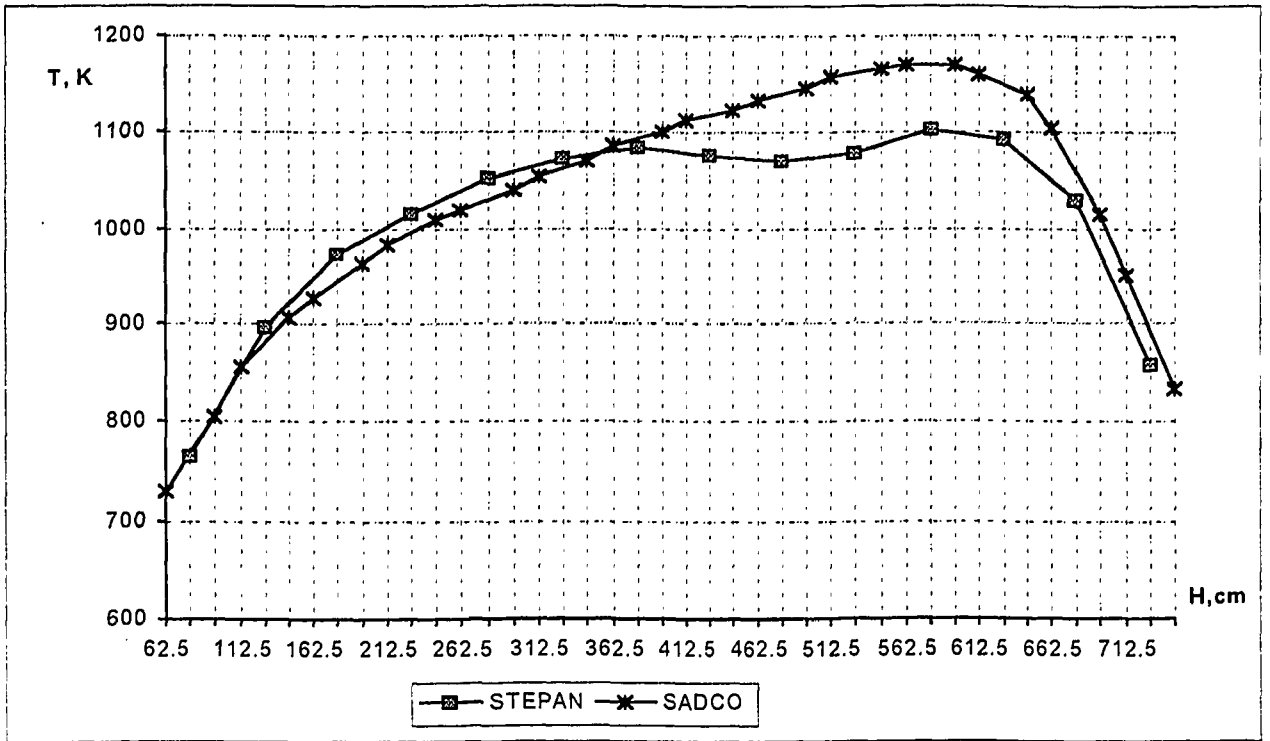


Fig. 41 Axial average fuel temperature distribution (core position 40-42; bottom of the core at 7 m)

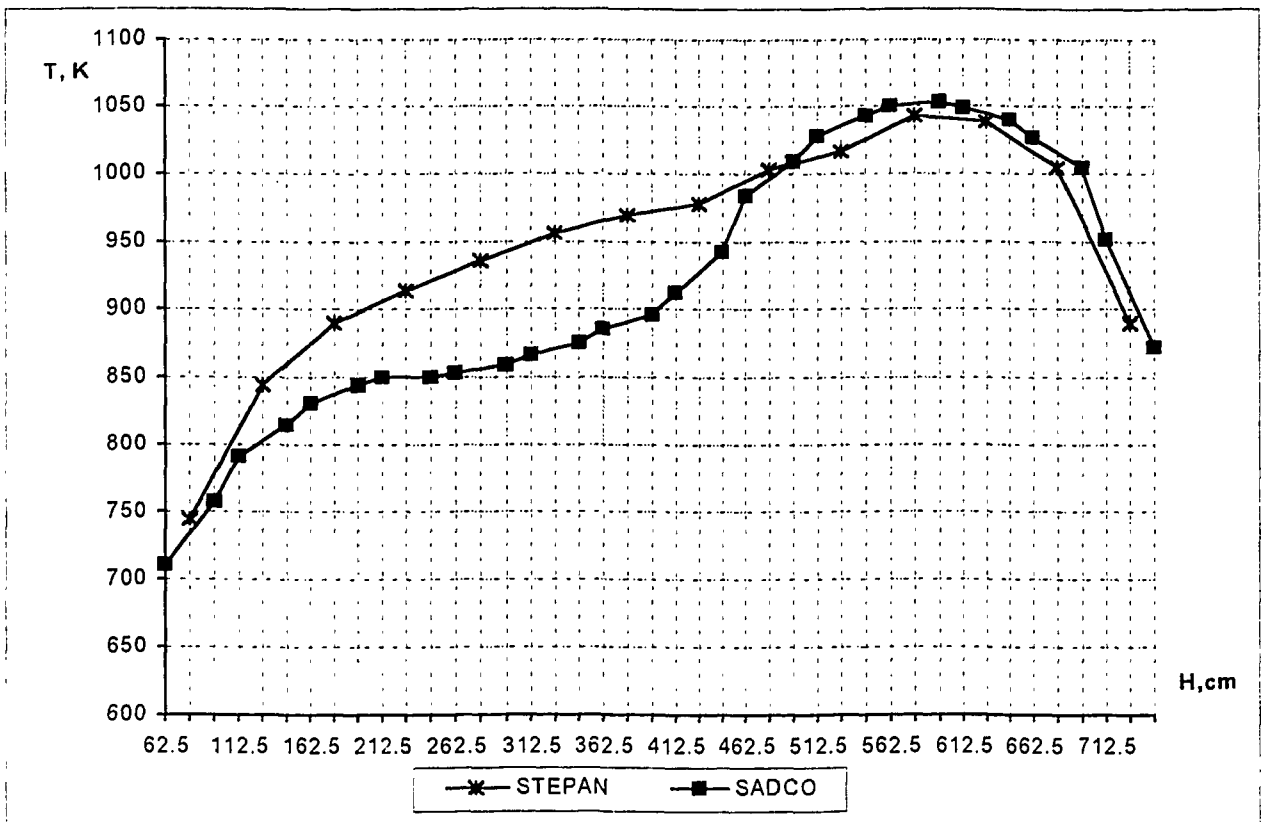


Fig. 42 Axial average fuel temperature distribution (core position 24-46; bottom of the core at 7 m)

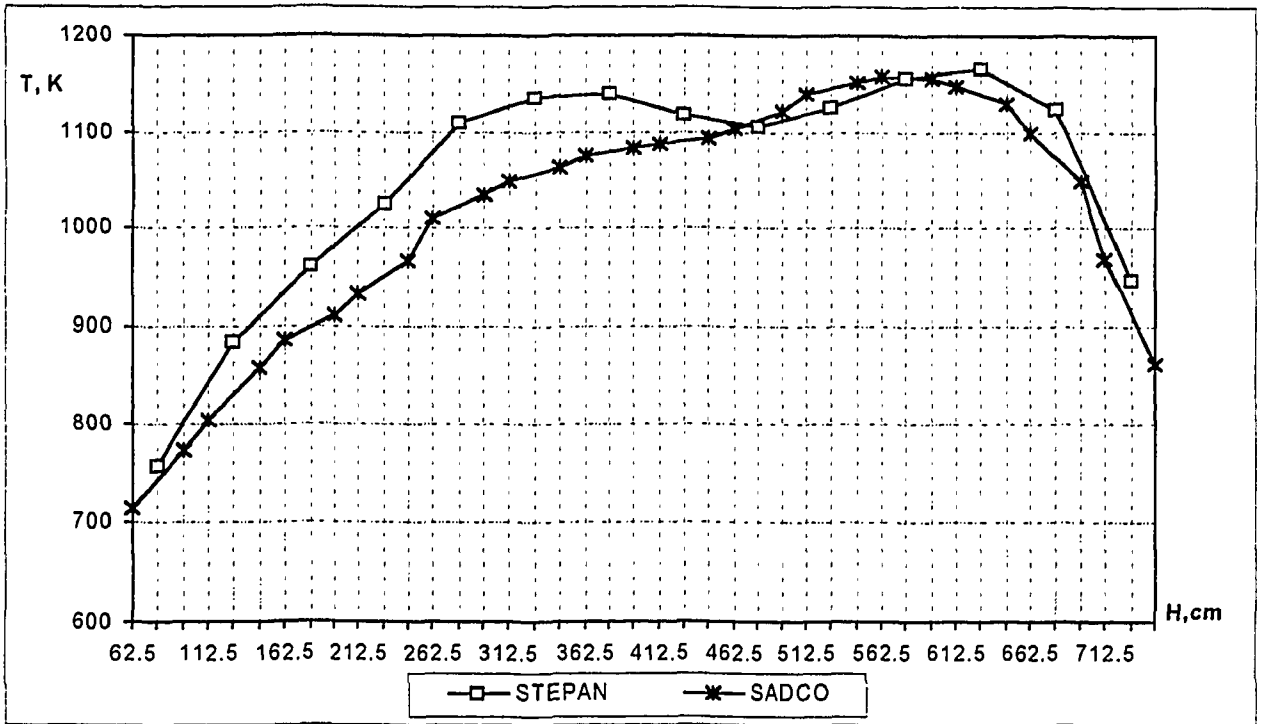


Fig. 43 Axial, average fuel temperature distribution (core position 35-35; bottom of the core at 7 m)

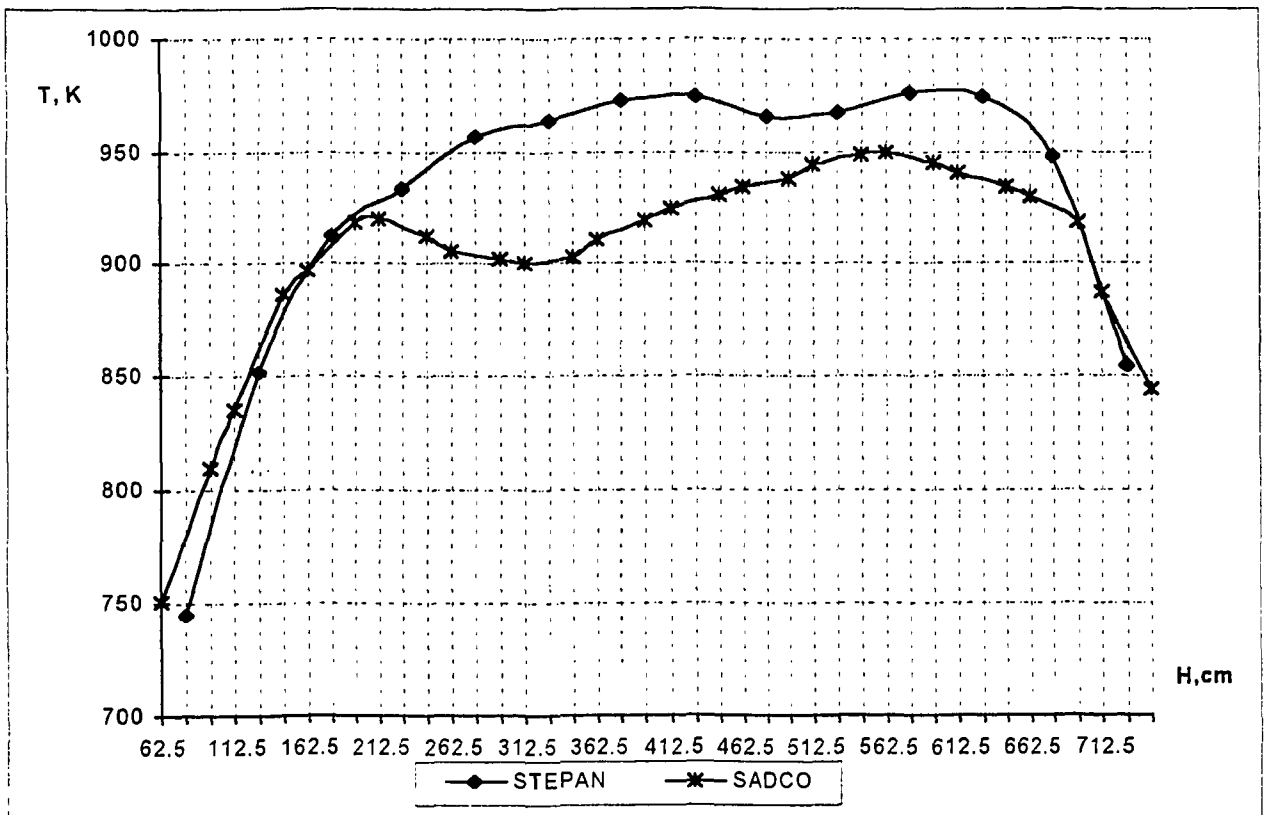


Fig. 44 Axial average fuel temperature distribution (core position 45-31; bottom of the core at 7 m)

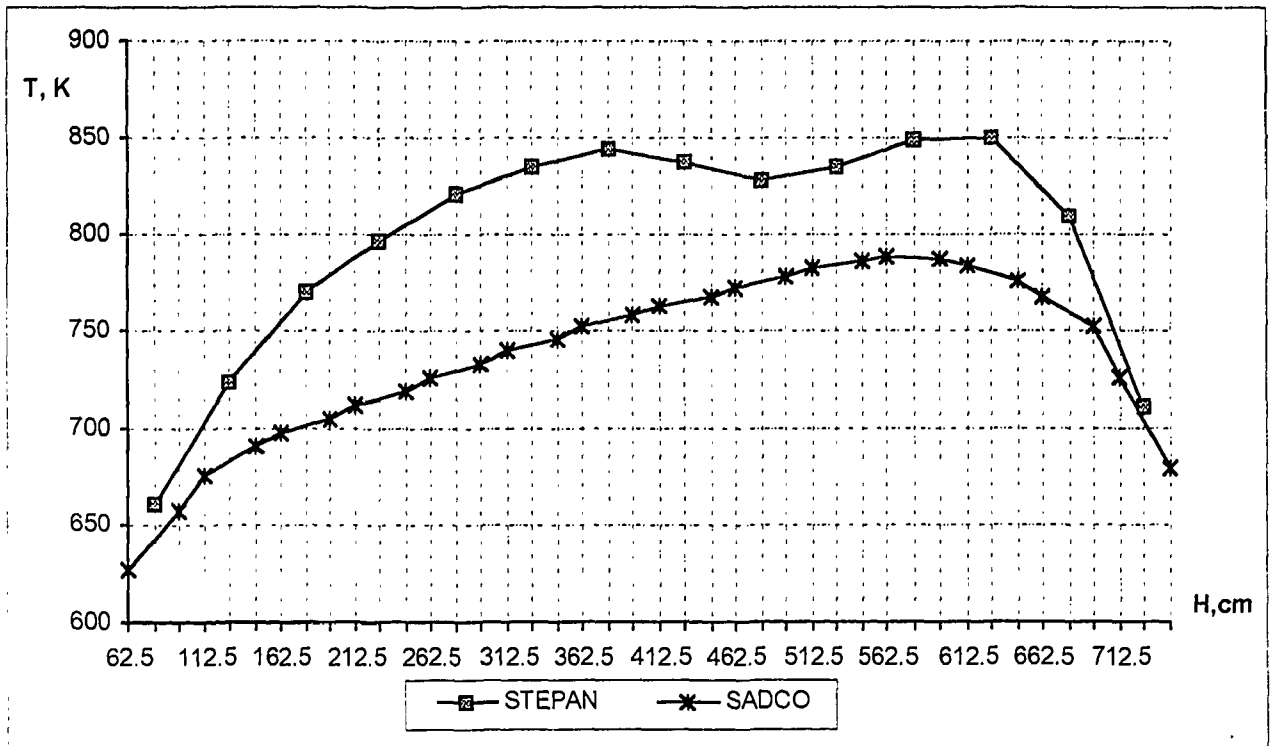


Fig. 45 Axial average graphite temp. distribution (core position 40-42; bottom of the core at 7 m)

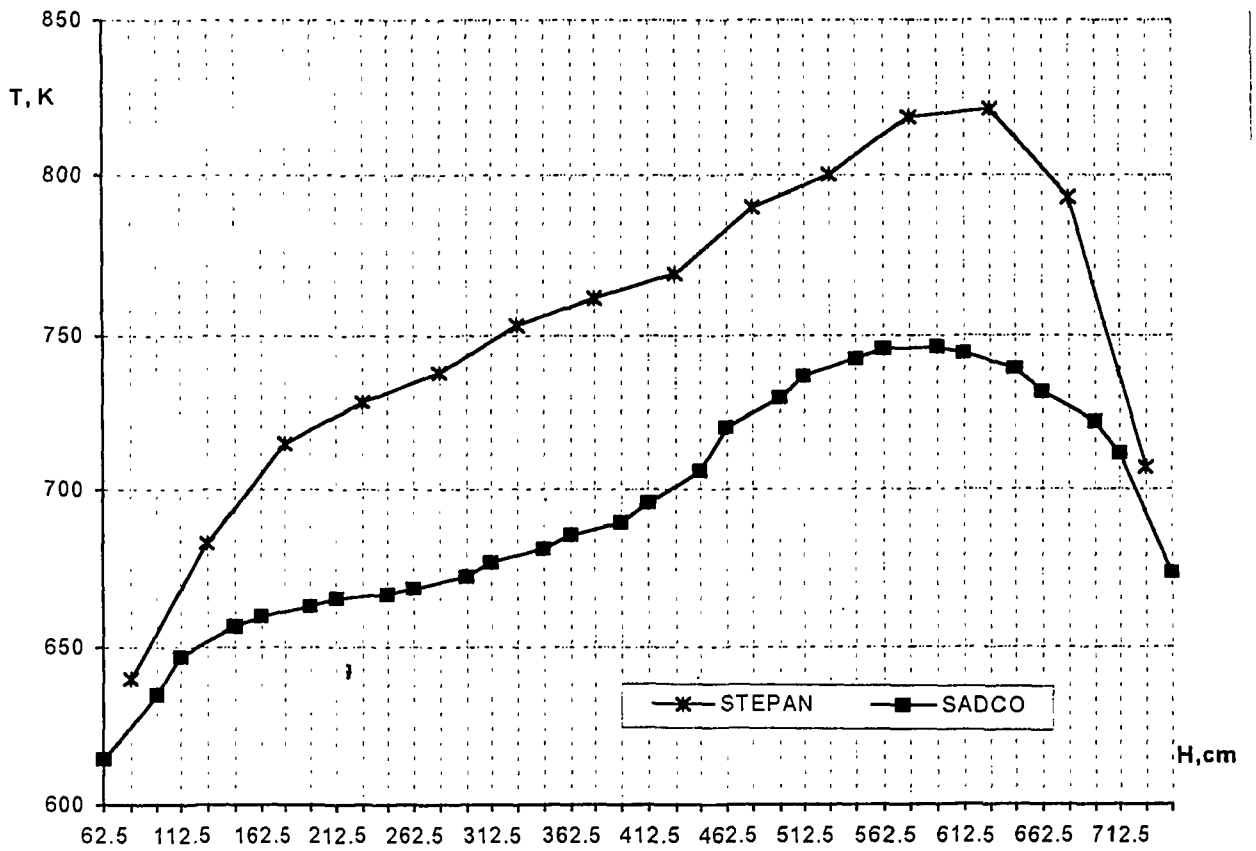


Fig. 46 Axial average graphite temp. distribution (core position 24-46; bottom of the core at 7 m)

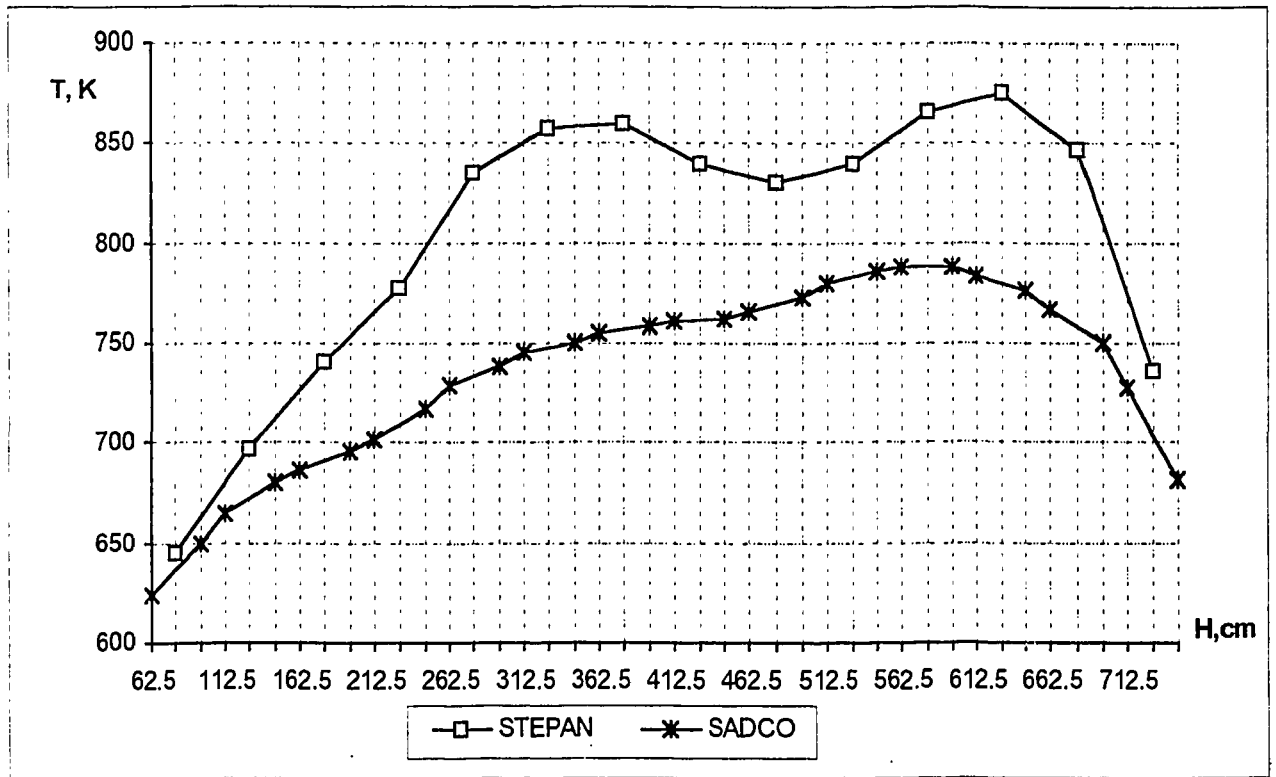


Fig. 47 Axial average graphite temp. distribution (core position 35-35; bottom of the core at 7 m)

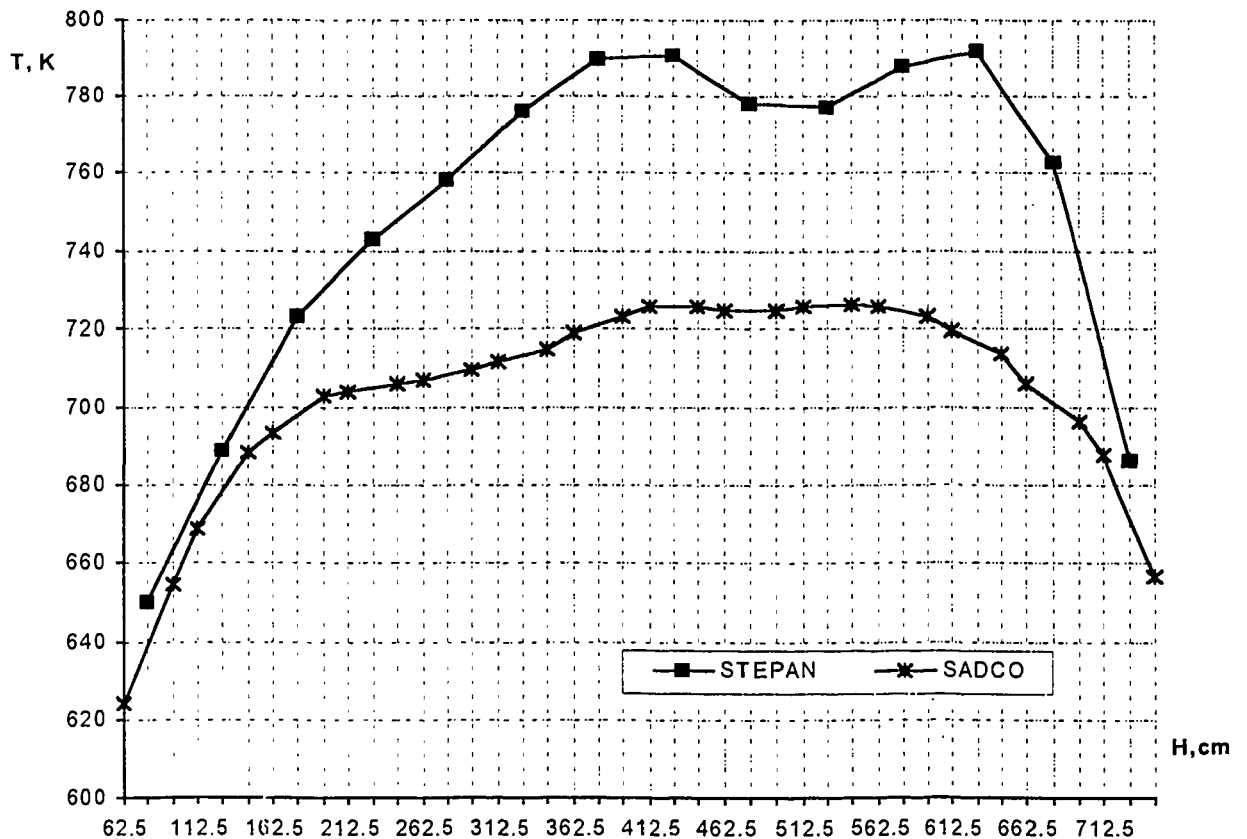


Fig. 48 Axial average graphite temp. distribution (core position 45-31; bottom of the core at 7 m)

5.4 Shutdown reactivity at hot zero power

The shutdown reactivity at hot zero power was determined for two different reactor states. In the first state fuel and graphite temperatures, coolant density, xenon poisoning, and their respective distributions were assumed to be identical with the corresponding equilibrium conditions at 90% of nominal power prevailing prior to reactor shutdown. In the second case, the more realistic situation was investigated which takes into account void collapse and the reduction of the fuel temperature shortly (usually a few seconds) after shutdown, when the graphite temperature - because of the large time constant of the graphite in the order of half an hour - did not yet significantly change. The calculations were performed in accordance with the conditions defined in Table 10. Three different modes of shutdown were considered: shutdown provided by SDS-1 plus SDS-2, shutdown provided by SDS-2 and shutdown provided by SDS-1 respectively. The analyses were performed for two voiding conditions in both, the fuel and the CPS channels. These conditions are either solid water (+) or no water (-) in the channels.

Table 10: Matrix for the analyses of the hot zero power cases

Mode of Reactor shutdown	Water in Fuel Channels	Water in CPS Channels
SDS-1 plus SDS-2	+	+
SDS-1 plus SDS-2	+	-
SDS-2	+	+
SDS-2	+	-
SDS-1	+	+
SDS-1	+	-

When only the fast system (SDS-1) is used for reactor shutdown, all the remaining other rods are assumed to stay in positions corresponding to critical operating conditions. The calculated k_{eff} values obtained by SADCO/STEPAN are shown in Tab. 11 for the first case.

Table 11: k_{eff} values for hot zero power conditions (xenon, fuel, graphite temperatures and water density at equilibrium prior to shutdown)

Water in CPS circuit	Mode of reactor shutdown		
	SDS-1 plus SDS-2	SDS-2	SDS-1
+	0.9281/0.92901	0.9437/0.94434	0.9847/0.98274
-	0.9238/0.92491	0.9404/0.94154	1.0052/1.00675

The void reactivity effect of the CPS circuit if the CPS rods are inserted is slightly negative except for the case when shutdown is provided by SDS-1 only. This case is considered a hypothetical situation by the designer since it presumes a CPS LOCA and the simultaneous failure of all the other control rods to insert when called upon. In the West regardless of its probability to fail, any fast shutdown system has to be able to shut the reactor down and maintain subcriticality from any operational occurrence and any accident to be considered [6]. The void reactivity effect of the CPS circuit exceeds the effectiveness of the SDS-1 for this assumption and the reactor is or almost is prompt critical ($0.9/1.1 \beta_{eff}$).

For the second case the calculations were performed for (full power) equilibrium xenon and graphite temperature conditions prevailing at the beginning of the cooling down process after shutdown. The fuel and coolant temperatures were assumed to be isothermal and equal to 557°K. The primary coolant density was 0.78 g/cc (solid water at saturation temperature). These

conditions correspond to the so called hot zero power standby conditions in use in western reactor design. The calculations were performed for the six reactor states described above. The calculated k_{eff} values are shown in Table 12.

Table 12: k_{eff} values for hot zero power standby conditions (Full power equilibrium xenon and graphite temperature, fuel and water temperature 557 K).

Water in CPS circuit	Mode of reactor shutdown		
	SDS-1 plus SDS-2	SDS-2	SDS-1
+	0.9445/0.9362	0.9584/0.9487	0.9912/0.9838
-	0.9407/0.9351	0.9555/0.9485	1.0130/1.0035

The reactor's subcriticality under these conditions is less than just after shutdown because of the lower fuel temperature and the larger coolant density. Both, SDS-1 plus SDS-2 and SDS-2 are able to shut the reactor down and maintain the required shutdown reactivity for the voided and unvoided CPS circuit. Since the reactivity achievable by the insertion of the SDS-1 rods only is about $+2.2/0.6 \beta_{off}$, it is obvious that in case of the voided CPS circuit the reactor cannot be shutdown by the fast acting scram system. Therefore this system does not comply with the international requirements on the basic principles for reactor shutdown systems.

5.5 Shutdown reactivity at cold zero power

The most reactive state the shutdown system has to be able to cope with is characterised by the temperatures which fuel, water and graphite assume after long term cool down and after xenon decays to zero. Consequently, the analysis was performed for the reactor at zero power in a cold unpoisoned state (zero xenon concentration) with isothermal temperatures for all core components (330/343°K). Since there is no requirement for the SDS-1 to be able to shut the reactor down and maintain subcriticality under these conditions only two modes of shutdown were analysed: shutdown by SDS-1 plus SDS-2 and shutdown by SDS-2.

Again two voiding conditions in the CPS cooling system were considered: zero void (+) or 100% void (-). The calculated k_{eff} values are shown in Table 13.

Table 13: k_{eff} values for cold zero power, zero xenon conditions, isothermal temperatures for water, fuel, and graphite (330/343 K).

Water in CPS circuit	Mode of reactor shutdown	
	SDS-1 plus SDS-2	SDS-2
+	0.9615/0.9584	0.9741/0.9701
-	0.9549/0.9557	0.9698/0.9682

The void reactivity effect of the CPS circuit in the cold unpoisoned zero power state with inserted CPS rods is slightly negative both for the inserted and the fully withdrawn SDS-1 rods. The shutdown reactivities of SDS-1 plus SDS-2 and of SDS-2 alone both meet the requirements in force in Russia asking for a 2% margin under the conditions investigated.

5.6 Maximum allowable operative reactivity margin (ORM)

The operative reactivity margin is defined as the excess reactivity of the unrodded core (all control rods fully withdrawn) and is expressed by the equivalent (fictive) number of fully inserted control rods necessary to reduce it to zero. At full power the ORM is now equal to 43-48 rods. Compared to pre Chernobyl cores it was increased to assure a less positive void reactivity coefficient in the power range RBMK are currently operated. This higher ORM leads to a reduction of the subcriticality achievable by the reactor shutdown systems. It therefore deemed necessary to determine the upper limit for the ORM (UL ORM) which would be acceptable from a shutdown reactivity point of view.

Since the investigation of this problem originally was not intended as part of this project a new task was defined to analyse this effect. A potential temporary increase of the ORM during transients (xenon burn out for example) was not included in this task but has to be given special consideration in the safety analysis for each plant. The main attention was devoted to an intentional increase of the ORM for example by a reduction of the discharge burn up of the fuel e.g. an increase of the refuelling rate. To determine the UL ORM, calculations using a special version of the STEPAN code were performed. A three dimensional supercell, comprising 12x12 core positions, was considered to adequately represent the whole core for this purpose. The investigations were covering time spans of about two years to obtain a realistic response of the core to a long term change of the ORM. On-line refuelling is modelled in this calculation. An initial steady-state reactor condition with 2.4% enriched fuel and an ORM equivalent to 45 CRs at full power was assumed. The subcriticality analysis was performed for the following reactor conditions:

- full power, all control rods fully inserted;
- zero power, all Control rods fully inserted, coolant density 0.8 g/cm³;
- zero power, all SDS-2 control rods fully inserted, coolant density 0.8 g/cm³;
- zero power, all control rods fully inserted, coolant density 0.8 g/cm³, fuel and graphite temperatures are decreased to 284 °C;
- zero power, all control rods fully inserted, coolant density 1g/cm³, fuel and graphite temperature 70 °C;
- zero power, all control rods fully inserted, coolant density 1 g/cm³, fuel and graphite temperature at 70 °C, no xenon.

There are two ways available to compensate the ORM in the reactor: One by fully inserting and two by only partly inserting the control rods.

5.6.1 Compensating the ORM by fully inserted control rods.

In order to exclude the distortions of the axial neutron field and burn up distributions due to partially inserted control rods from our considerations, firstly configurations with fully inserted rods only were analysed. Configurations involving partly inserted rods will be discussed later. Two options to increase the ORM were investigated as shown in Table 14 and Table 15 respectively:

- the number of additional absorbers (AA) is kept constant (1). The ORM is increased by an increase of the refuelling rate;
- the number of AA is decreasing in time to keep void reactivity and burn up at the initial level (2).

According to the results of Table 14 the change of subcriticality due to an increase of the ORM may be expressed as $\delta\rho_s/\delta\rho_{ORM} = -0.5\%/10CR$. The typical average value of the cold zero power shutdown reactivity for the second generation units presently is about 3%. According to the regulatory requirements the shutdown margin under these conditions must not be less than 2% corresponding to an ORM of 63-68 CR. If the ORM is increased by a reduction of the number of the additional absorbers in the core, the value $\delta\rho_s/\delta\rho_{ORM} = -0.3\%/10CR$. This smaller value is explained by the change of the reactivity effect due to the unloading of the additional absorbers (AA).

Table 14: Shutdown reactivities at different reactor states. Number of additional absorbers NAA=78.

Reactor state	ORM=45	ORM=75	ORM=105
All control rods are inserted (ARI)	7.6	6.3	5.2
ARI, zero power, no boiling (water density $\gamma = 0.8 \text{ g/cm}^3$)	5.9	4.6	3.4
The same as (2) but FASS rods are withdrawn	4.1	2.8	1.6
ARI, hot zero power (core temperature 284°C)	5.4	4.2	2.8
ARI, cold zero power (core temperature 70°C, water density $\gamma = 1.0 \text{ g/cm}^3$)	5.3	3.8	2.5
ARI, cold zero power, no xenon	2.9	1.4	-0.2

In Table 15 the shutdown reactivities are given for the same reactor states but for different numbers of additional absorbers.

Table 15: Shutdown reactivities for different reactor states and various initial ORMs. Number of additional absorbers parameter.

Reactor state	ORM=45 NAA=78	ORM=75 NAA=39	ORM=105 NAA=0
All control rods are inserted (ARI)	7.6	6.3	5.1
ARI, zero power, water density $\gamma = 0.8 \text{ g/cm}^3$	5.9	4.9	3.8
The same as (2) but FASS rods are withdrawn	4.1	3.0	1.8
ARI, hot zero power, isothermal core temperature 284°C	5.4	4.3	3.2
ARI, cold zero power, core temperature 70°C, water density $\gamma = 1.0 \text{ g/cm}^3$	5.3	4.2	3.4
ARI, cold zero power, no xenon	2.9	2.0	0.9

The safety related neutron characteristics for various values of the ORM are presented in Table 16.

α_ϕ void reactivity coefficient

ρ_{CPS} void reactivity effect in CPS loop

ρ_i reactivity effect due to uniform core heating

The value of average burn up is also presented

Table 16: Neutron characteristics for various ORM

ORM, rods	Number of AA	Burn up Mwd/kg	α_ϕ, β	ρ_{CPS}, β	$\rho, \%$
45	78	10.6	0.81	4.0	+0.02
75	78	9.6	-0.10	3.1	+0.10
105	78	8.6	-1.00	2.2	+0.15
75	39	11.1	0.65	3.1	-0.09
105	0	11.5	0.48	2.2	-0.35

These results give us the values of derivatives:

$$\frac{\partial \alpha_\phi}{\partial \rho_{ORM}} = -0.3\beta / 10CR$$

$$\frac{\partial \alpha_\phi}{\partial n_{AA}} = -0.19\beta / 10AA$$

$$\frac{\partial \rho_{CPS}}{\partial \rho_{ORM}} = -0.3\beta / 10CR$$

The subcriticality for the variants of reduced NAAs unloading is decreasing more slowly because of the change of reactivity effect due to core cooling. Thus the value of $\partial \rho_s / \partial \rho_{ORM} = -0.36\%/10CR$. This means the maximum allowable ORM value is 71-76 CR (for limiting subcriticality 2%).

5.6.2 Compensating the ORM by partly inserted rods.

Another, more realistic way of compensating the ORM is by means of partly inserted control rods. In order to quantify the effect on the ORM all manual control rods in the supercell, fully withdrawn in the previous analysis were now inserted 1.5 m into the core. The rest were fully inserted. Consequently the ORM increases by 30 CR to 75 CR. For comparison the standard version with an ORM of 45 CR but redistributed in the upper part of the core was also investigated. Table 17 presents the control rod configurations investigated, showing number and axial insertion of 45 rods normally distributed and redistributed in the upper core region.

Table 17: The axial distribution of ORM.

Height of core, m	The number of control rod-absorbers in polycell	
	Normal distribution	Redistribution in the upper part of core
0 (bottom)	4 (2 MCR, 2 SBR)	2 (2 SBR)
2	4 (2 MCR, 2 SBR)	2 (2 SBR)
3	3 (2 MCR, 1 SBR)	1 (1 SBR)
4	3 (2 MCR, 1 SBR)	1 (1 SBR)
5	2 (2 MCR)	0
6	4 (4 MCR)	2 (2 MCR)
7	5 (5 MCR)	12 (12 MCR)

It was considered in the calculations that the redistribution occurs instantaneously. Then the reactor continues to operate and transfers into a new steady-state with new fixed positions of CR.

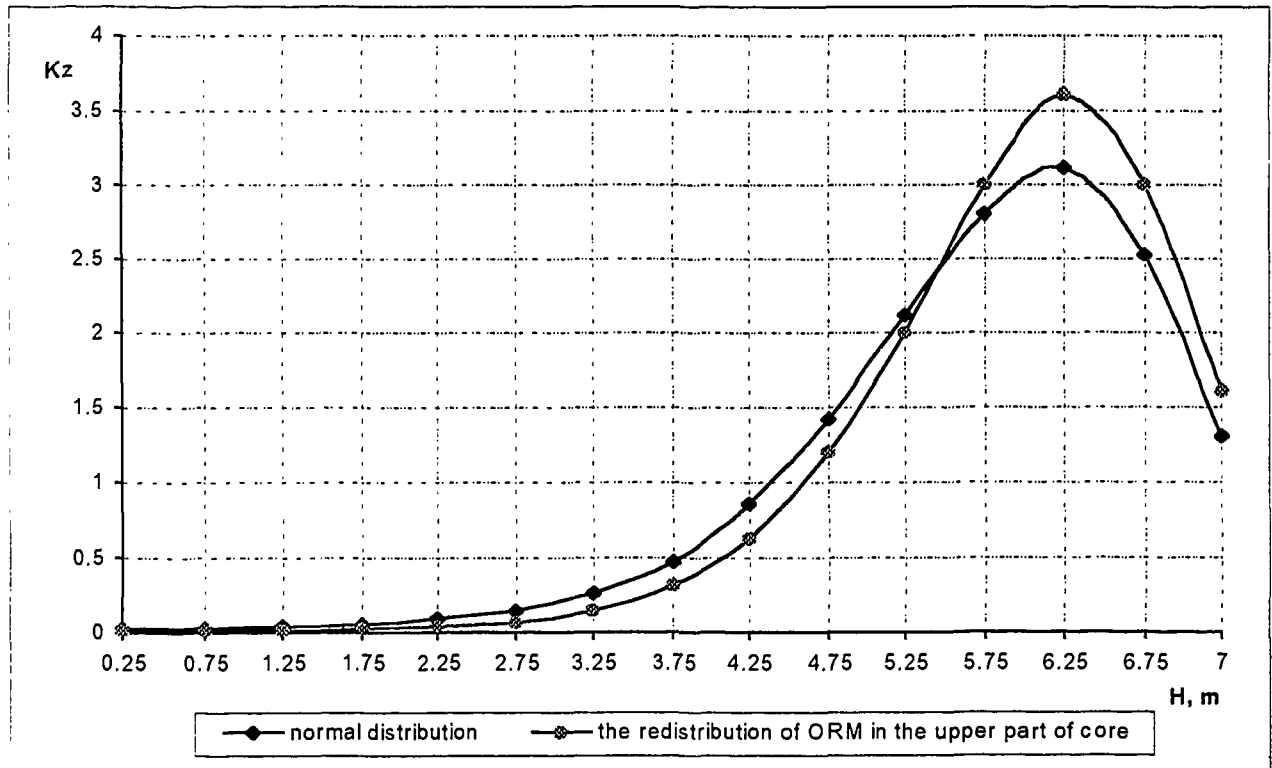


Fig. 49 Axial neutron flux distribution and local ORM distrib. (ORM=45); (top of the core at 7 m)

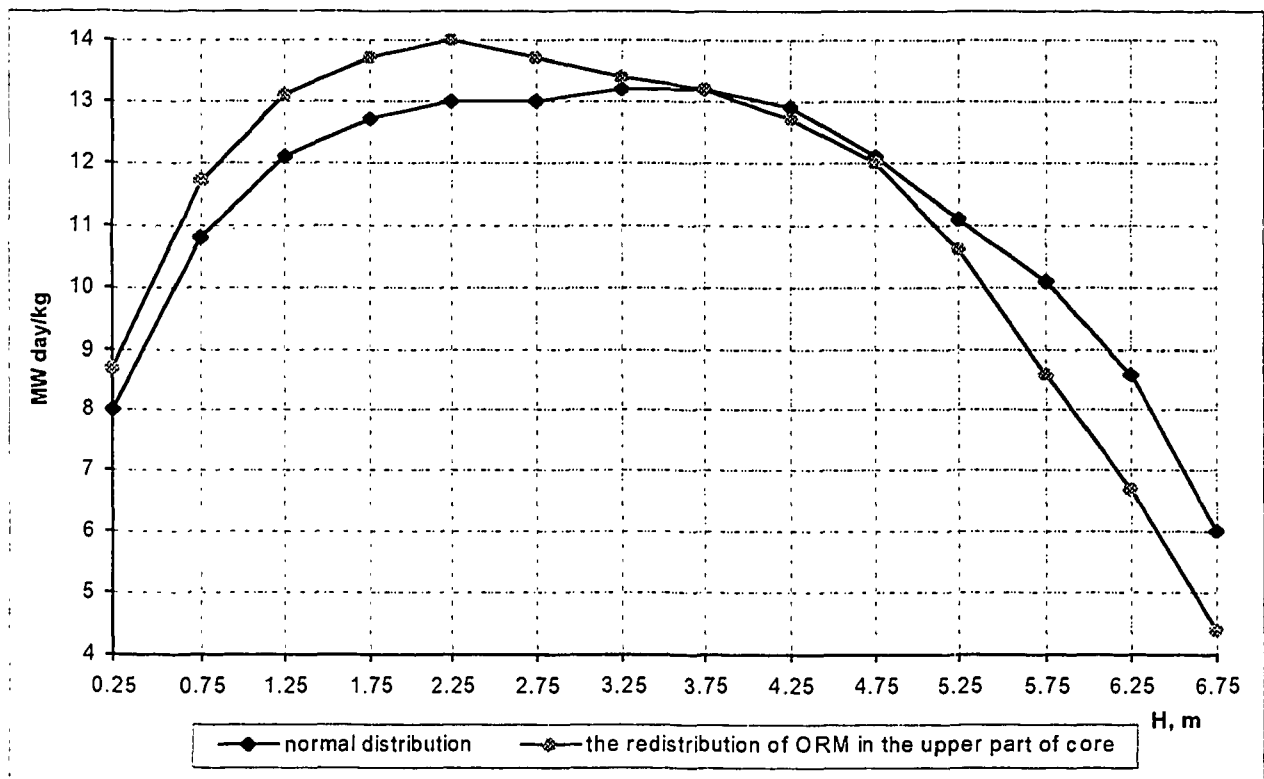


Fig. 50 Axial burn up distribution and local ORM distrib. (ORM=45); (top of the core at 7 m)

Table 18 shows the cold zero power shutdown reactivities achievable for an ORM of 45 and 75 rods respectively. The rods are redistributed as shown in Table 17. In case of an ORM of 45 CR the shutdown reactivity initially is increased as a result of the redistribution.

Table 18: Cold zero power shutdown reactivities $\Delta\rho$ for the redistributed cases versus time after control rod swamp.

Elapsed time (days)	Shutdown reactivity $\Delta\rho$ (%)	
	75 rods	45 rods
0	1.88	3.56
200	0.14	1.56
400	-0.26	1.14
600	-0.25	0.72
800	-0.27	0.66
1000	-0.25	0.68

But after about 600 full power days as a result of the axial neutron field and burn up redistribution (Fig. 49-50) the subcriticality is decreased to a level less than 1% (Table 18). The same picture of the time behaviour of subcriticality is true also for the case of an ORM of 75 CR. But in this case in the new steady-state following the redistribution, the shutdown reactivity is negative and the reactor cannot be shutdown (note that in the Table negative shutdown reactivities are used for $\Delta\rho > 0$).

Conclusions:

- The decrease of subcriticality with an increasing ORM is about 0.5% for each 10 CR of the ORM. Hence the upper limit of the ORM for the required subcriticality of 2% is 63-68 CR and for a subcriticality of 1% is-83-88 CR.
- These limits are valid for the reactors of the second generation and they are optimistic. If we take into account the possible ORM redistribution in the axial direction during an increase of the ORM then the limiting values will be smaller and in the worst case the limit is close to the present ORM.
- To obtain more precise results for this limit full scale 3-D calculations with proper modelling of refuelling are required.
- In addition a set of calculations was performed using the SADCO code. To determine the maximum permissible ORM we have decreased the average fuel burn-up in the core from 9.18 Mwd/kg to 8.72 Mwd/kg to obtain a subcriticality of 1% for the cold unpoisoned state. The control rod arrangement has been optimised to provide the according nominal power distribution. With this burn up reduction the ORM increased from 45 to 80 effective control rods, and may be considered as the upper ORM limit for the SMOLENSK NPP unit-3.

6. Transient analysis of SMOLENSK -3

To assess the shutdown rate of the existing shutdown systems, three different accident scenarios were investigated:

- the LOCA of the main circulation circuit (MCC-LOCA);
- the LOCA of the CPS circuit (CPS-LOCA);
- the erroneous control rod withdrawal accident (ECRWA).

As in the steady state analysis the reactor condition prevailing on December 28,1993 was investigated. The results of the calculations performed by STEPAN + KOBRA are presented below. The full scale three dimensional model representing all the 1661 fuel channels was used. The thermohydraulic part of the code (KOBRA) describes the core with a boundary condition for the system pressure at the core outlet, and forcing functions for enthalpy and flow rate at the inlet.

The KOBRA code is based on a non-equilibrium and inhomogeneous two phase flow model. The model incorporates four basic conservation equations: conservation of mixture mass, mixture momentum, mixture energy and liquid energy. The KOBRA code uses a slip model to describe phase separation and thus void fraction. The slip ratio (the ratio of gas velocity to liquid velocity) is represented by an empirical correlation with a modification for counter current flow conditions. The fuel temperature is calculated for one average fuel pin in each assembly. Models for the local automatic control system (LAC), the local scram system (LSS), and the global protection system using excor detectors were included in the analyses.

Also the three dimensional transient code TRIADA was used for the transient analyses. This code is broadly used at RDIPE for safety analysis. It is a one energy group coarse mesh neutron diffusion code. The core is represented by polycells each comprising 4x4 core channels. The coupling of these large nodes is established by a finite difference scheme.

6.1 LOCA analysis of MCC (ultimate design base accident)

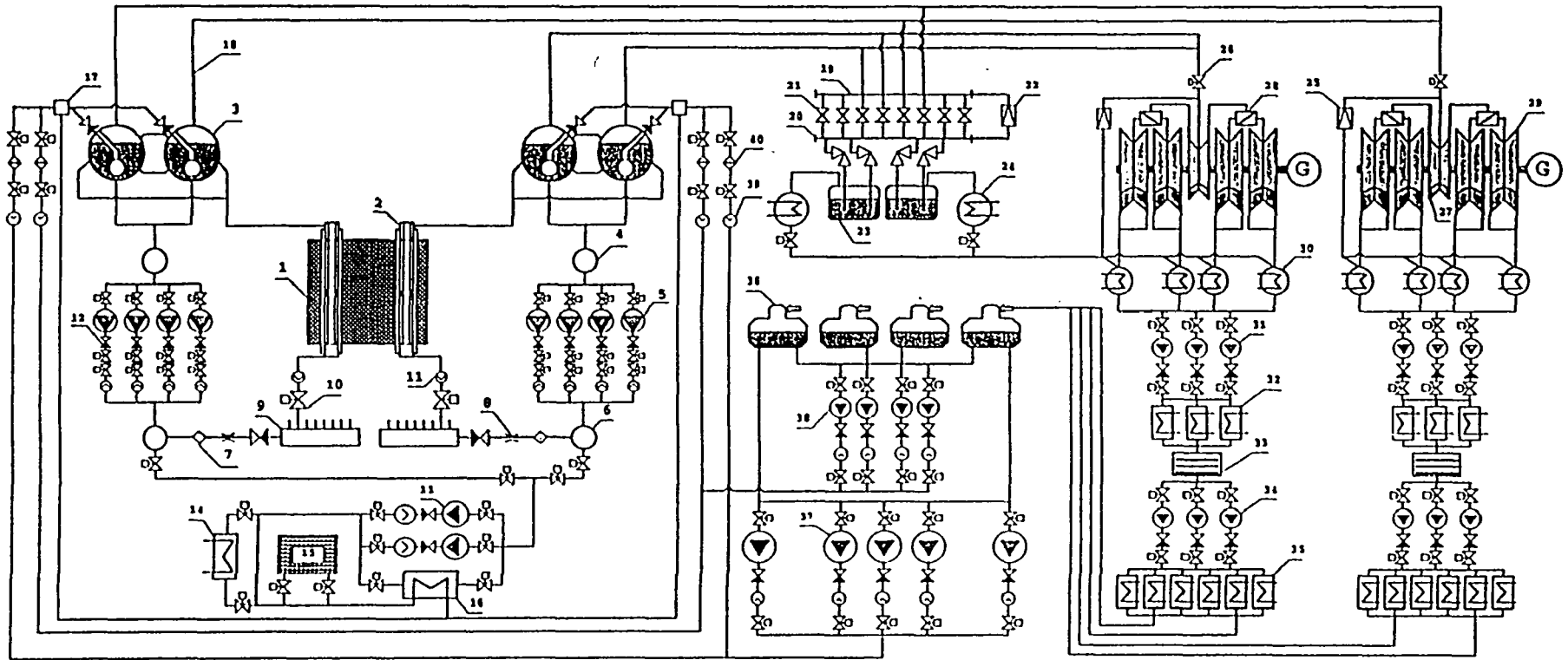
The heat transport process in SMOLENSK-3 is arranged as a direct forced circulation cycle circuit. A schematic is presented in Figure 51. The boiling light water coolant supplies steam to two turbines. There are two independent loops, one for each core half and turbine, comprising the main circulation circuit. The coolant, driven by 3 pumps (three in operation one in stand-by) in each loop is pumped to the 1661 fuel channels via a system of headers and pipelines. The water in the channels heats up to boiling and partially evaporates. The resulting steam water mixture flows from the fuel channels via steam water lines to the steam drum separators, two in each loop, where the steam is separated from the water. The saturated steam passes the steam collectors and via the steam lines is transported to the condensing turbines. The feedwater is delivered by the main feedwater pumps to the drum separators in each loop.

A guillotine type double ended break of the main pressure header, diameter 900 mm and supplying cooling water to one core half is considered the ultimate design base accident for RBMK.

The following assumptions were made in the analysis:

- nominal operating conditions;
- only two out of three trains of the ECCS are available;
- all SDS-1 and SDS-2 rods are inserted, in a second case no scram was assumed;
- control rod insertion times: 2.5 seconds for SDS-1 and 12 seconds for SDS-2 rods;
- reactor scram on pressure in leak tight compartment.

Fig. 51 Typical RBMK heat transport diagram



- | | | | | |
|---------------------------|----------------------------------|-------------------------|-------------------------------|-------------------------------|
| 1 - Reactor | 9 - Distribution header | 17 - Mixer | 25 - BRUK-valves | 33 - Condensate cleanup |
| 2 - Fuel channel | 10 - Isolation and control valve | 18 - Steam lines | 26 - Stop and control valve | 34 - 2-grade condensate pumps |
| 3 - Steam drum-separator | 11 - Flow measurement | 19 - High pressure ring | 27 - High pressure turbines | 35 - Preheaters |
| 4 - Suction header | 12 - Check valves | 20 - Low pressure ring | 28 - Reheaters | 36 - Deaerators |
| 5 - Main circulation pump | 13 - Cooldown pump | 21 - Main relief valve | 29 - Low pressure turbines | 37 - Main feedwater pump |
| 6 - Pressure header | 14 - Blowdown after-cooler | 22 - BRUB-valves | 30 - Turbine condenser | 38 - Small feedwater pump |
| 7 - Mechanical filter | 15 - Bypass cleanup | 23 - Bubbler | 31 - 1-grade condensate pumps | 39 - Flow measurement |
| 8 - Limiter | 16 - Blowdown regenerator | 24 - Heat exchanger | 32 - Preheaters | 40 - Mechanical filters |

- during the first 15 seconds only water is discharged through the break;
- film boiling from the beginning of the accident, zero heat transfer between the cladding and the steam after voiding of the fuel channels, film boiling after the initiation of the ECCS injection in the reflood phase;
- all check valves at the distribution group headers close.

Right after the break, assumed at time zero, voiding in the core half of the ruptured pressure header starts and the coolant density of this half of the reactor core rapidly - within 2 seconds - drops down to almost zero (Fig. 52). The rate of voiding is different in channels with different power (Fig. 53). The analysis was performed starting from nominal power, nominal power distribution, nominal system pressure, system flow and inlet subcooling conditions.

6.1.1 Reactor shutdown by SDS-1 plus SDS-2

The void reactivity coefficient for the initial conditions investigated (90% reactor power) is rather small. Since the rise of the reactivity due to voiding is initially also compensated by the local automatic control (LAC) system there is no neutronic signal to trigger the reactor scram. This was considered in the analysis by using the pressure increase after the break in the leak tight compartment to actuate the scram. Within 1.2 seconds after the break occurred the pressure rise in the leak-tight compartment is high enough to reach the scram set point. It was assumed that the ECCS begins to inject water into the core half involved 3.5 seconds thereafter. Reactivity and -neutron power versus time during the first 15 seconds into the transient are shown in Fig. 54 and 55. Fuel and clad temperatures in the hot channel are shown in Fig. 56 and 57.

The LOCA analysis of the MCC was also performed by TRIADA. The corresponding neutron power and reactivity behaviour are shown in Fig. 66. The value of the void reactivity coefficient α_{ϕ} is $0.25 \beta_{\text{eff}}$ the prompt power reactivity coefficient α_{ω} is $-3.0 \cdot 10^{-4} \beta_{\text{eff}}/\text{MW}$ for nominal power. These values were calculated assuming 97 additional absorbers and an ORM of 45 control rods. The predicted value of the core void reactivity effect under operating conditions $\Delta\rho_{\text{void}}$ is $0.15 \beta_{\text{eff}}$. Correspondingly voiding of one circulation loop results in a reactivity effect less than $0.1 \beta_{\text{eff}}$. A comparison of STEPAN + KOBRA and TRIADA results may be performed on the basis of Figures 54, 55 and 66.

6.1.2 No actuation of shutdown and ECCS system.

In the above analysis the assumption was made that the reactor scram would be triggered by the pressure increase in the leak tight compartment. It was already stated that this pressure increase is the first signal available, since there are no neutronic signals due to the small void reactivity coefficient. It is common practice to assume failure of the first signal in the safety analysis of nuclear power plants. Even though there is some discussion going on, on how to apply this principle to RBMK, the analysis was repeated under the assumption that the scram systems are not actuated and the reactor continues to operate at full (90%) power after the break.

The results of the analyses are shown in Fig. 58-65. Because of the heat up of the core half concerned, the reactivity tends to fall due to the Doppler effect in the fuel. The LAC system tries to maintain the power level and worsens the situation (Figure 58). The changes of neutron power, coolant density, fuel and cladding temperatures are shown in Fig. 59 - 65. Since the ECCS is only actuated after the reactor is scrammed, the cooling of the core half concerned will not be restored during this scenario and sooner or later the core will melt down.

Calculational difficulties in the thermal hydraulics of SADCO do not permit the code to describe the rise of the clad temperature beyond 900 C. Therefore the temperature behaviour of the fuel and channel components for the case without scram should be investigated separately.

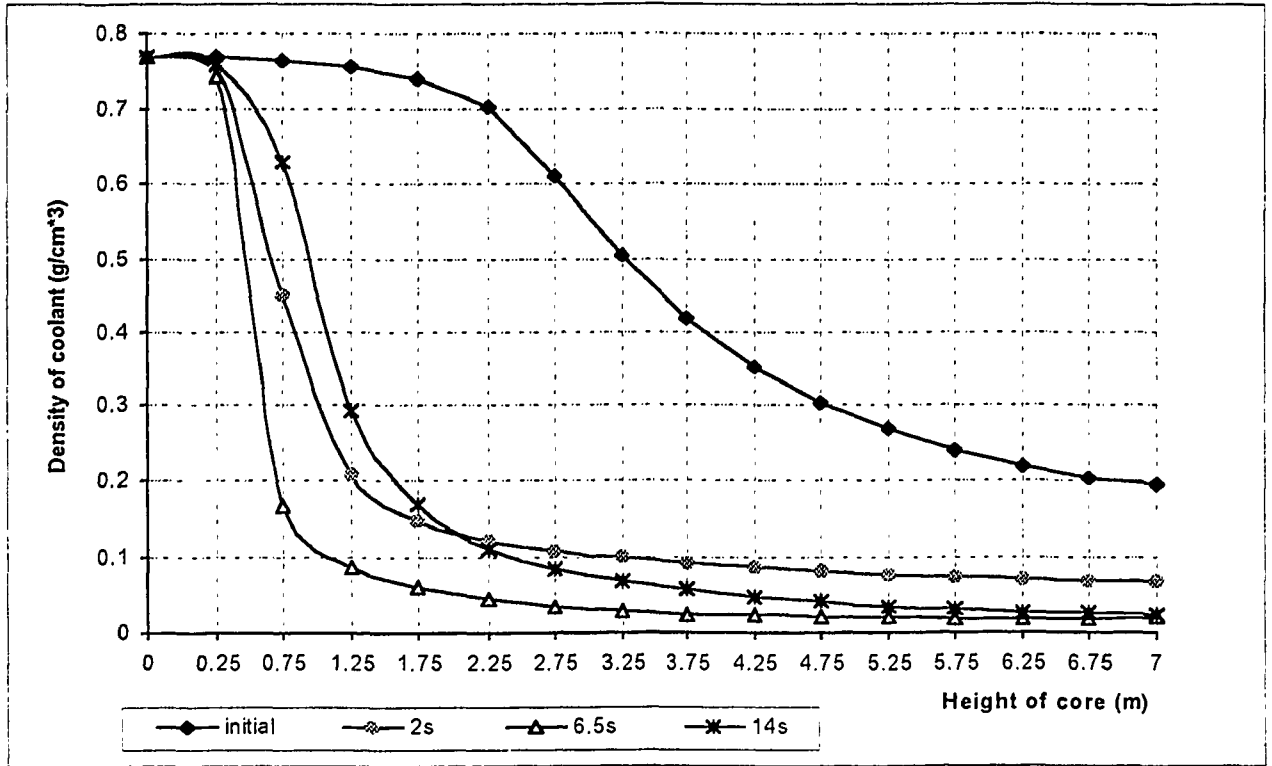


Fig. 52 Average coolant density in the voided core half during loss of coolant accident; (top of the core at 7 m)

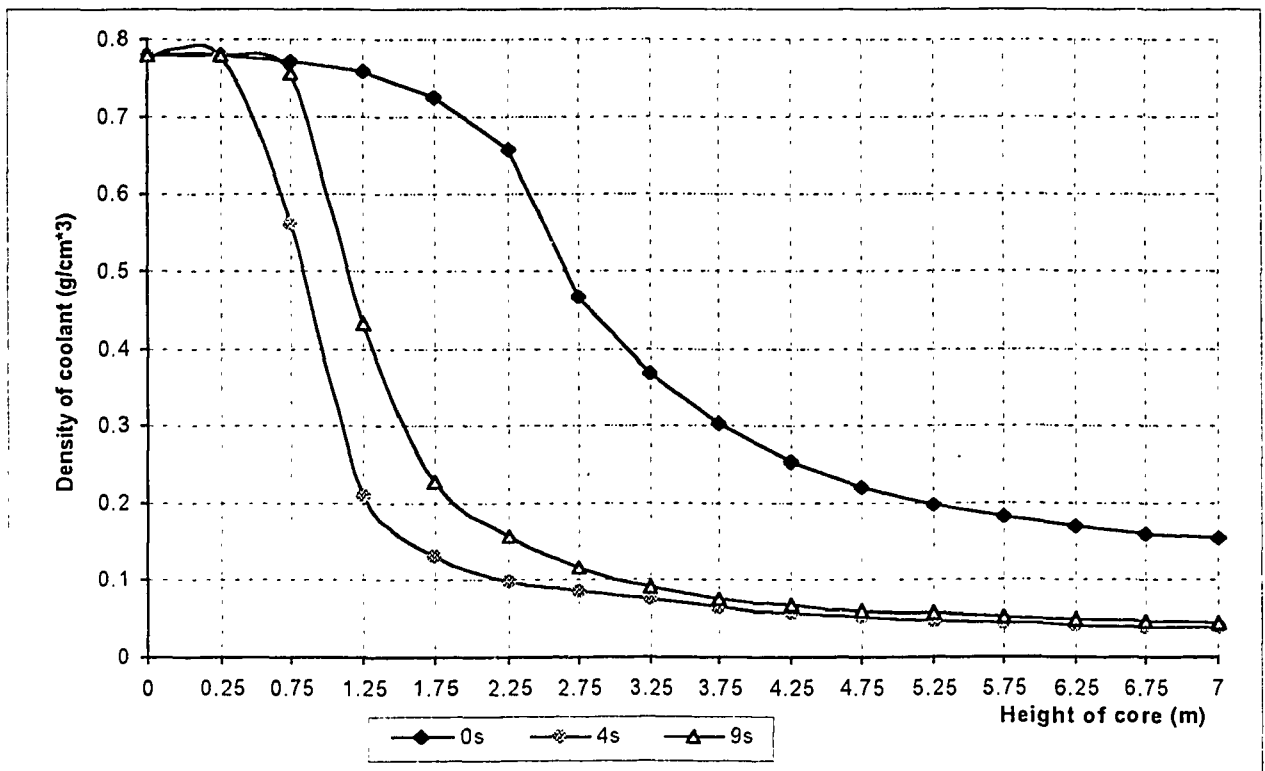


Fig. 53 Coolant density in hot channel (3MW); (top of the core at 7 m)

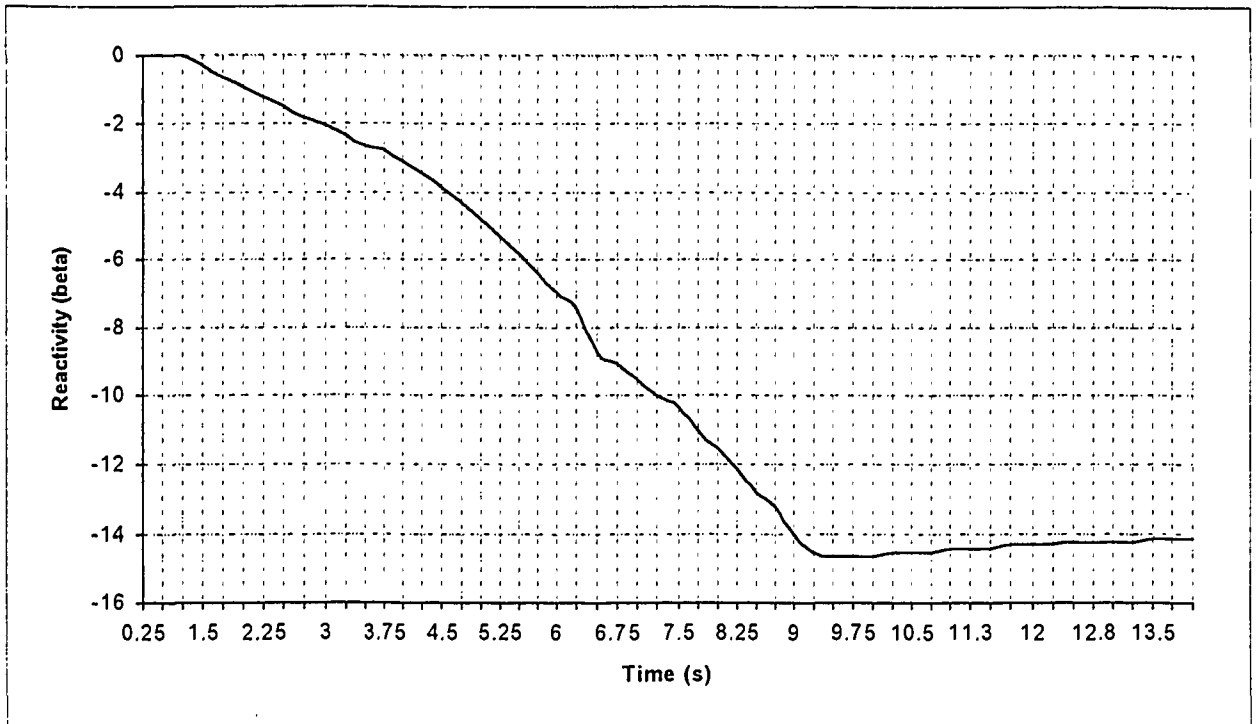


Fig. 54 Total reactivity vs. time during loss of coolant accident

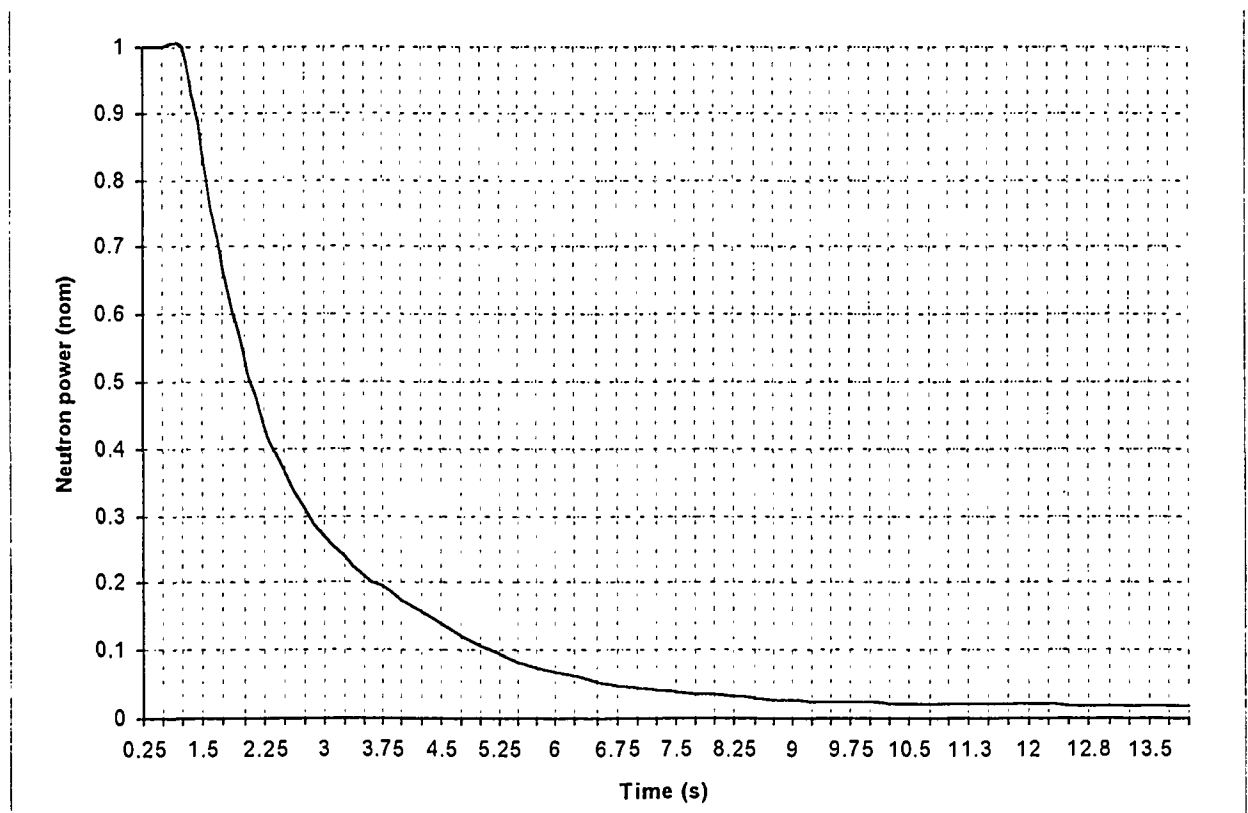


Fig. 55 Neutron power vs. time during loss of coolant accident.

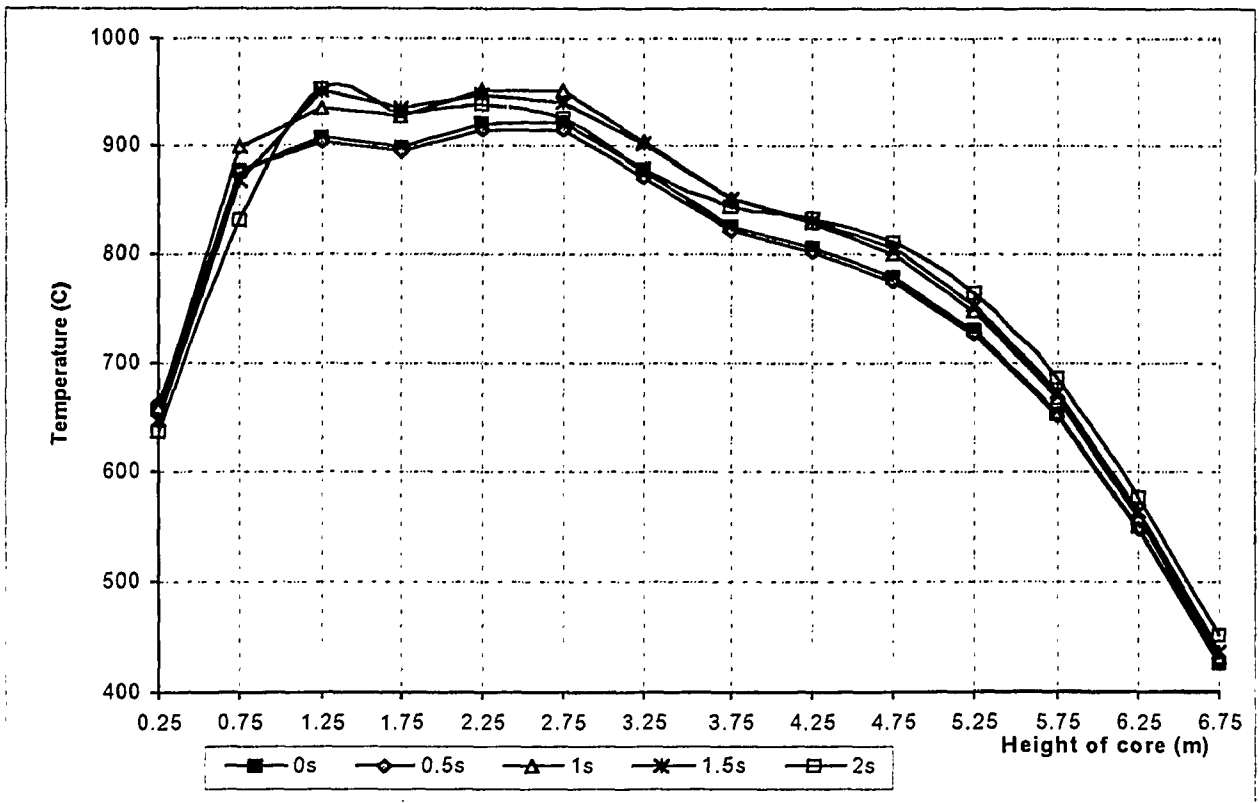


Fig. 56 Hot channel axial average fuel temp. distribution during LOCA; (top of the core at 7 m)

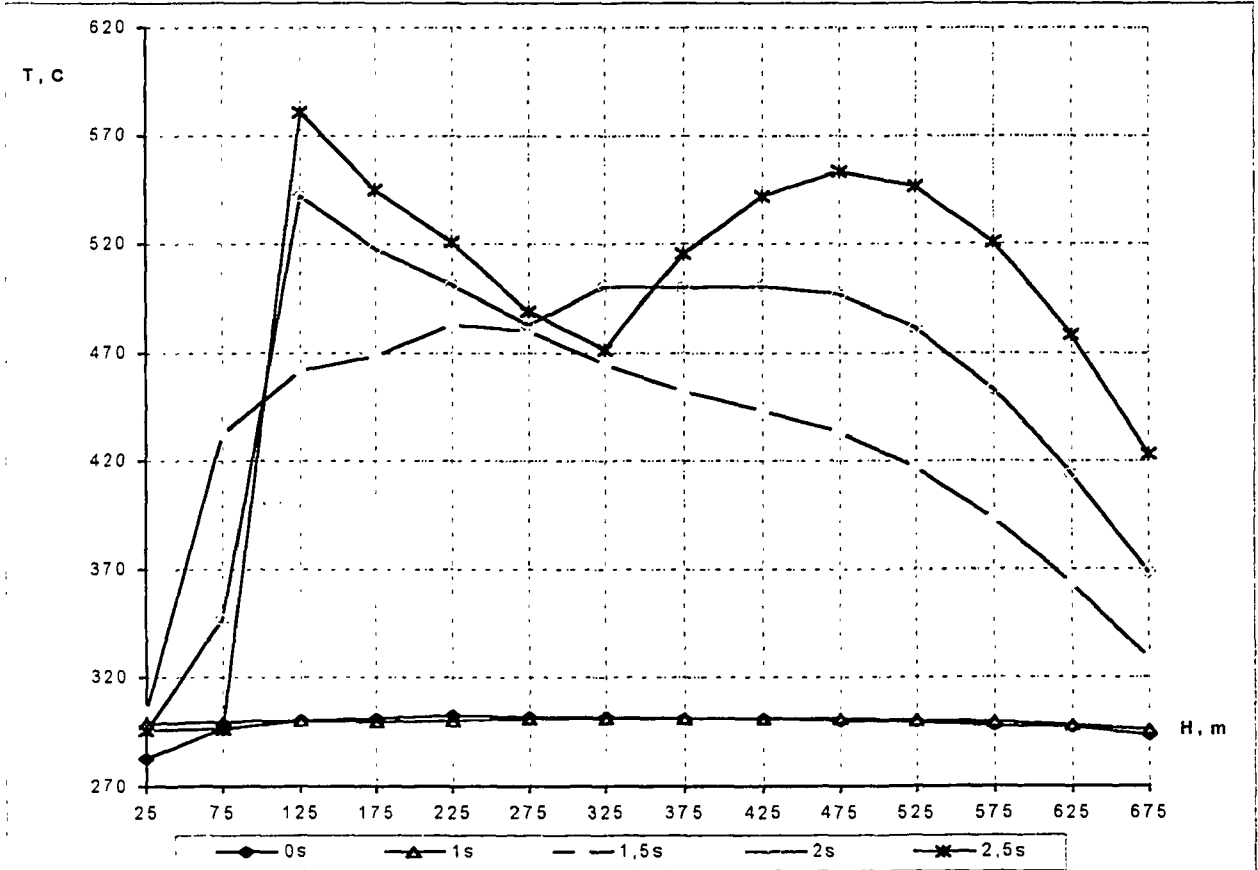


Fig. 57 Hot channel axial clad temp. distribution during LOCA; (top of the core at 7 m)

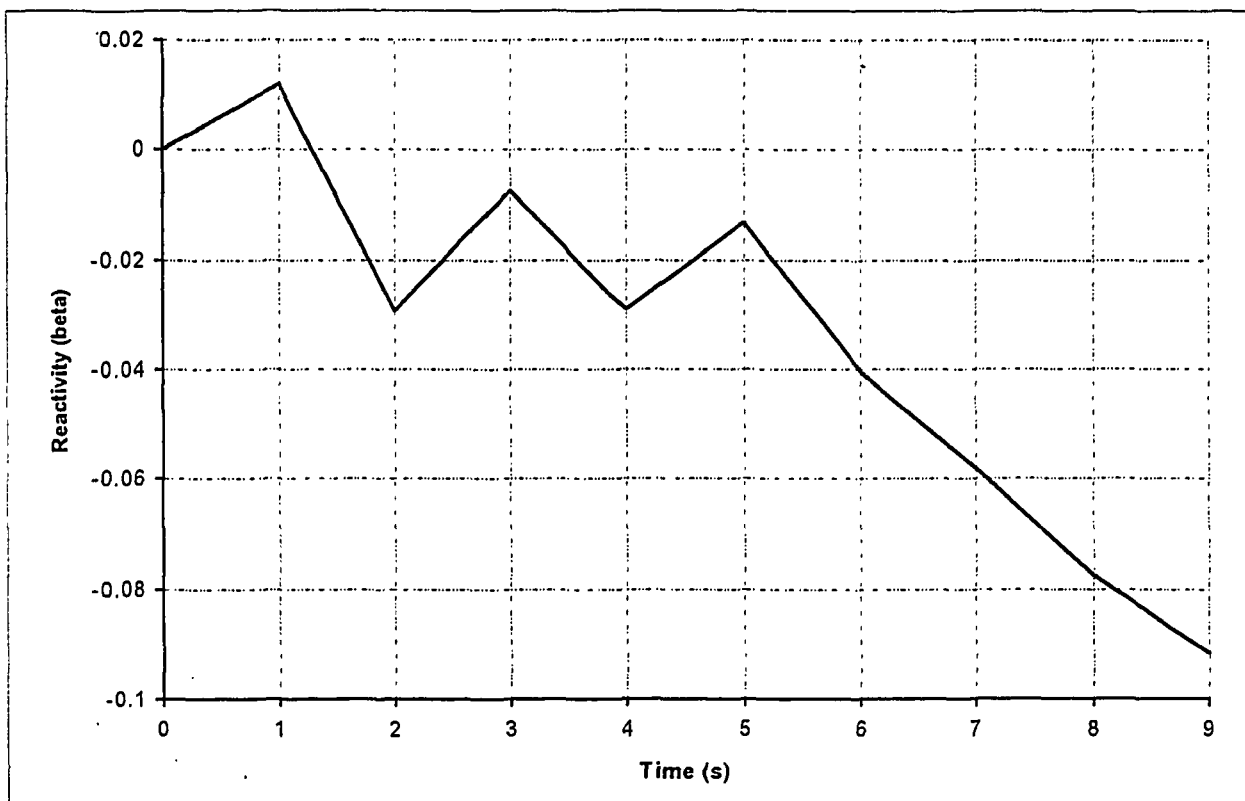


Fig. 58 Reactivity vs. time during LOCA without scram (no ECCS); (top of the core at 7 m)

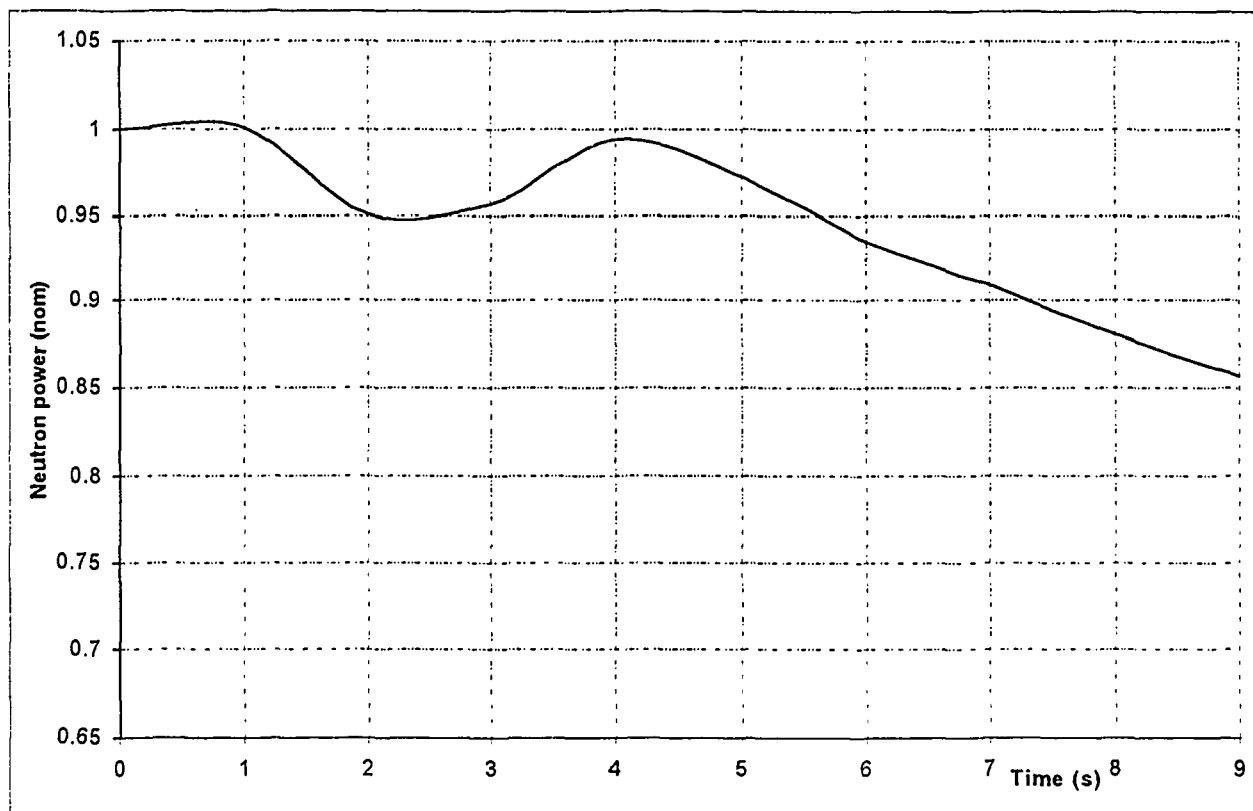


Fig. 59 Neutron power vs. time during LOCA without scram (no ECCS); (top of the core at 7 m)

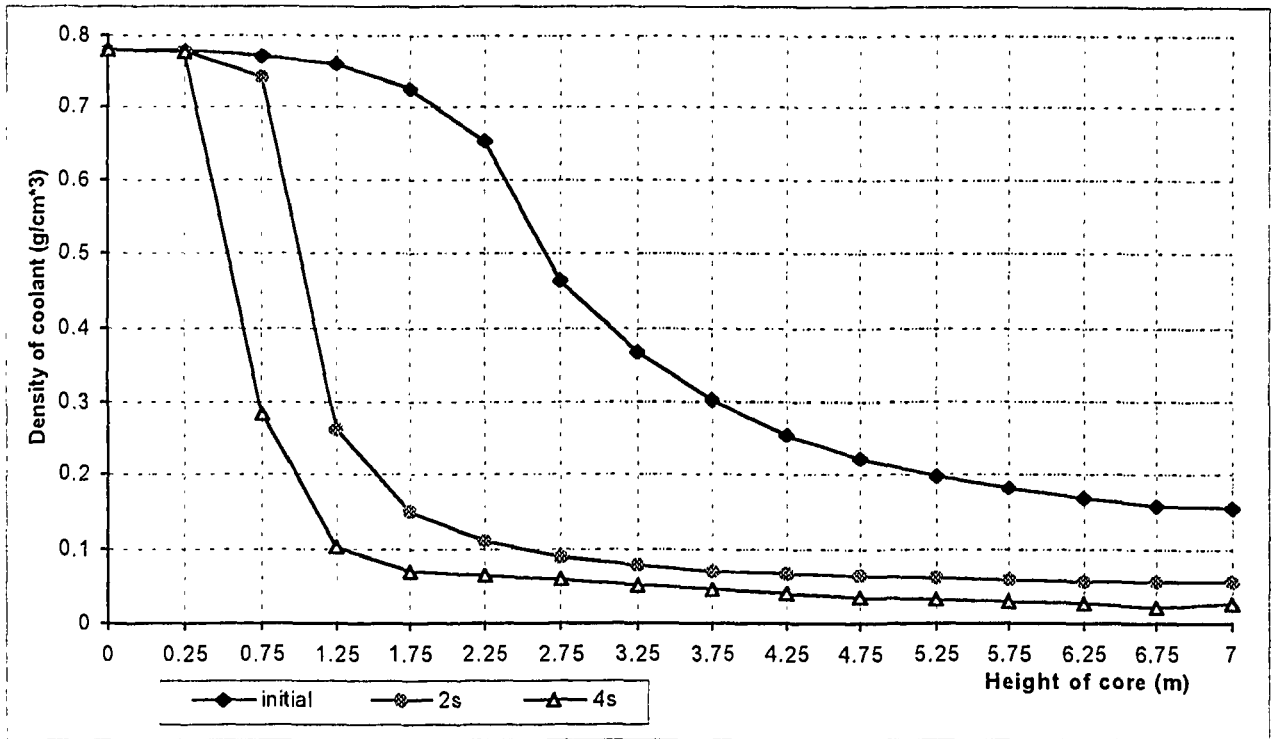


Fig. 60 Axial coolant density distribution in hot channel during LOCA without scram (no ECCS)

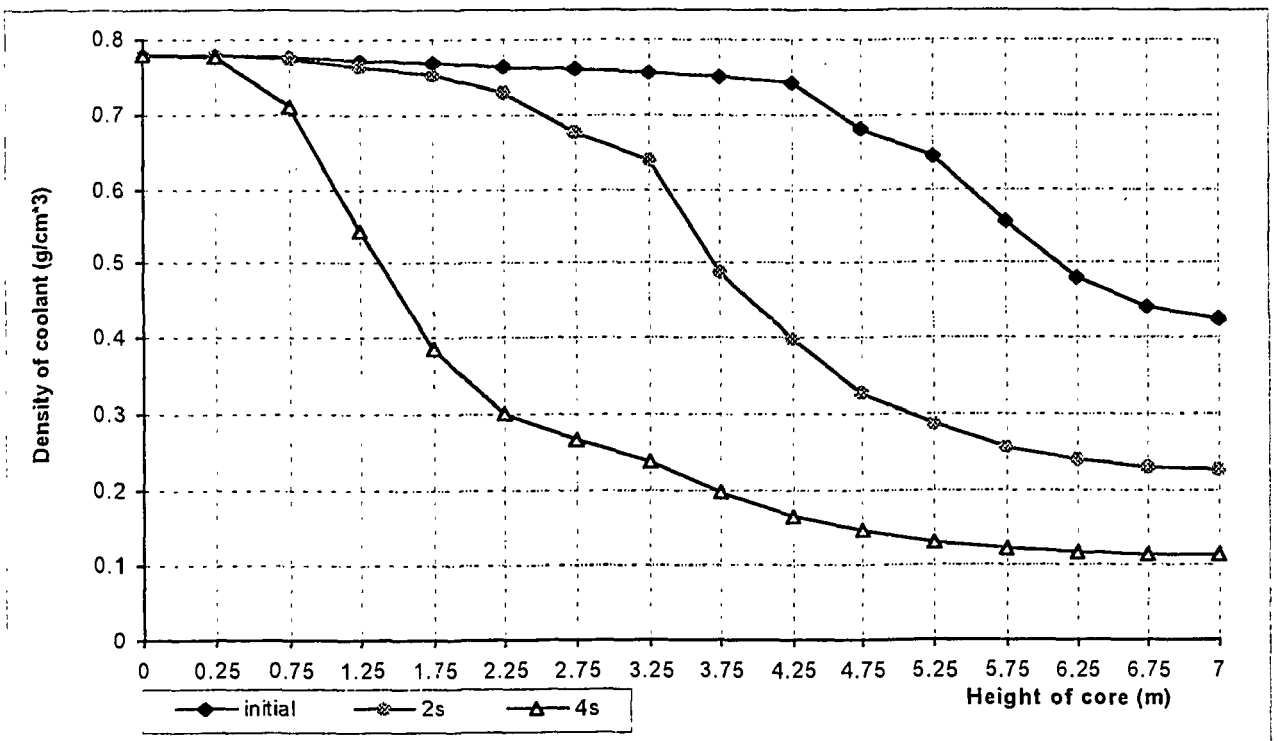


Fig. 61 Axial coolant density distribution in low power channel (0.8 MW) during LOCA without scram (no ECCS)

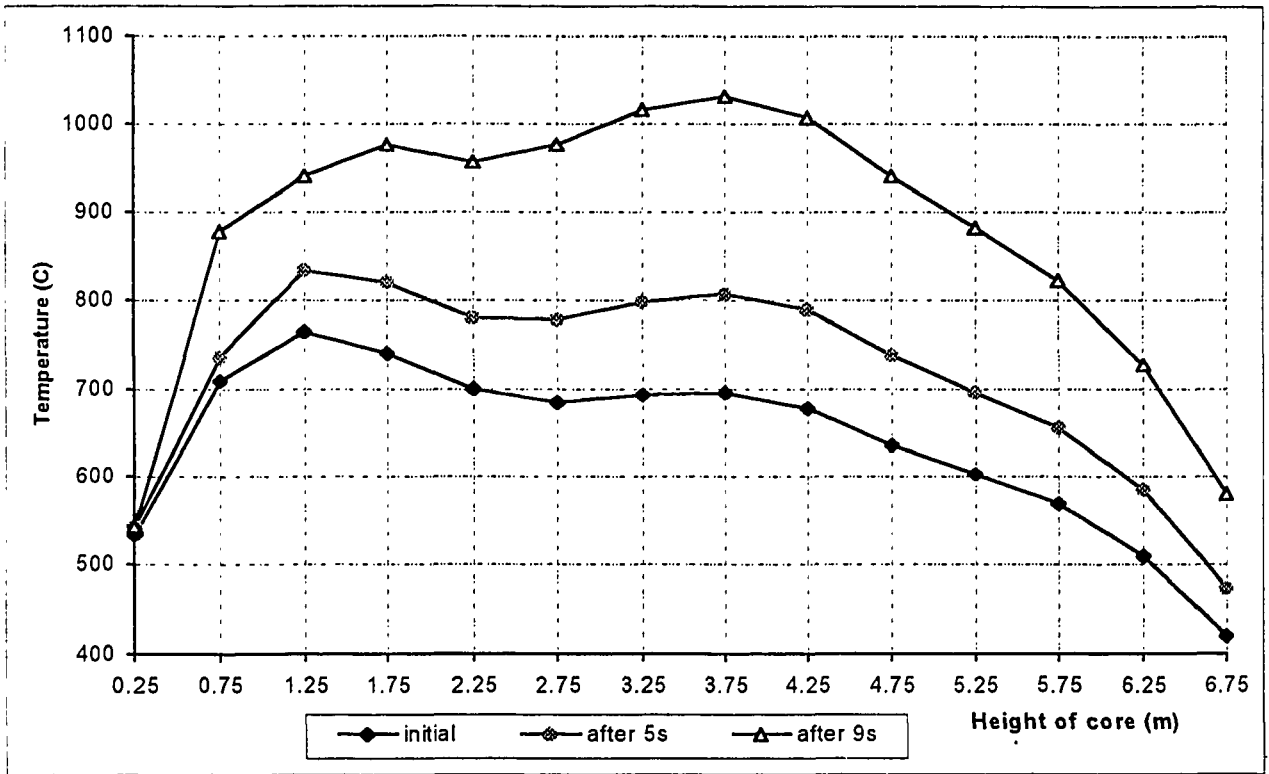


Fig. 62 Hot channel average fuel temperature distribution during LOCA without scram (no ECCS); (top of the core at 7 m)

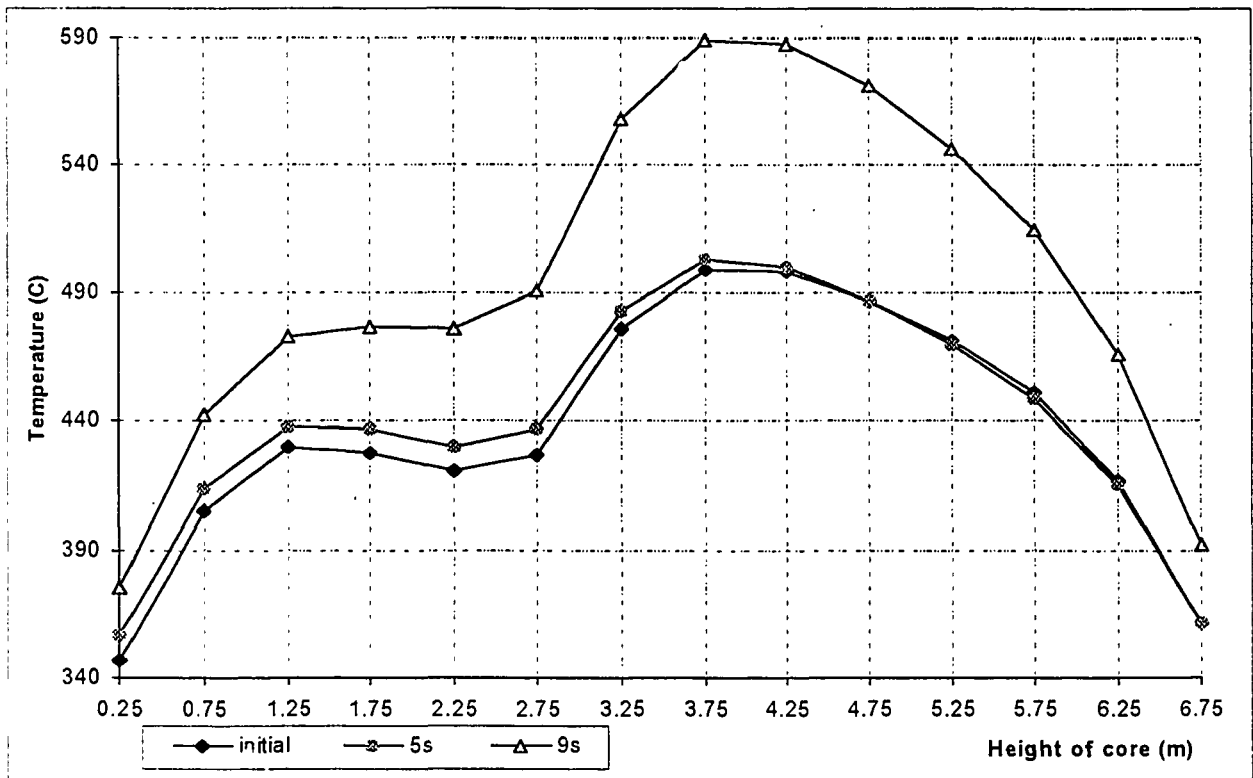


Fig. 63 Low power channel (0.8 MW) average axial fuel temperature distribution during LOCA without scram (no ECCS); (top of the core at 7 m)

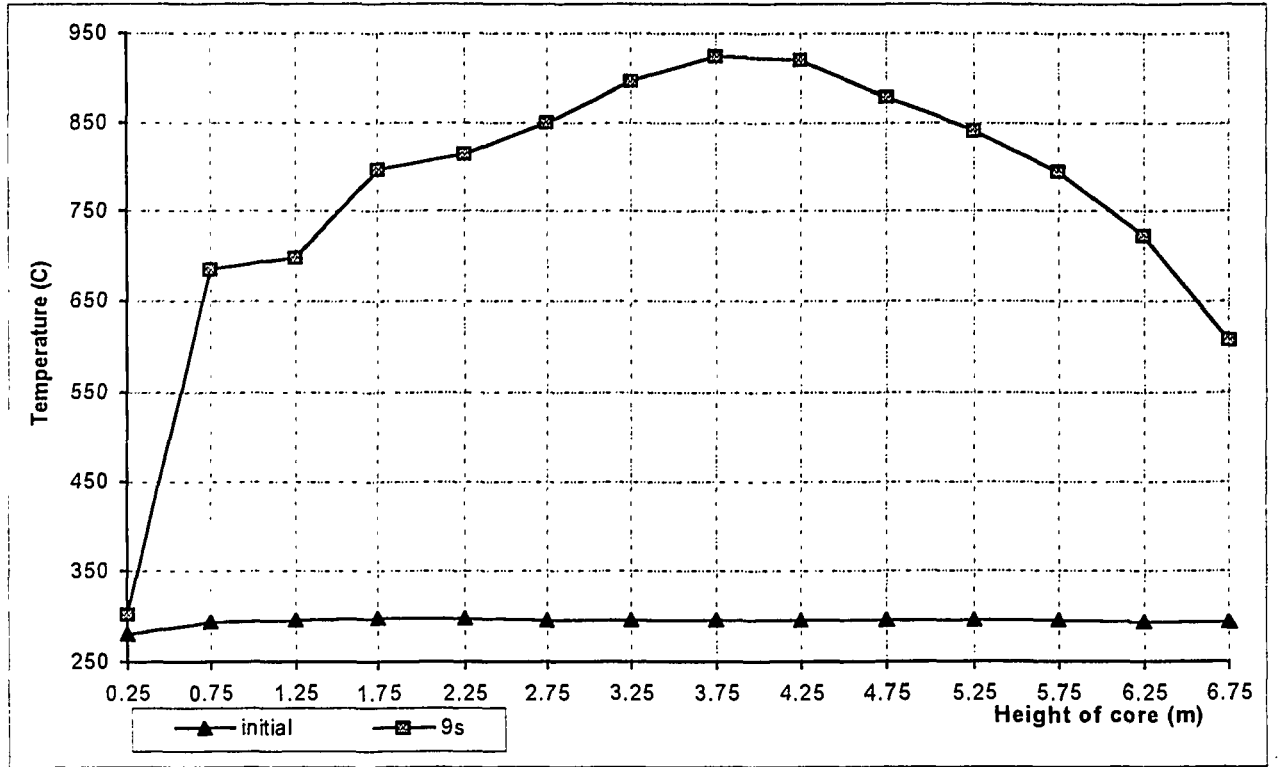


Fig. 64 Hot channel average axial fuel temperature distribution during LOCA without scram (no ECCS), (top of the core at 7 m)

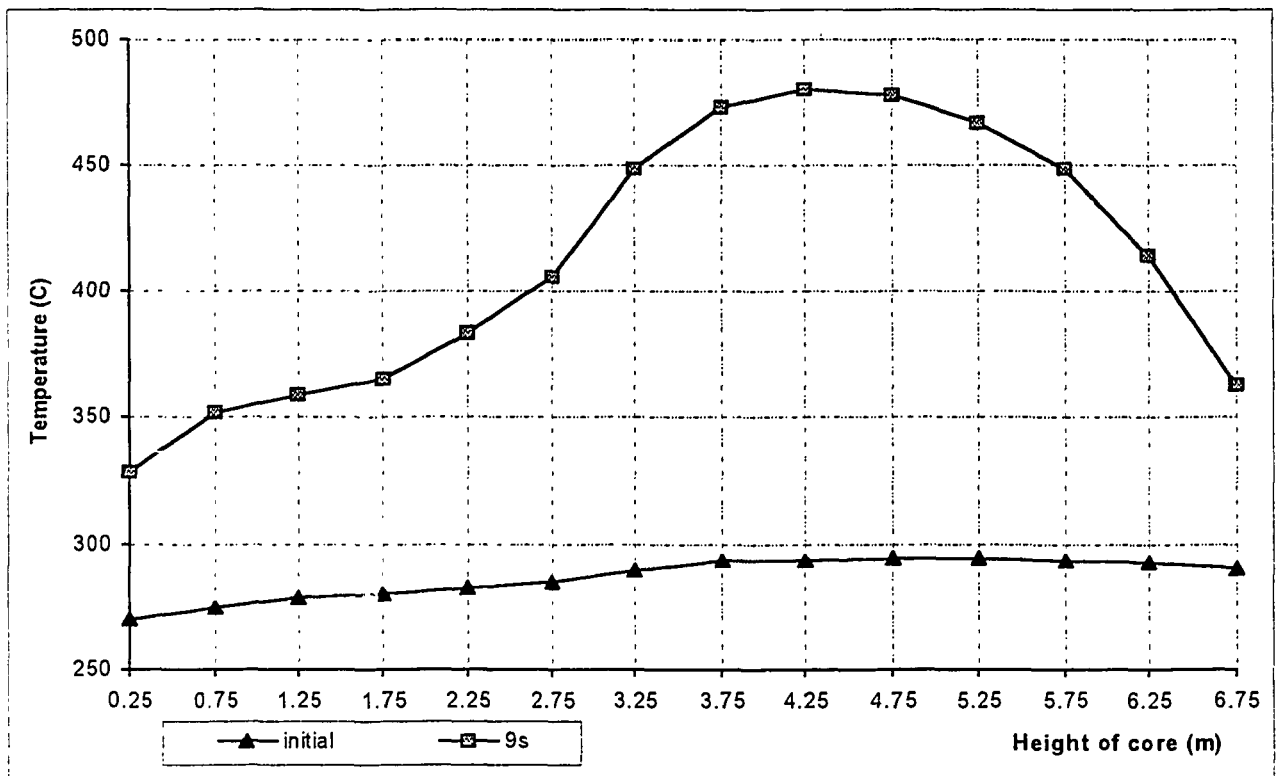


Fig. 65 Low power channel (0.8 MW) axial cladding temperature distribution during LOCA without scram (no ECCS); (top of the core at 7 m)

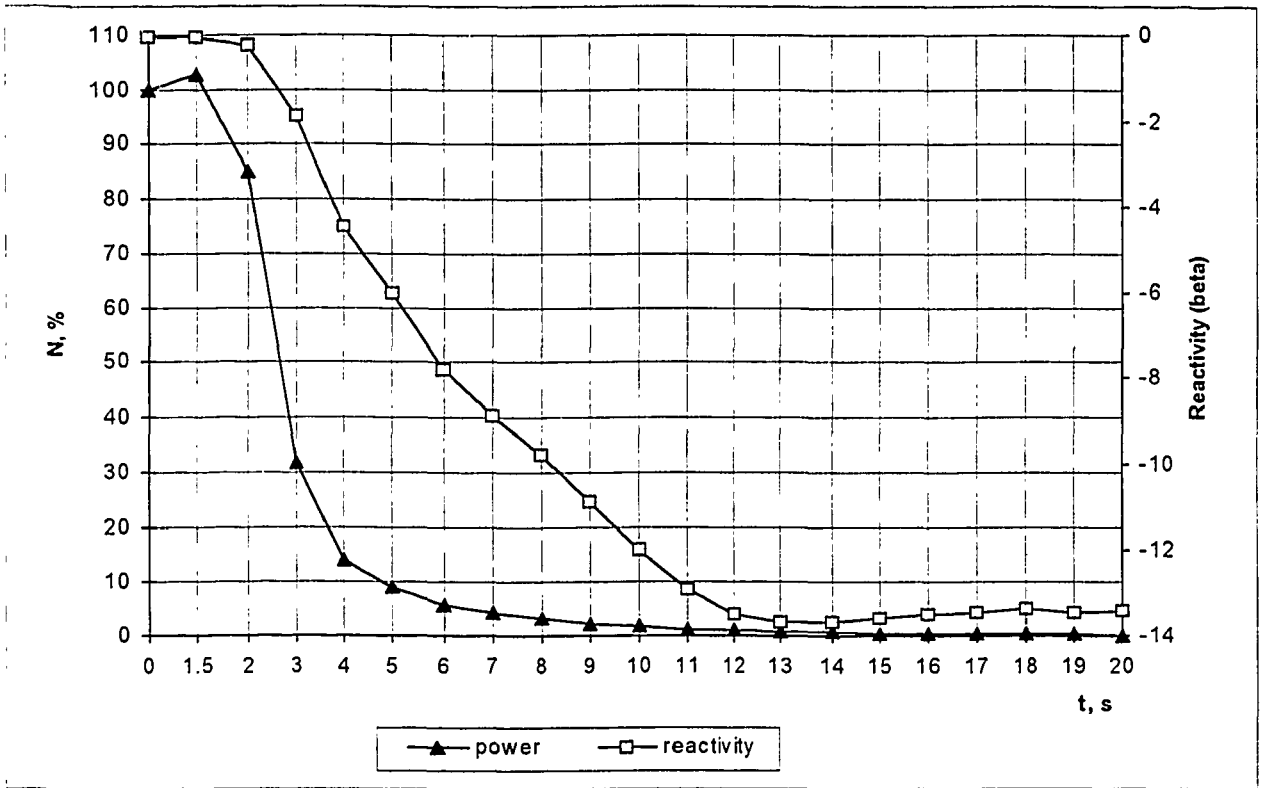
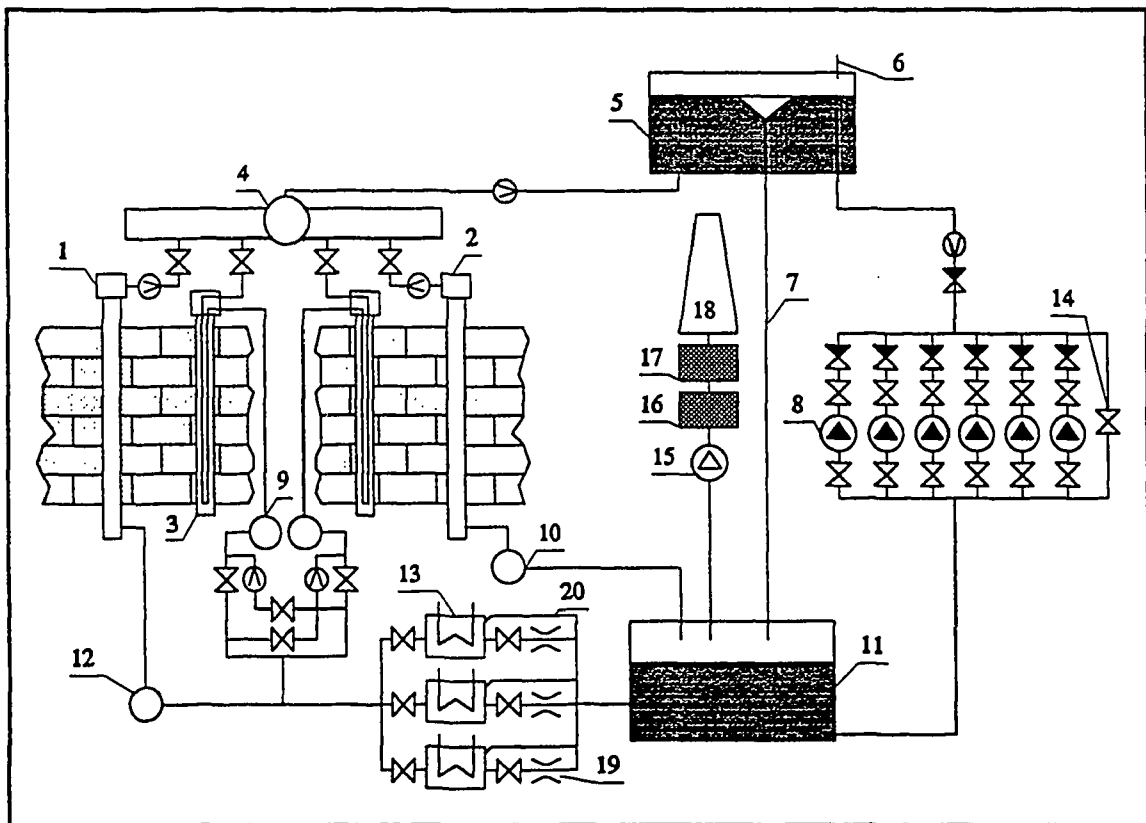


Fig. 66 Reactivity and neutron power vs. time during LOCA (TRIADA analysis)

6.2 LOCA analysis of CPS circuit

The CPS cooling system consists of two lower and one upper storage tank, four pumps which raise the water from the lower tanks to the storage tank, and pipelines and heat exchangers associated with the system. Two pumps are needed to maintain the level in the storage tank, a third pump is in an automatic stand-by mode. The coolant circulation is based on gravity. Without pumps, the level in the discharge tank will be lost in 7 minutes. It takes 40-45 seconds for the level to drop from the core outlet to the core inlet. The inventory of the cooling water is controlled by measuring the level in the storage tank, and the pressure and water flow-rate in each channel. Three out of four pumps are operated by a Diesel backed electrical system. A schematic of the system is presented in Figure 67.



- | | | | |
|-------------------------------|-----------------------------|-----------------------------|-----------------------------------|
| 1 - SUZ channel | 6 - Air vent | 11 - Circulation tank | 16 - Burning of combustible gases |
| 2 - Fast scram (BAZ) channel | 7 - Bypass pipeline | 12 - Drainage header of SUZ | 17 - Cooling chamber |
| 3 - Reflector cooling channel | 8 - SUZ pumps | 13 - Heat exchanger | 18 - Ventilation stack |
| 4 - Distribution header | 9 - Drainage header of KOO | 14 - Bypass of SUZ pumps | 19 - Throttling orifice |
| 5 - Emergency tank | 10 - Drainage header of BAZ | 15 - Gas fans | 20 - Discharge pipelines |

Fig. 67 Basic diagram of the cooling circuit for the control and protection channels and reflector cooling channels

The CPS-LOCA was analysed under the assumption of a break of the distribution header. Since the CPS system is an open loop operating at atmospheric pressure, the water in these channels will not flash, but merely void the system by draining the channels. There will always be a well defined water level which was assumed to drop from the top of the core down to the bottom within 40 seconds. Another possibility to void these channels might be by air ingress which already occurred in some RBMK. Under the conditions of air ingress the channels may be voided much faster than under LOCA conditions. Presently the CPS system is not modelled in our thermal hydraulic codes. Consequently air ingress cannot be analysed in a realistic way. To overcome this problem the attempt was made to simulate air ingress by parameterizing the time for the water level to drop from the top of the core down to the bottom.

With regard to the time it takes the channels to run dry, three cases were investigated

Case	Time to empty channels (sec.)
1	40
2	5.0
3	2.5

The analysis was done under the assumption that reactor shutdown was provided by the simultaneous actuation of the two shutdown systems SDS-1 plus SDS-2 as in any RBMK accident. In order to evaluate the shutdown effectiveness of SDS-1, the fast acting scram system only was used for reactor shutdown in a further analysis.

6.2.1 Shutdown by SDS-1 plus SDS-2

In order to demonstrate adequate shutdown rate, in the analysis the reactor was scrammed on neutronic signals only even though there are three diverse technological signals available for shutdown:

- the flow rate in CPS loop;
- the water level in the upper storage tank;
- the pressure in the distribution header of the CPS loop.

The results of the TRIADA calculations are presented in Fig. 68 and 69, which show the reactivity insertion as a function of water level and as a function of time respectively. If the water level drops slowly enough (case 1 and 2) the LAC system is able to keep the power under control during the first few seconds. When the LAC cannot prevent a power increase anymore the scram system is actuated as a result of the increasing neutron power (Fig. 70). When the CPS channels are emptied within 2,5 seconds only (case 3) the scram system cannot compensate the positive reactivity insertion during the first few seconds. A power burst up to about 25 times nominal may be the result of this transient as shown by STEPAN analyses (see Fig. 71 and 72). It is expected that even under these conditions the fuel might not be in jeopardy since the duration of the power burst is very short and the energy deposited in the fuel is estimated to remain below the limit for fuel fragmentation. Further analyses are necessary.

TRIADA calculations of the CPS LOCA were also performed for the cases of 45s, 5s and 2.5s to empty the CPS channels. The predicted steady state value of the void reactivity effect of the Control and Protection System is $3.9 \beta_{\text{eff}}$. The results are presented in Fig. 73-75.

As in the analyses presented above it was assumed that the insertion time of the control rods is independent of the run dry time of the channels as long as the latter is higher than the former. This assumption is no longer valid if the rods are „overtaken“ by the water level and move within emptied channels. This is particularly the case if the water level drops to the bottom of the core in no more than 2.5 seconds. If one takes this effect into account, the value of the peak core reactivity is decreased from $2 \beta_{\text{eff}}$ (Figure 75) to $1.4 \beta_{\text{eff}}$ (Figure 76) and the peak of the neutron burst is decreased from 19 times nominal -which is close to the STEPAN + KOBRA results- to 6 to 7 times nominal as may be seen by comparing Fig. 75 and Figure 76.

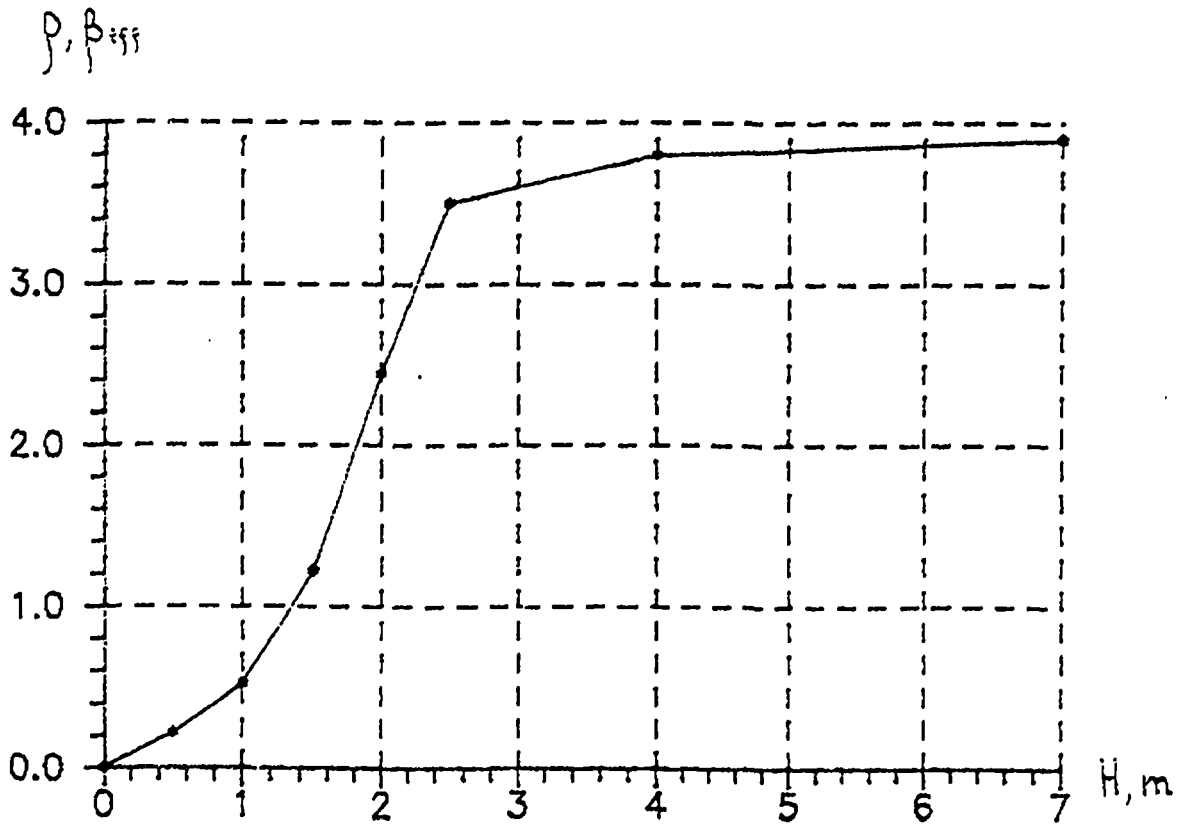


Fig. 68 Reactivity vs. water level in CPS channels; (top of the core at 0 m)

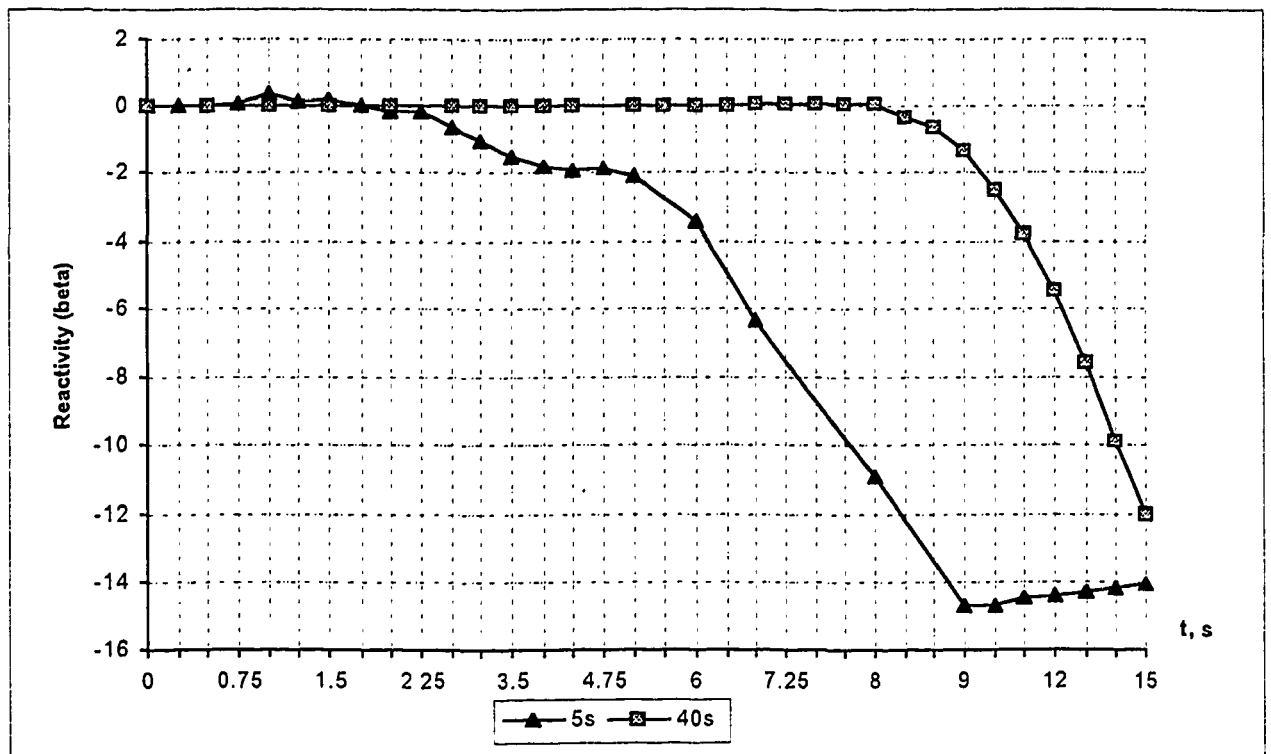


Fig.69 Reactivity vs. time during CPS-LOCA (parameter: time to empty channel)

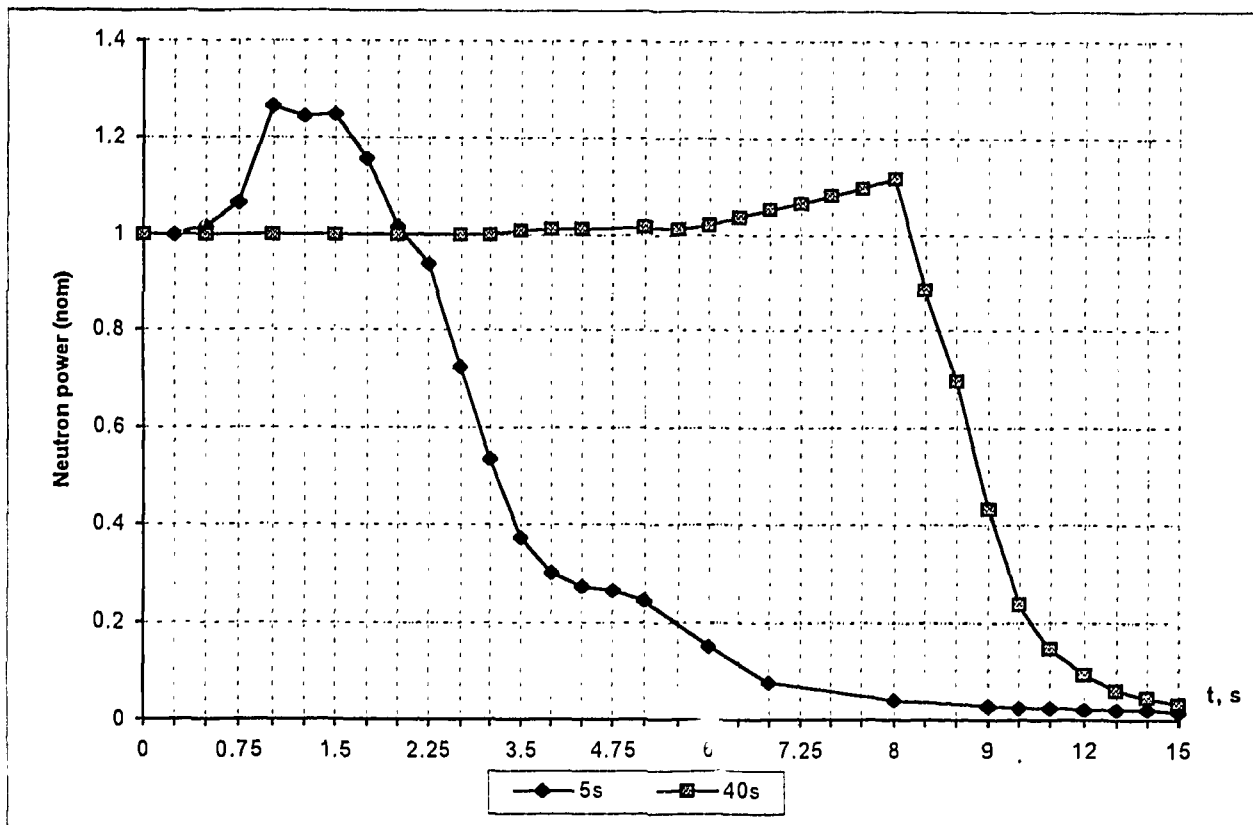


Fig. 70 Neutron power vs. time during CPS-LOCA (parameter: time to empty channel)

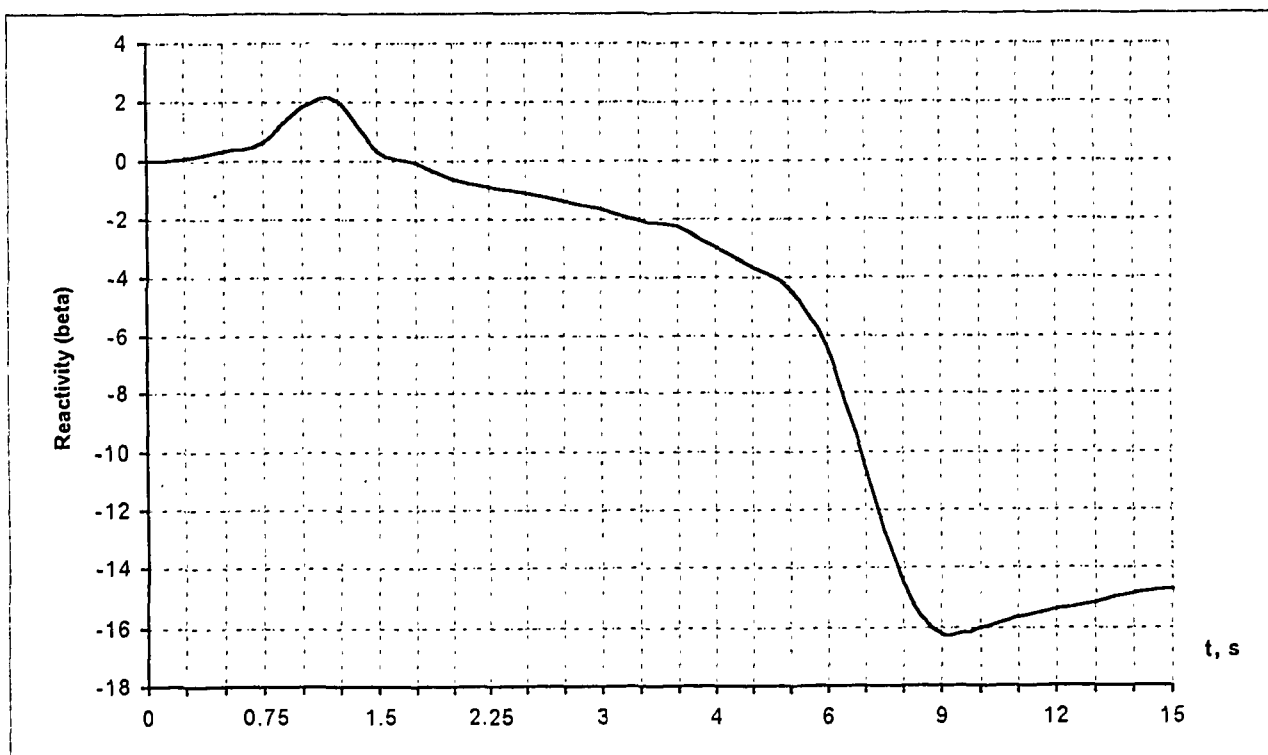


Fig. 71 Reactivity vs. time during CPS-LOCA (time to empty channels 2.5 sec.)

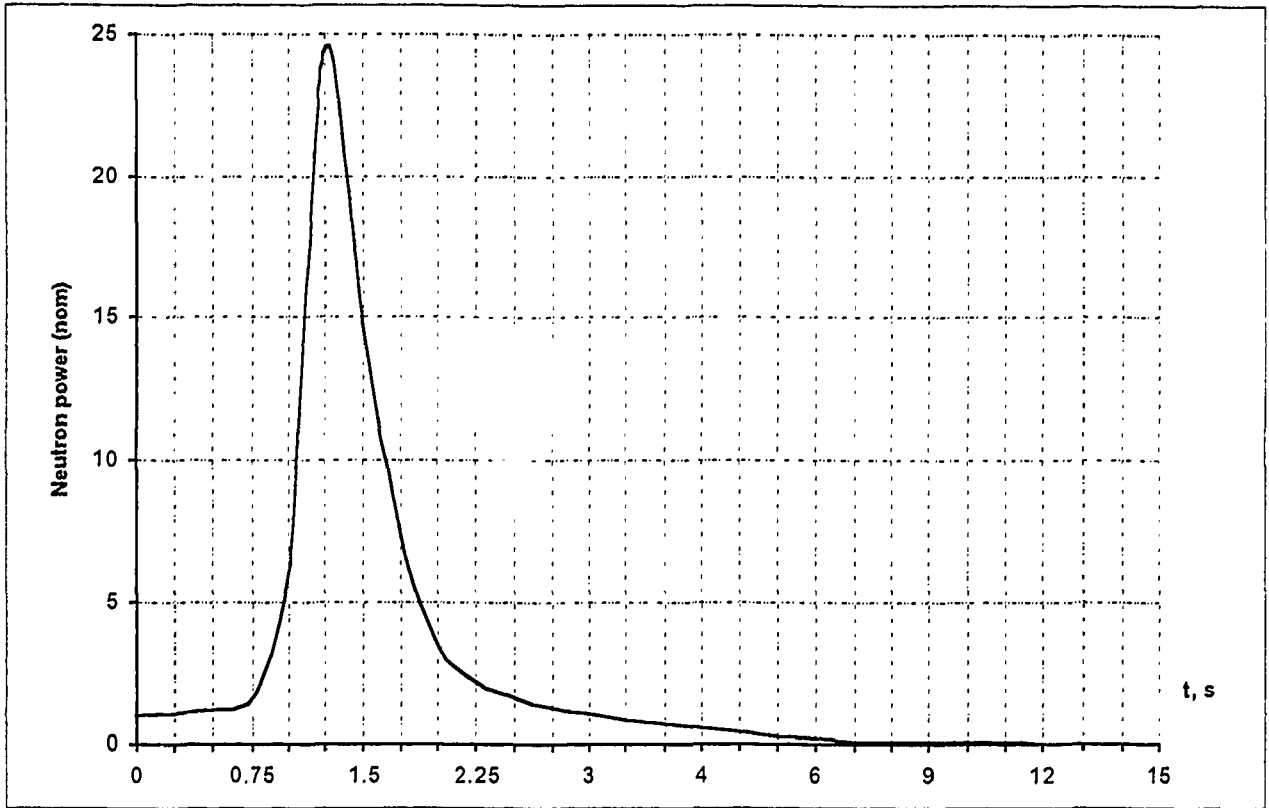


Fig. 72 Power burst during CPS-LOCA (time to empty channel 2.5 sec.)

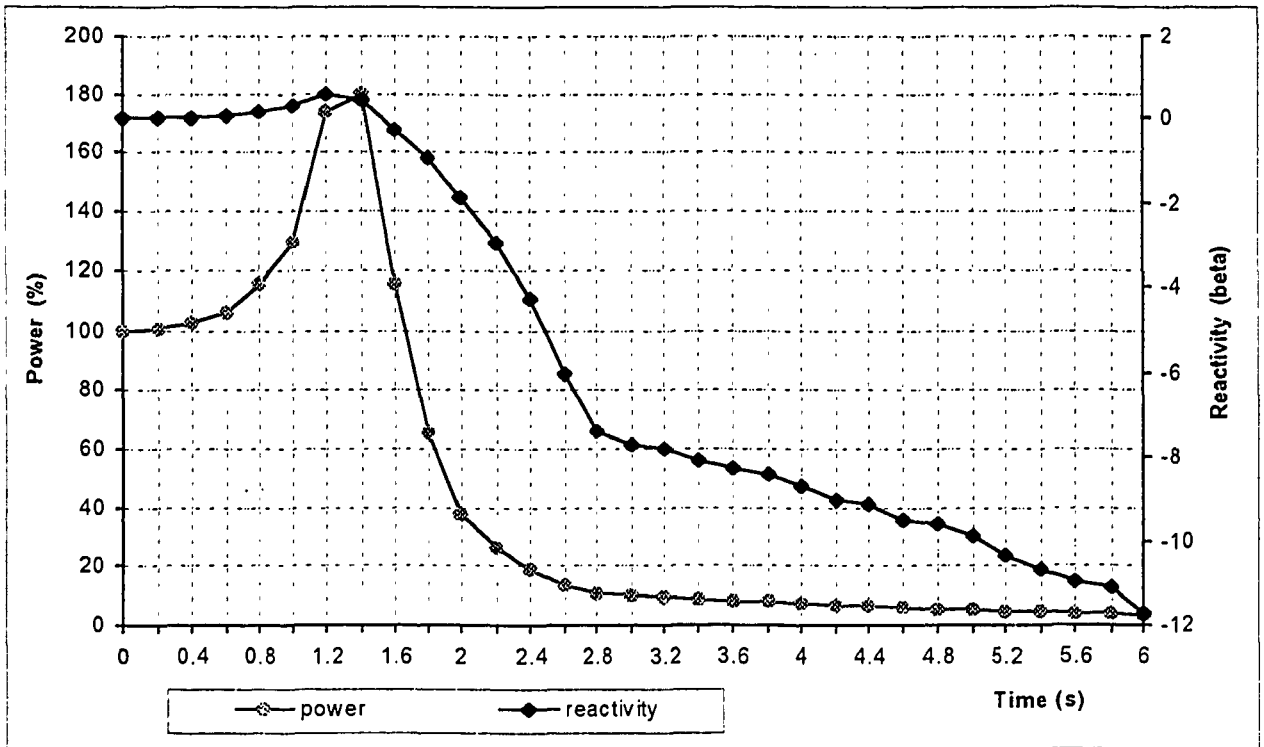


Fig. 73 Reactivity and power vs. time during CPS-LOCA, TRIADA analysis (time to empty channels 45 sec.)

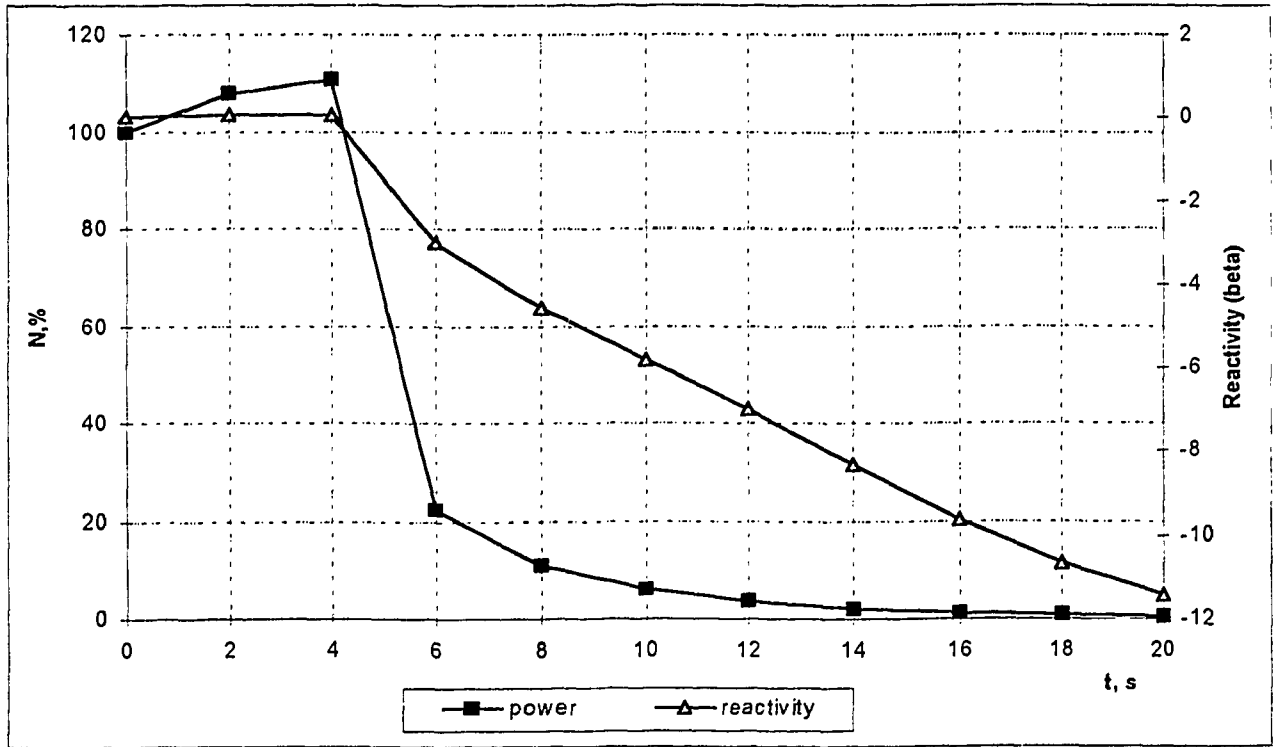


Fig. 74 Reactivity and power vs. time during CPS-LOCA. TRIADA analyses (time to empty channels 5 sec.)

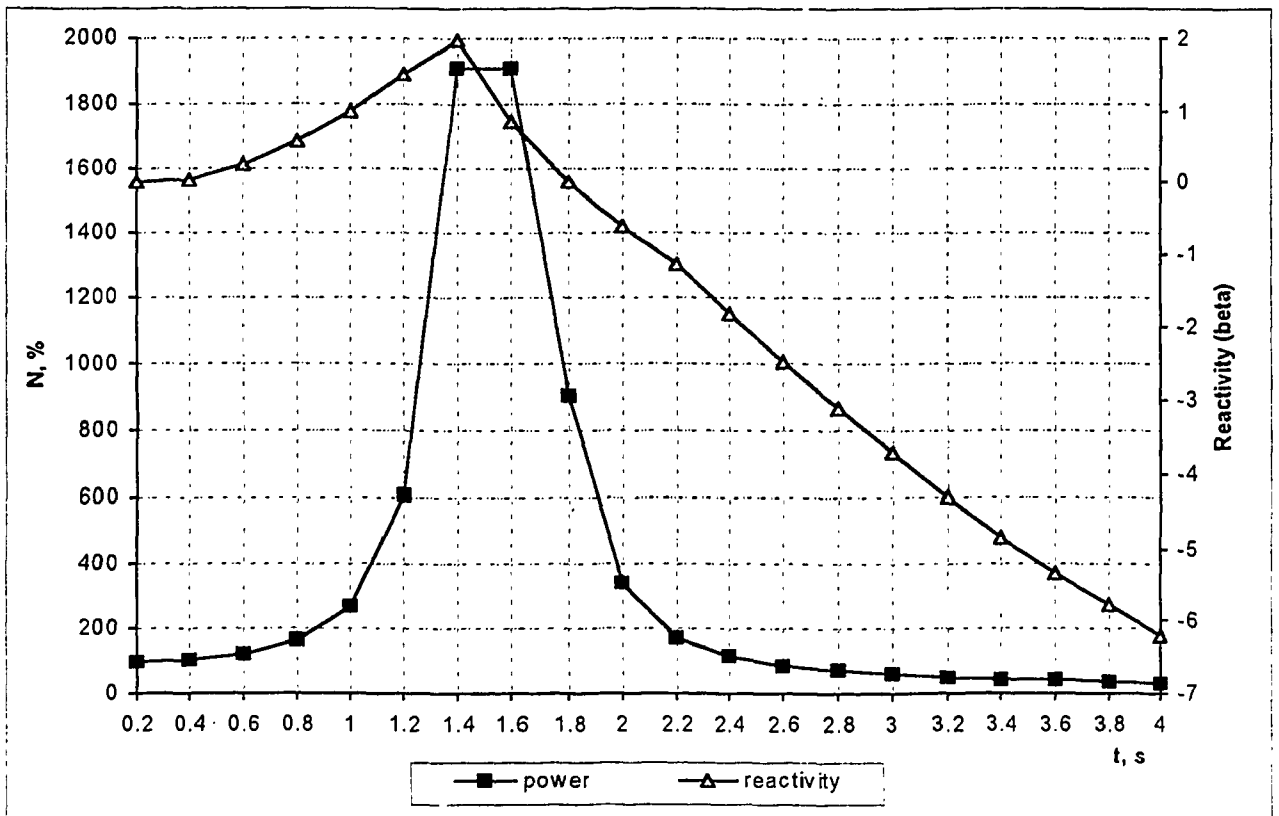


Fig. 75 Reactivity and power vs. time during CPS-LOca. TRIADA analysis (time to empty channels 2.5 sec.)

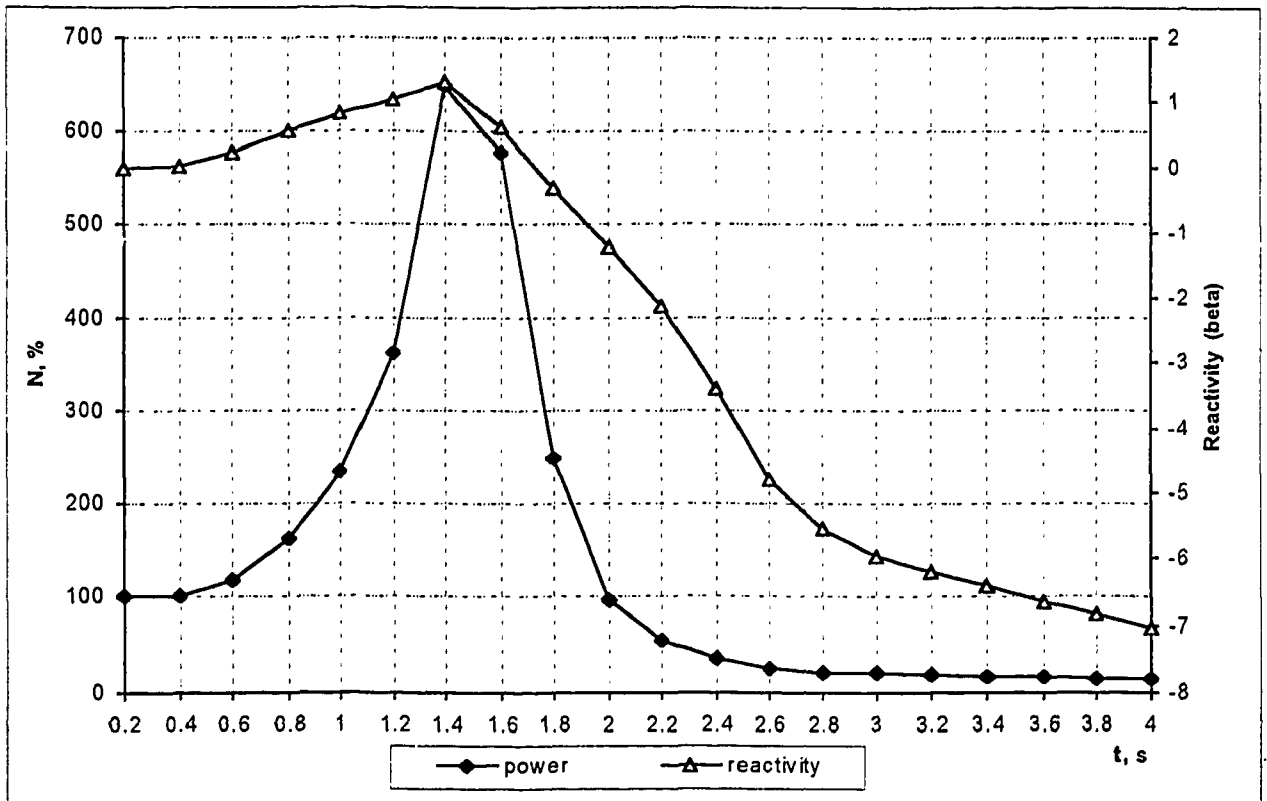


Fig. 76 Reactivity and neutron power vs. time during CPS-LOCA. TRIADA analyses (time to empty channels 2.5 sec. reduced control rod insertion time).

6.2.2 Shutdown by SDS-1 only

The CPS LOCA was also analysed under the assumption that only the 24 fast acting rods of SDS-1 are available for reactor shutdown. The worth of these 24 rods is not enough to suppress a power excursion caused by voiding of the CPS channels (40 seconds). The resulting net reactivity insertion is approximately $0,4 \beta_{\text{eff}}$ and the power excursion is terminated by the Doppler effect in the fuel only at a power level of about 1.5 times nominal. The behaviour of neutron power and reactivity is presented in Fig. 77 and 78 which show results of the STEPAN analyses. TRIADA results are shown in Fig. 79 and 80.

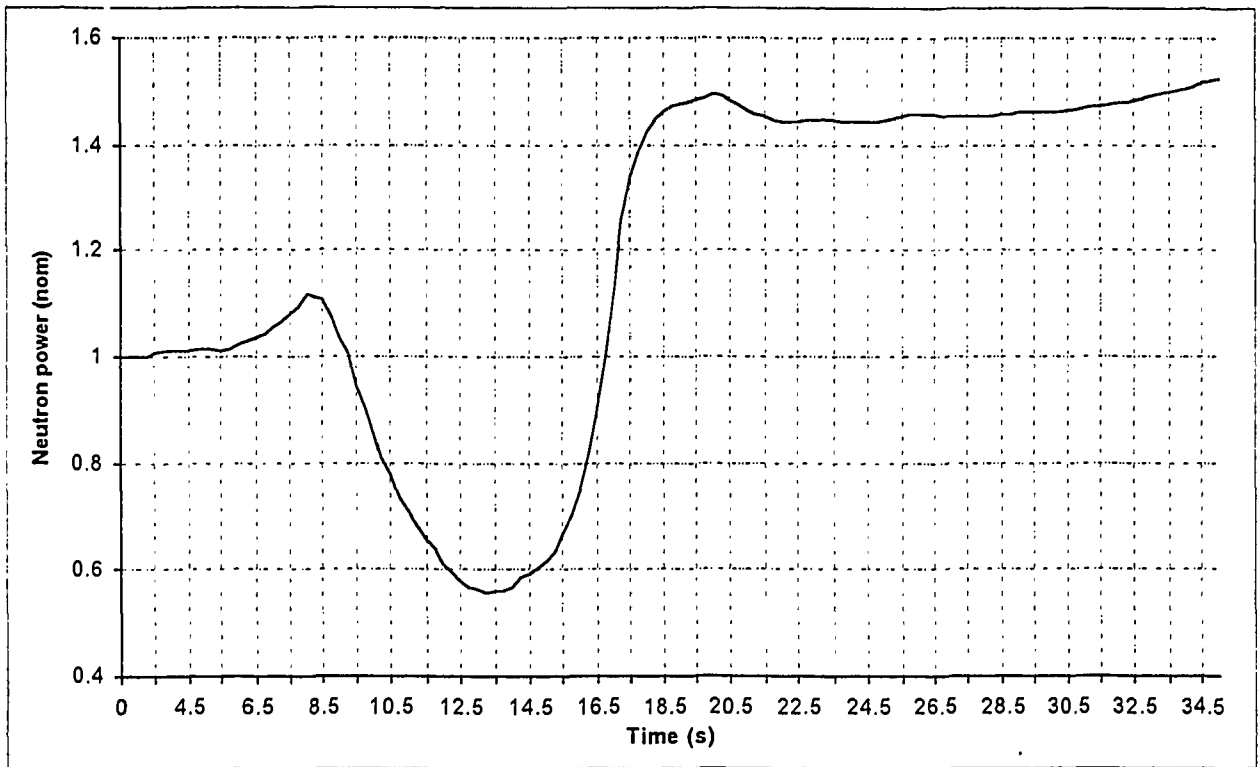


Fig. 77 Neutron power vs. time during CPS-LOCA, reactor chut down by SDS-1 only (time to empty channels 40 sec.)

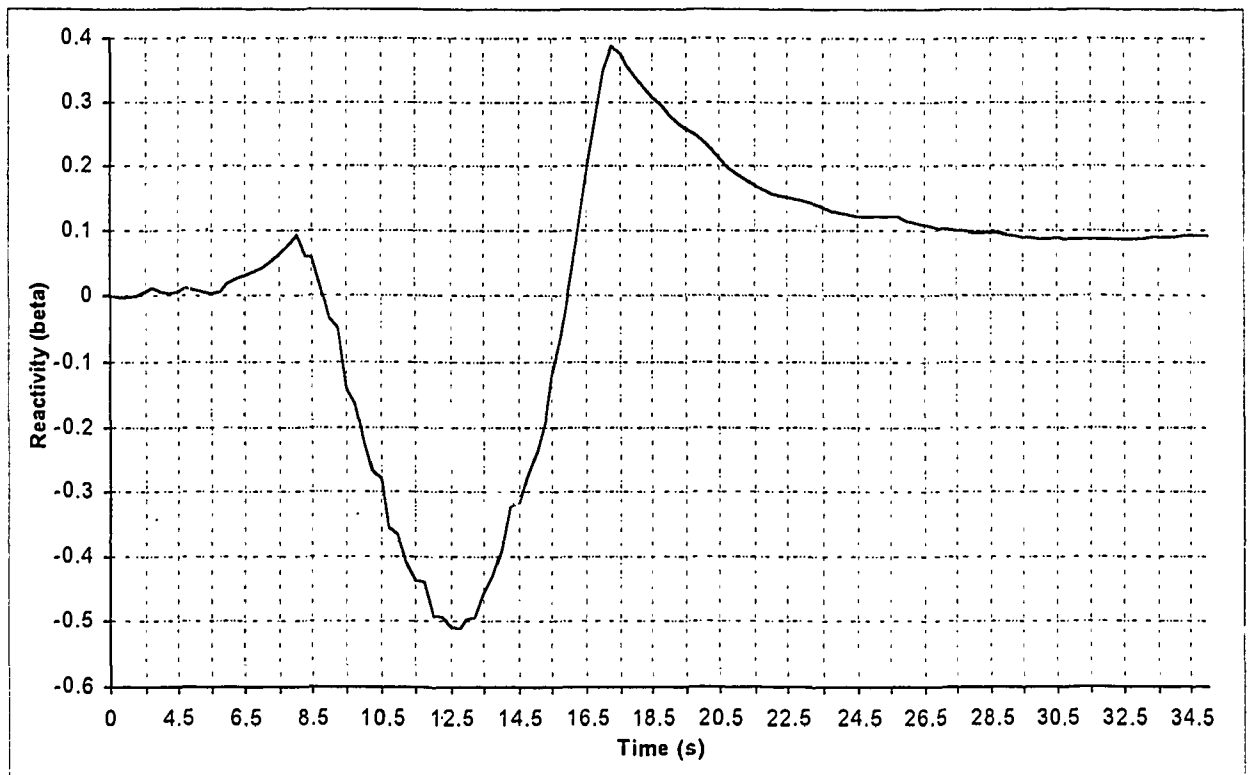


Fig. 78 Reactivity vs. time during CPS-LOCA, reactor shutdown by SDS-1 only (time to empty channels 40 sec.)

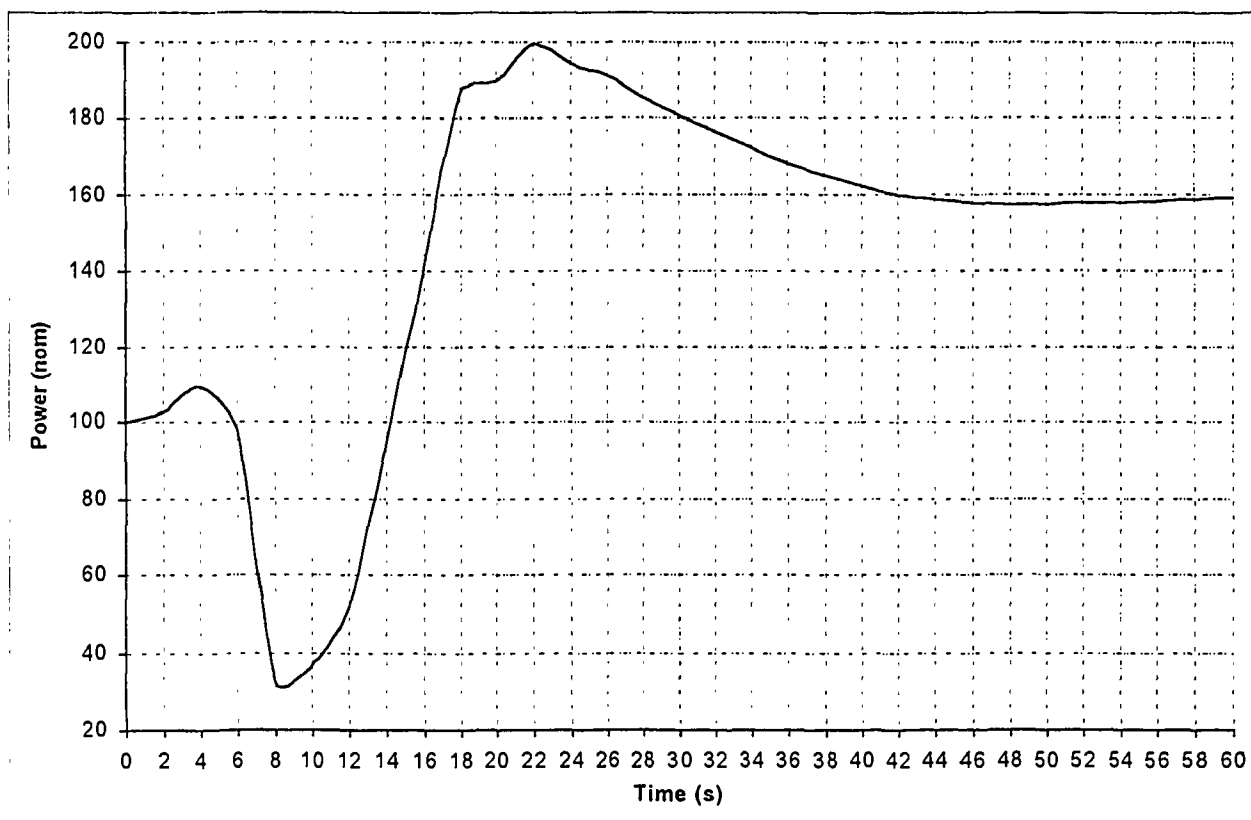


Fig. 79 Neutron power vs. time during CPS-LOCA, reactor shutdown by SDS-1 only TRIADA analysis (time to empty channels 40 sec.)

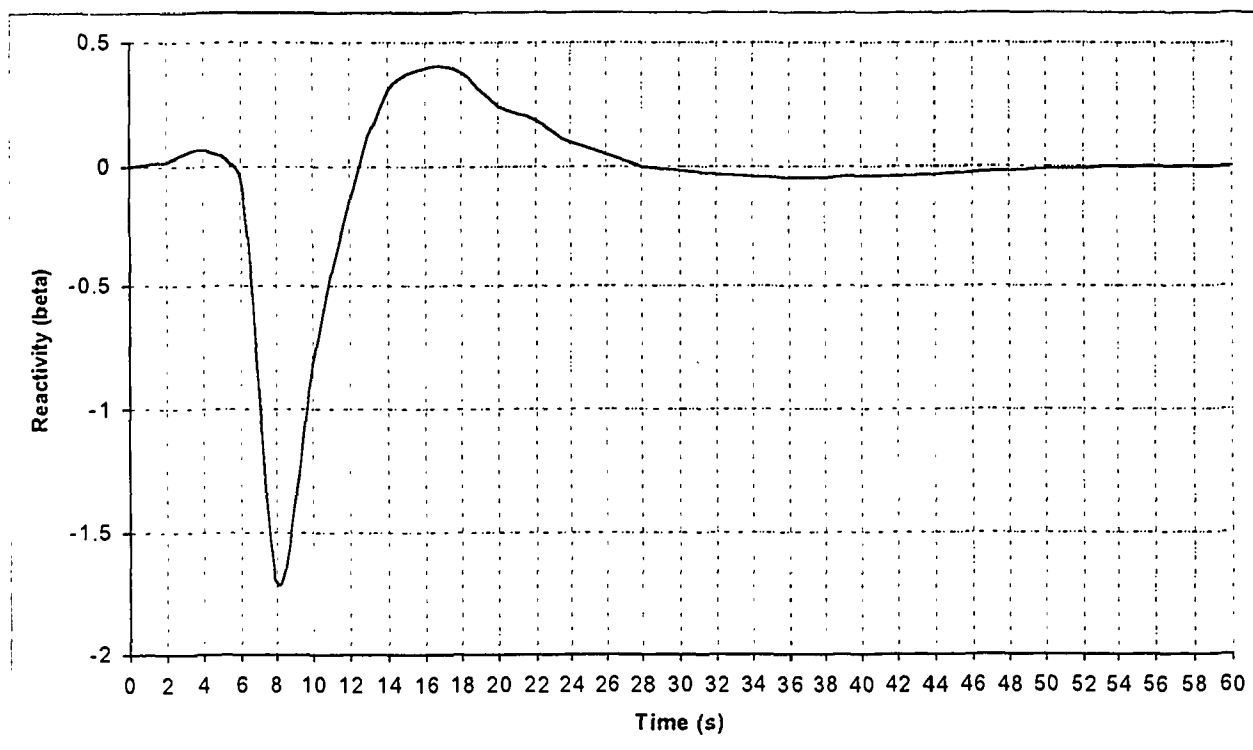


Fig. 80 Reactivity vs. time during CPS-LOCA, reactor shutdown by SDS-1 only TRIADA analysis (time to empty channels 40 sec.)

6.3 Erroneous control rod withdrawal accident (ECRWA)

The analyses of erroneous control rod withdrawal were performed by the STEPAN + KOBRA code for the SMOLENSK-3 reactor state of 25.05.93. For the analyses five different, nearly fully inserted manual control rods were chosen. The calculations were made in two-steps:

- steady-state calculations without LAC-LSS;
- transient calculations with LAC-LSS system in operation.

The comparison of these two calculations demonstrates the capability of the local automatic control (LAC) and local safety system (LSS) to cope with this accident. Five different initial control rod positions were investigated. The changes of the channel neutron power due to full CR withdrawal out of these positions are presented below. The Tables show the core position and the initial insertion depth of the control rod and the neutron power in the adjacent fuel assemblies prior to (upper Table) and after (lower Table) the rod withdrawal. They also present the k_{eff} value of the core after the rod has been withdrawn. The values in the Tables have been generated by steady state analysis. In each case for comparison also the maximum channel power after the rod withdrawal as calculated by the transient analyses are shown.

It may be seen that the steady state calculations without the LAC-LSS show an increase of the neutron power in the nearest fuel channel by a factor of about 3. This is nearly twice as high as the results of the transient analysis.

The increase of the nearest channel neutron power in the transient calculations is less than 100% as a rule. The ECRWA practically doesn't change the global core parameters (see Fig. 81 and 82) but locally the parameters are evidently changed. Fig. 83; and 89-92 demonstrate the change of the parameters in the fuel channel (56-56) next to the CR withdrawn (56-55). The fuel temperature (Fig. 89) rise is significant (the maximum increase is about 400 K), the flow rate in the channel is decreased by 10% (Fig. 91). The maximum clad temperature (Fig. 92) is changed only by about 5K and the neutron power in the channel is increased by about a factor of 2 (Fig. 83). Fig. 84 - 88 show some parameters for the cases of other rods withdrawal. Thus, the typical increase of the neutron power in the nearest fuel assembly in case a manual control rod is erroneously withdrawn from a fully inserted to a fully withdrawn position is about two times the initial value.

- Core position of Control rod 56-55. Initial rod insertion depth 680 cm
Channel power (MW) in adjacent fuel assemblies prior to rod withdrawal

2.38	2.03	2.01
1.86	C R	1.90
	1.52	2.04

Channel power (MW) in adjacent fuel assemblies after rod withdrawal, $k_{eff} = 1.00133$

6.58	6.43	5.84
5.73	C R	6.08/3.69 ²
5.22	4.58	5.53

- Core position of control rod 46-61. Initial rod insertion depth 620 cm
Channel power (MW) of adjacent fuel assemblies prior to rod withdrawal

2.28	2.39	2.21
1.81	C R	1.91
2.34	1.94	2.27

Channel power (MW) of adjacent fuel assemblies after rod withdrawal, $k_{eff}=1.00129$

0	6.62	5.65
4.92	CR	5.45/3.36 ³
5.63	5.28	5.72

- Core position of control rod 32-54. Initial rod insertion depth 670 cm
Channel power (MW) of adjacent fuel assemblies prior to rod withdrawal

1.74	1.61	1.87
1.81	C R	1.86
2.04	2.26	2.04

Channel power (MW) in adjacent fuel assemblies after rod withdrawal, $k_{eff}=1.00081$

3.13	3.25	3.34
3.73/2.29	CR	3.83
3.69	4.59	3.71

² nonstationary calculation with feedback and working LAR-LAP and shutdown system

³ nonstationary calculation with feedback and working LAR-LAP and shutdown system

- Core position of control rod 30-33. Initial rod insertion depth 620 cm.

Channel power (MW) in adjacent fuel assemblies prior to rod withdrawal

2.11	2.04	2.06
1.85	C R	1.87
2.09	1.90	2.08

Channel power(MW) in adjacent fuel assemblies after rod withdrawal, $k_{\text{eff}}=1.00081$

3.64	3.97	3.57
5.55	C R	3.61/2.88 ⁴
3.62	3.72	2.62

- Core position of control rod 60-37. Initial rod insertion depth 650 cm.

Channel power (MW) in adjacent fuel assemblies prior to rod withdrawal

2.12	2.02	2.19
2.12	C R	1.97
2.19	1.43	2.39

Channel power (MW) in adjacent fuel assemblies after rod withdrawal, $k_{\text{eff}}=1.00131$

4.74	5.10	4.89
5.19/3.26 ⁵	C R	4.80
4.72	3.47	5.15

⁴ nonstationary calculation with feedback and working LAR-LAP and shutdown system

⁵ nonstationary calculation with feedback and working LAR-LAP and shutdown system

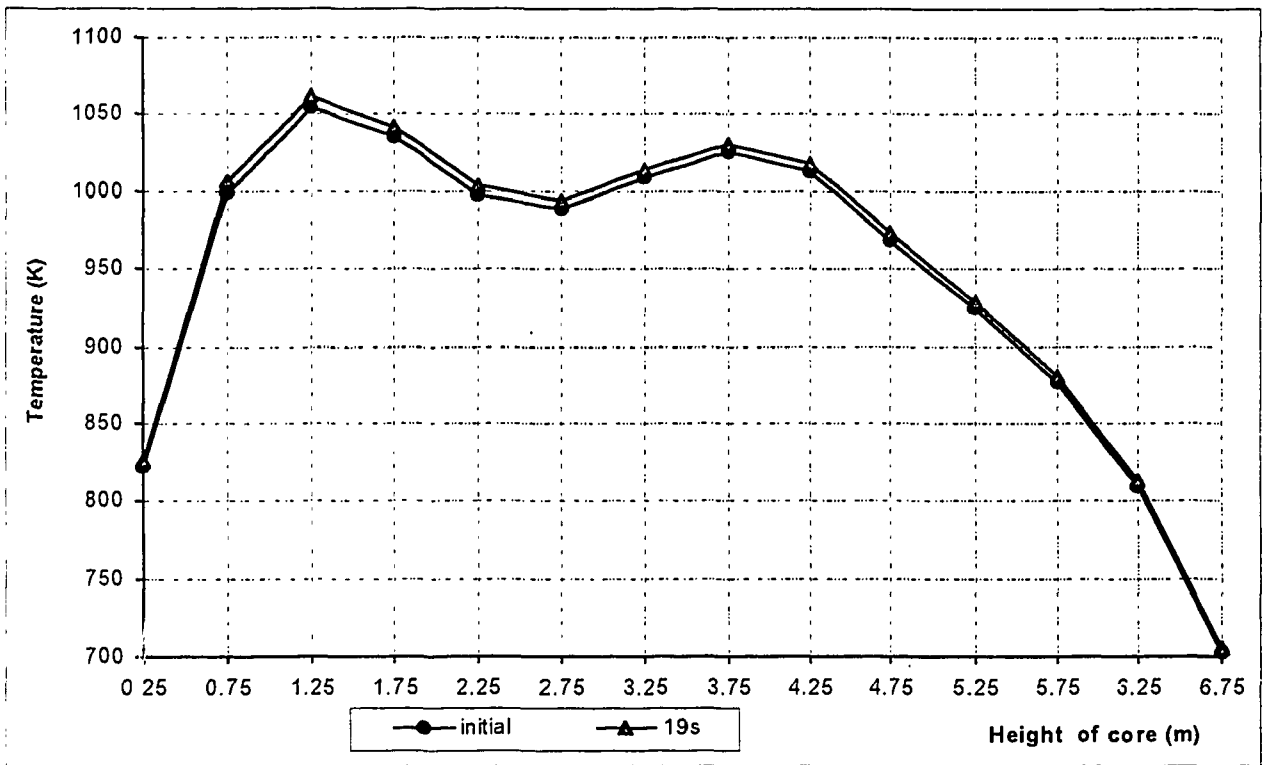


Fig. 81 Erroneous control rod withdrawal. Core average axial fuel temp.; (top of the core at 7 m)

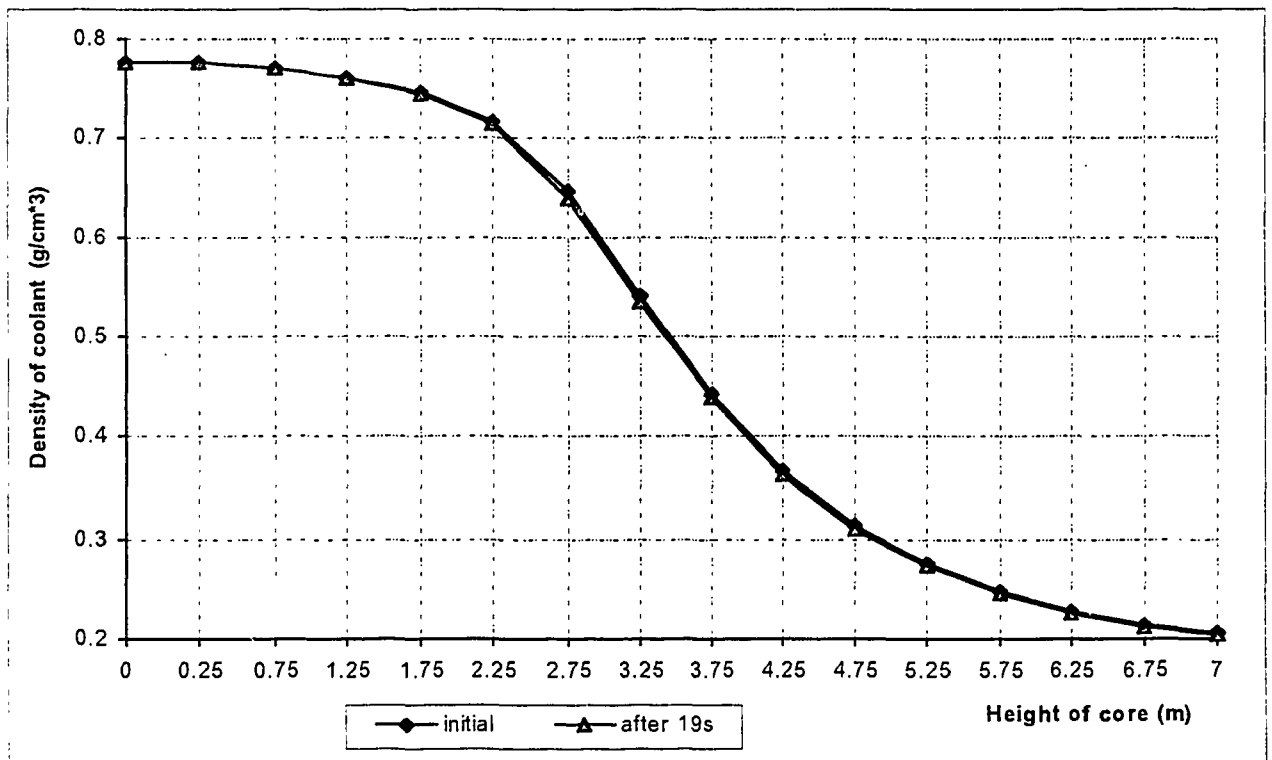


Fig. 82 Erroneous rod withdrawal. Core average axial water density distribution; (top of the core at 7 m)

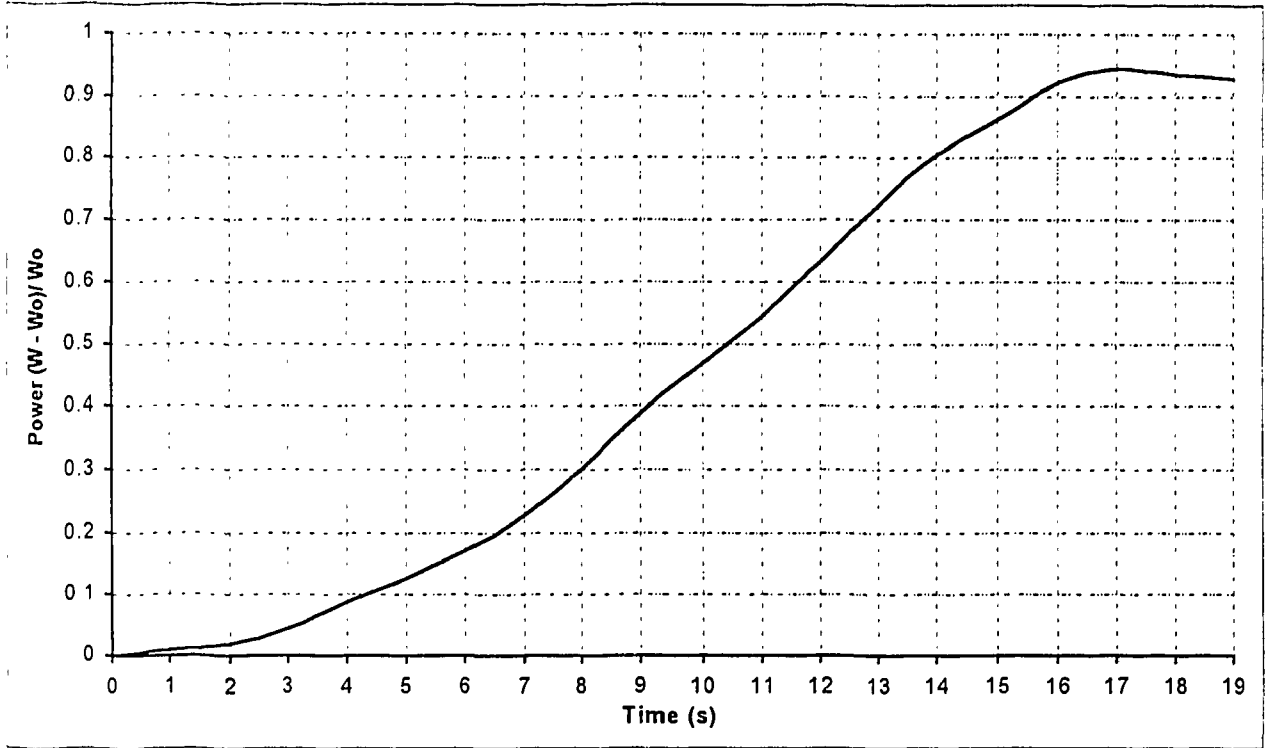


Fig. 83 Erroneous rod withdrawal. Power vs. time in channel 56-56, CR 56-55 withdrawn

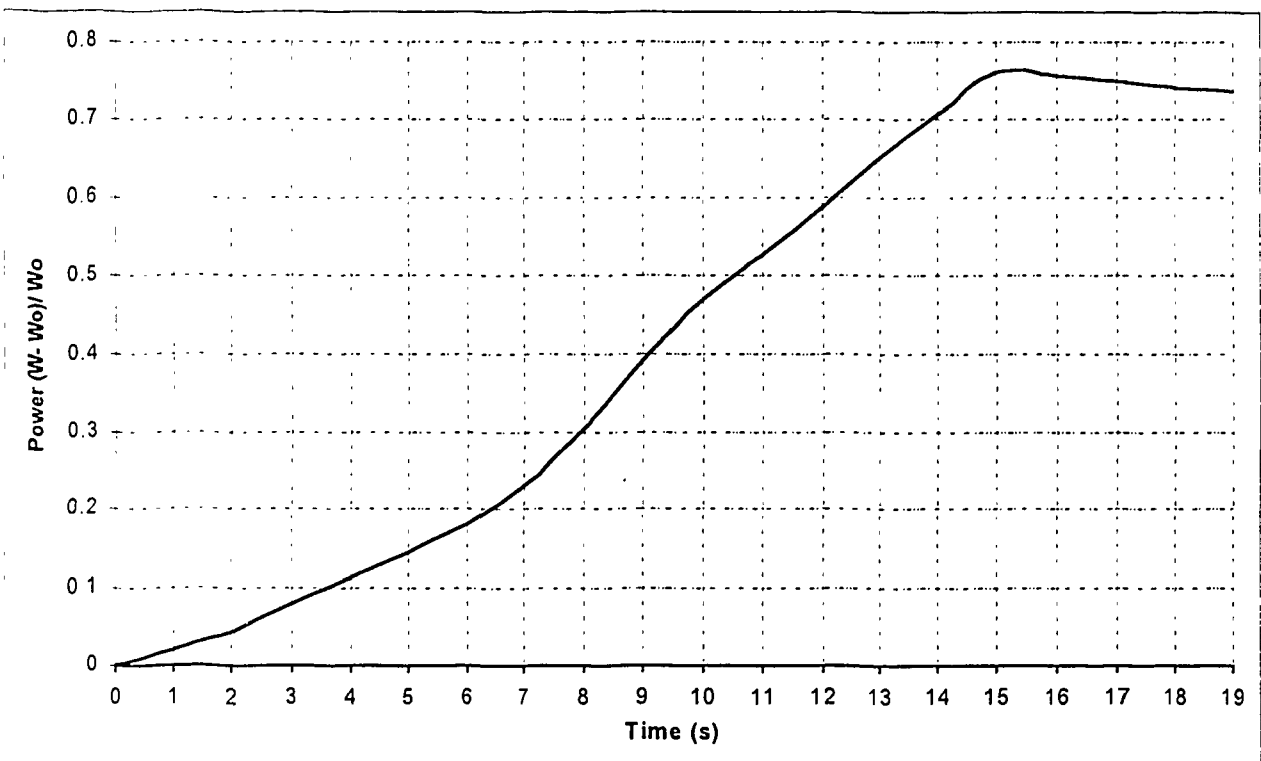


Fig. 84 Erroneous rod withdrawal. Power vs. time in channel 46-62, CR 46-61 withdrawn.

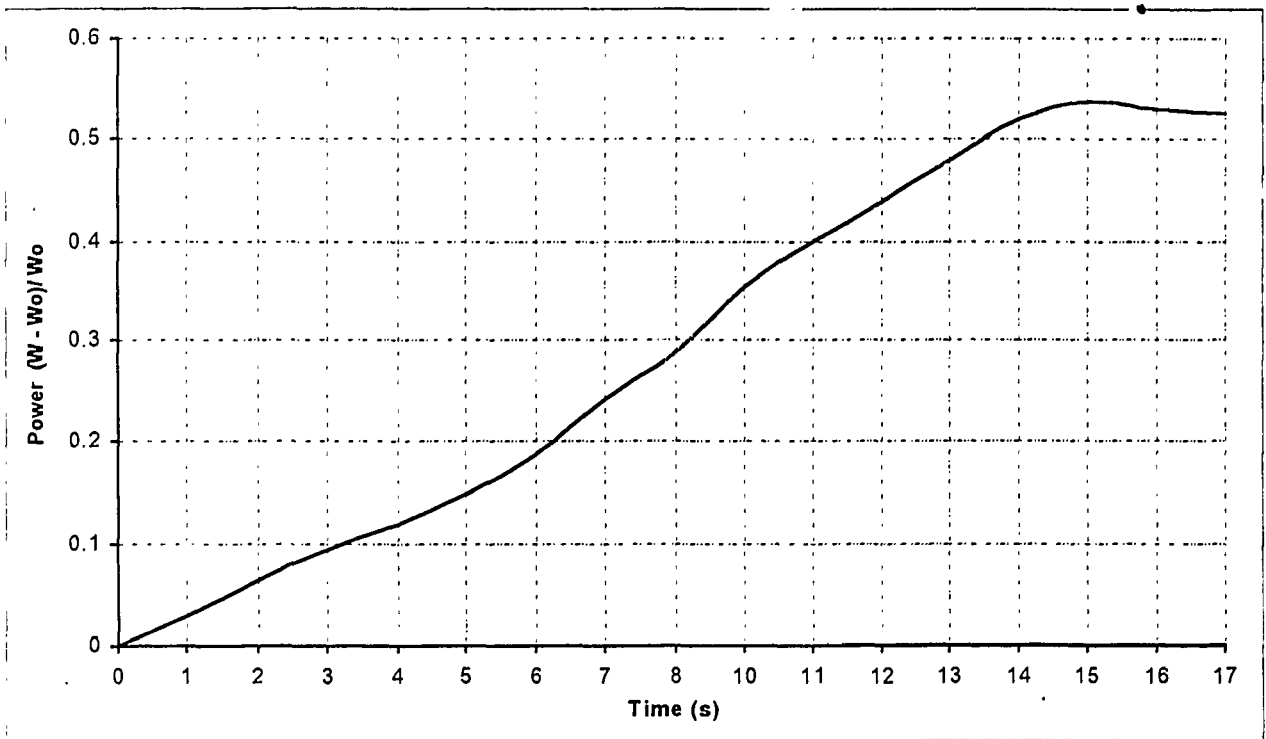


Fig. 85 Erroneous rod withdrawal. Power vs. time in channel 30-34, CR 30-33 withdrawn.

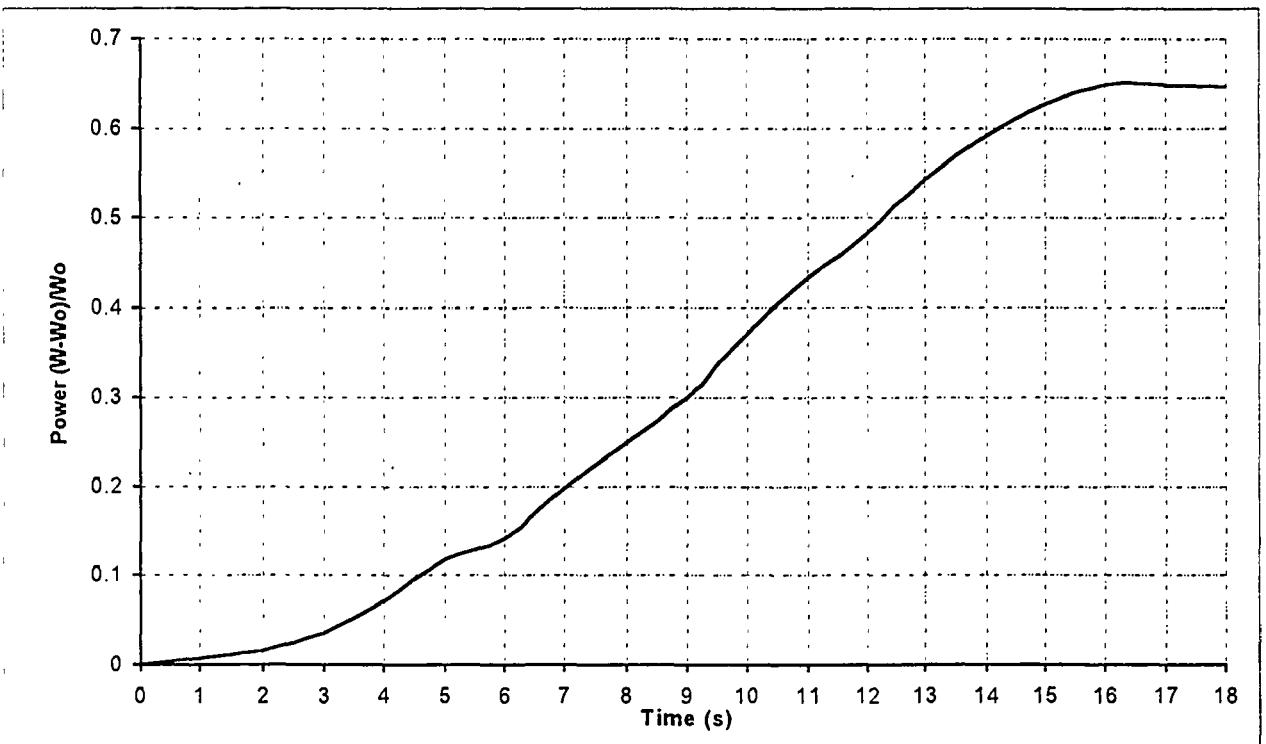


Fig. 86 Erroneous rod withdrawal. Power vs. time in channel 32-44, CR 32-45 withdrawn.

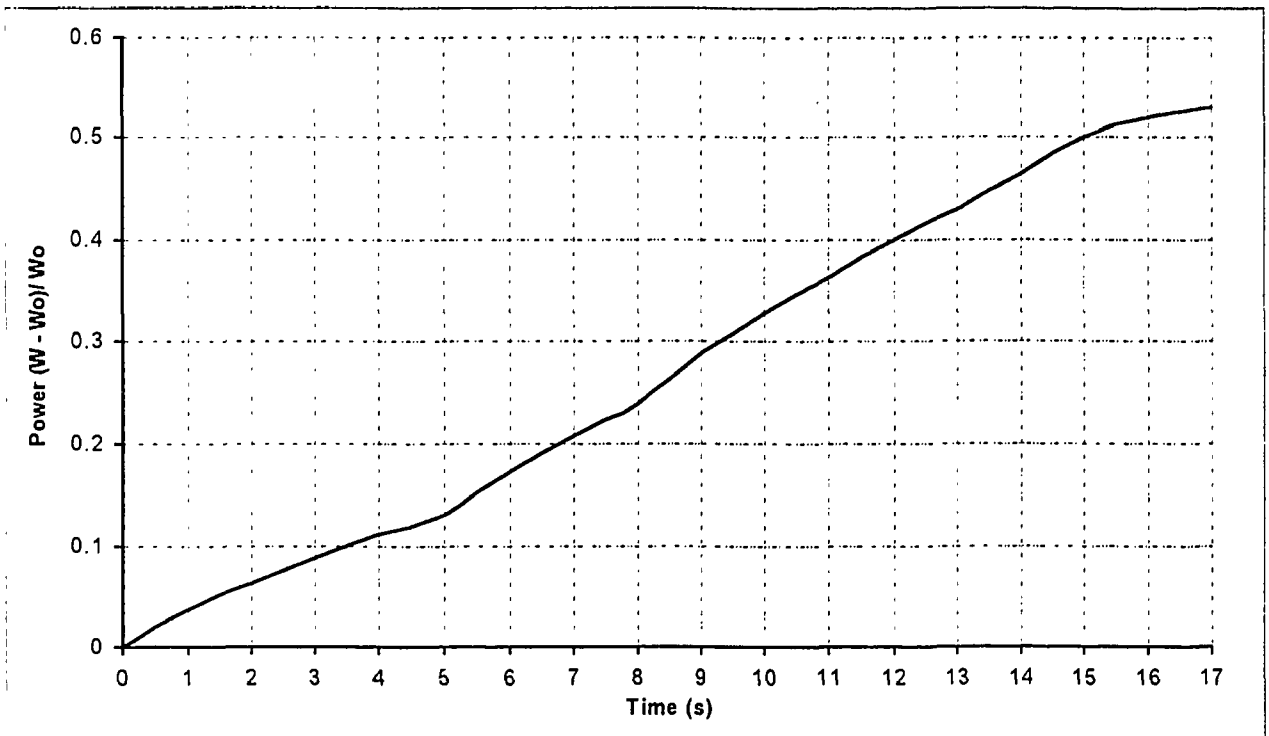


Fig. 87 Erroneous rod withdrawal. Power vs. time in channel 60-36, CR 60-37 withdrawn.

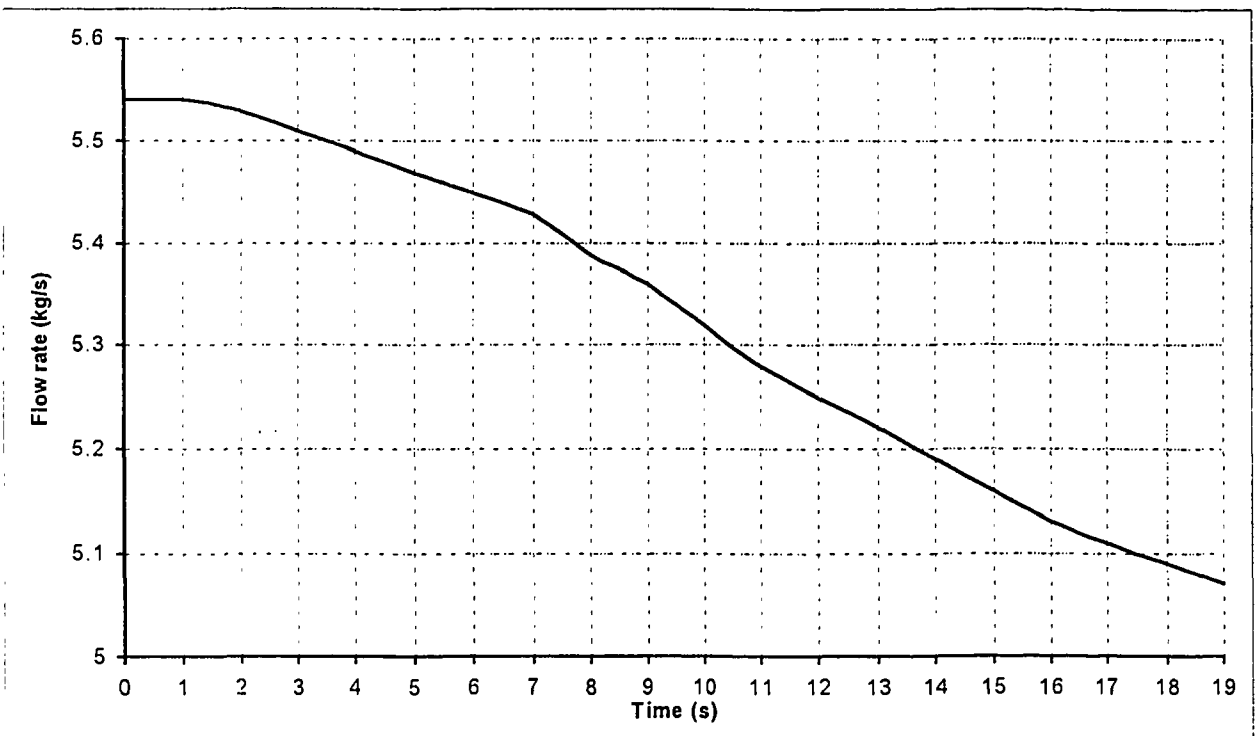


Fig. 88 Erroneous rod withdrawal. Flow rate vs. time in channel 46-62

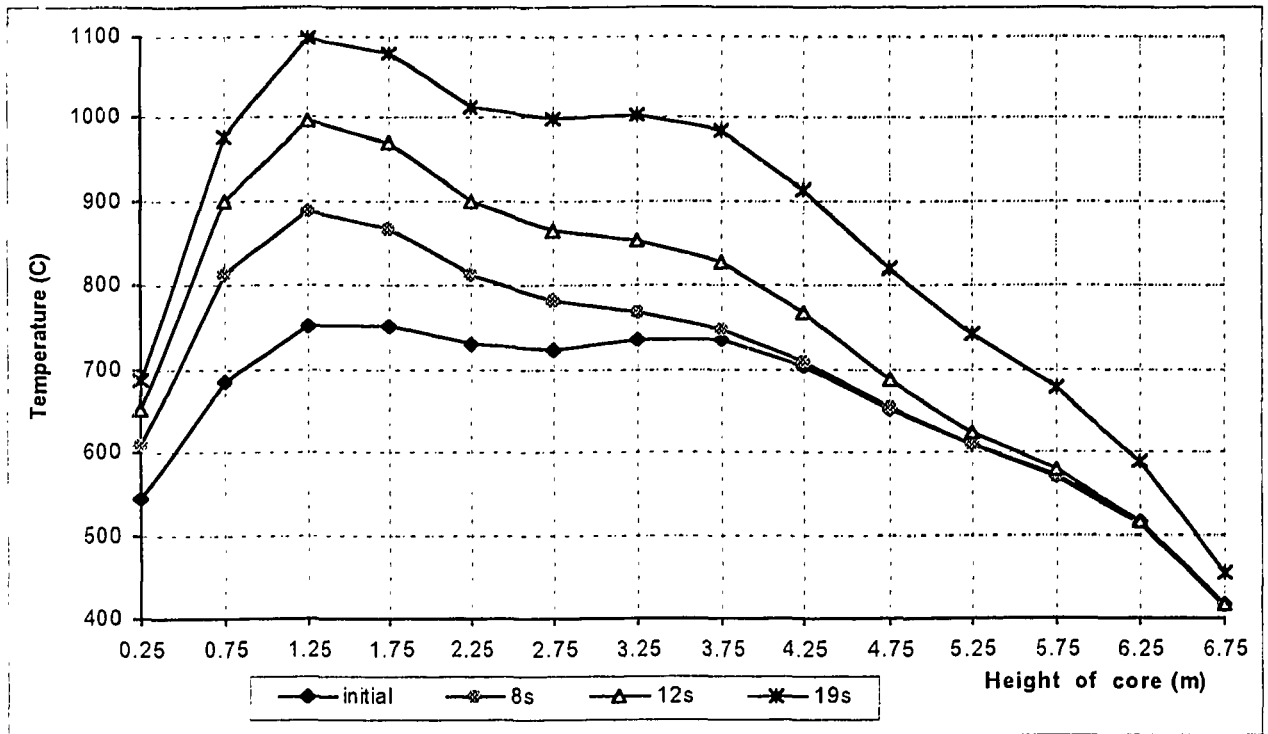


Fig. 89 Erroneous rod withdrawal. Average axial fuel temperature distribution in channel 56-56; (top of the core at 7 m)

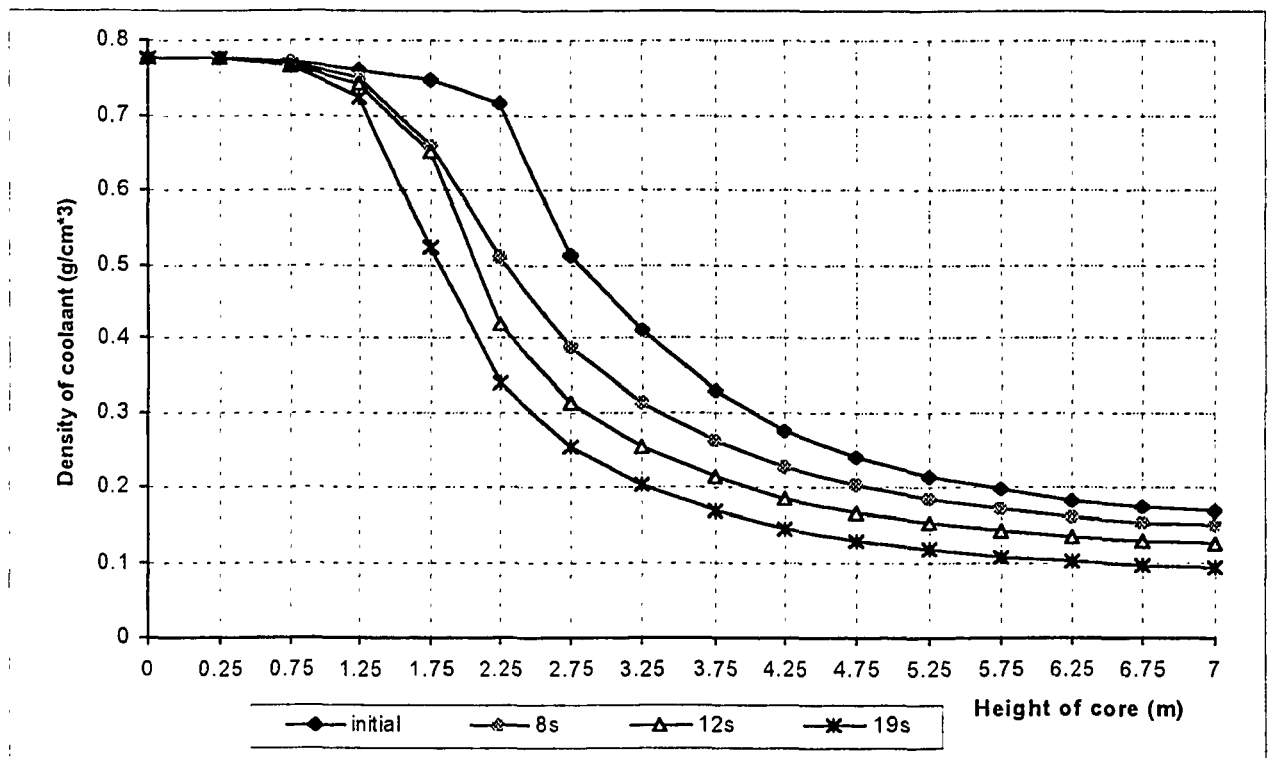


Fig. 90 Erroneous rod withdrawal. Axial water density distribution vs. time in channel 56-56.

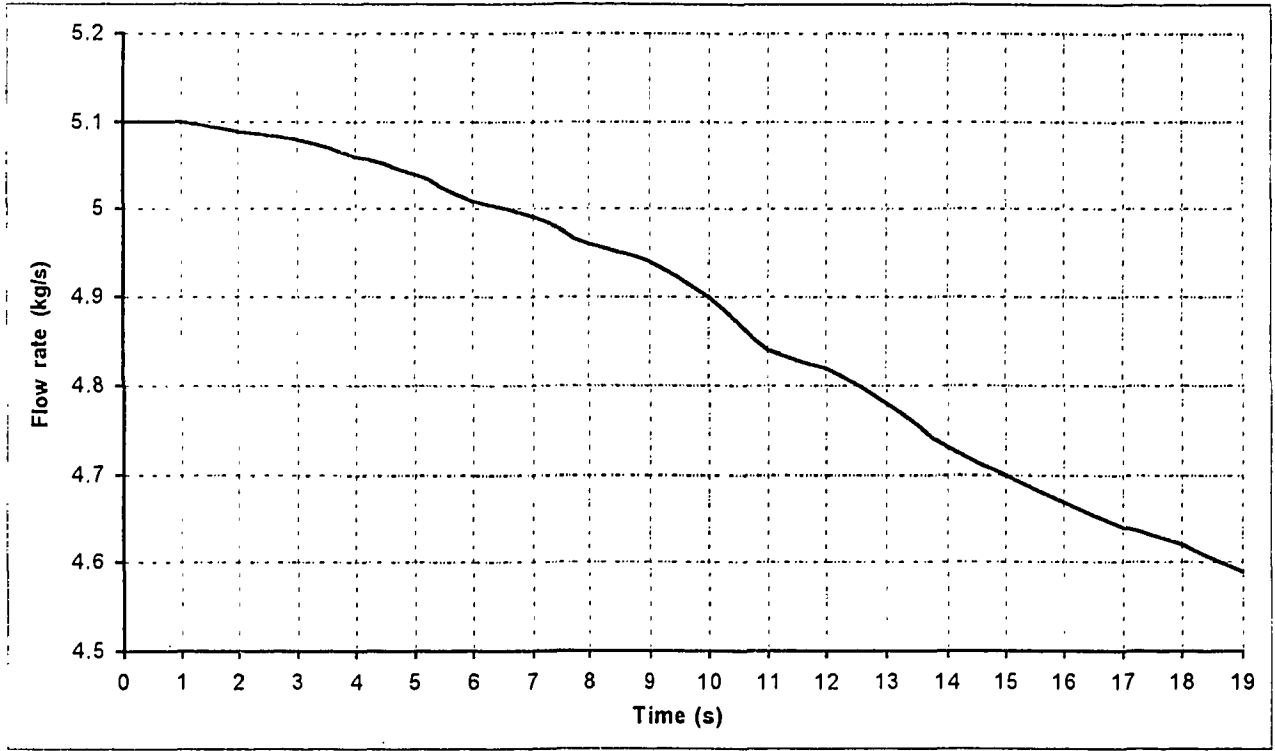


Fig. 91 Erroneous rod withdrawal. Flow rate vs. time in channel 56-56.

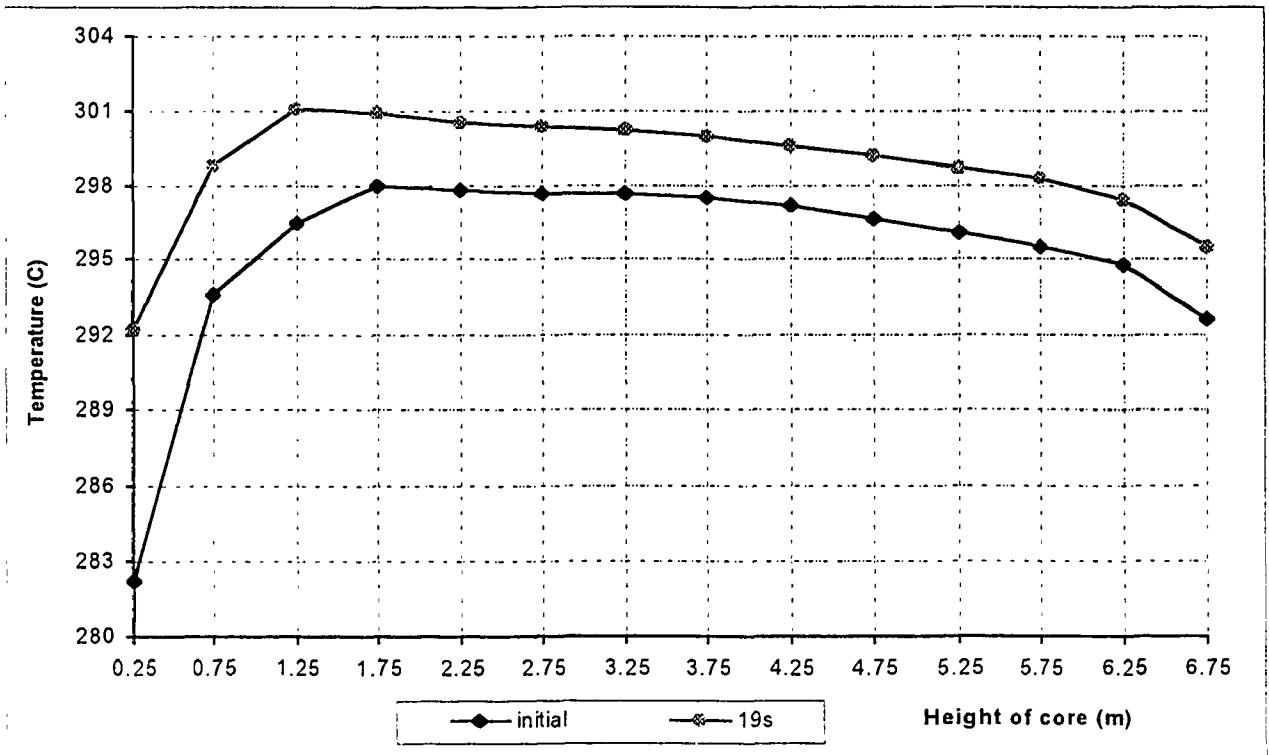


Fig. 92 Erroneous rod withdrawal. Axial fuel clad temperature distribution.

Conclusions

- The Ultimate Design Base Accident (LOCA of MCC) of the SMOLENSK Nuclear Power Plant Unit-3 was investigated. There is no significant power increase in this accident due to the small void reactivity effect. However, as a result and because of the corrective actions taken by the LAC system, there is no neutronic scram signal available to trigger reactor shutdown. The pressure rise in the leak-tight compartment is the only signal to actuate reactor scram.
- The CPS LOCA was analysed for various cases with the time to empty the CPS channels as parameter. If this time (time for the water level to drop from the top to the bottom of the core) is about 40s the reactor is scrammed within 10s after the level reaches the top of the core. The signal used in the analysis is based on neutron power. If the channels are drained within 2.5s a short neutron power burst terminated by the Doppler effect in the fuel at about 80000 MW cannot be suppressed by the shutdown systems. Since the duration of this burst is less than 1 second it is expected that there is no fuel fragmentation. Further analysis is necessary to clarify this question.
- The FSS rods only are not capable to scram the reactor and maintain subcriticality in case of the CPS -LOCA even if it takes 40 seconds for the water level to drop from the top to the bottom of the core.
- The typical local power increase after an erroneous withdrawal of a single manual control rod from its initially fully inserted to a final fully withdrawn position is about 100% in the fuel assembly next to the rod withdrawn. This increase is followed by a rise of fuel the temperature and a decrease of the channel flow rate. The clad temperature practically stays unchanged.

6.4 Transient ARROTTA analysis

Since the ARROTTA version available at the time when the project started did not allow to model moving manual control rods, the transient analysis performed by ARROTTA initially had to be restricted to the CPS LOCA analysis with only the SDS-1 system being available for shutdown.

The code was modified during the course of the project work and now the motion of the RBMK specific control rods may be modeled. As already stated earlier in this report these rods comprise an absorber and a graphite displacer separated from each other by a water region. Absorber and displacer are connected by a telescopic connecting piece. The problem to overcome was the proper modeling of the relative motion of the absorber and the graphite displacer on their way into or out of the core.

Since the fast acting shutdown rods of the SDS-1 don't have displacers the original code version already allowed to properly model their motion similar to LWR control rods. The same is true for the motion of the water level in the CPS channels which may be simply modeled as a group of moving control rods. Moreover, as the primary objective of the CPS-LOCA analysis was to demonstrate how the SDS-1 is able to cope with this accident it appeared desirable to run the case and compare the results with STEPAN analyses.

Two cases were investigated:

- the loss of coolant in the CPS system;
- the loss of coolant in a single CPS channel.

The second case was investigated since the concern was raised that the accident might not be detectable by the CPS system nor recognized by the operator and consequently timely action for mitigation might not be possible.

6.4.1 The loss of coolant in the CPS system.

As in all other transients the initial conditions assumed in the analysis of this accident were the working conditions prevailing on December 28, 1993. After a postulated break of the distribution header near the top of the core the water level in the CPS channels was assumed to drop with uniform velocity from the top to the bottom of the core within 44 seconds. The delay time for the shutdown rods to start moving was assumed to be 0.7 seconds after the signal for high power occurred. Reactor shutdown was provided by the SDS-1 rods only. The SDS-2 rods were assumed to remain in their critical positions prior to the accident.

In agreement with the steady state analysis the core experiences a power excursion after shutdown by the SDS-1 system. The power surge is terminated by the Doppler effect in the fuel only. The peak power occurs at approximately 20 seconds after reactor shutdown and exceeds 5000 MW as shown in Figure 93. After the power excursion is over a new equilibrium power level is established at about 3400 MW. Using the peak coolant enthalpy presented in Figure 94 an estimate of the critical heat flux ratio was made based on a modified Macbeth correlation in use at RDIPE for DNBR analyses. The estimate shows critical heat flux conditions during this accident even though the main circulation pumps keep running at full speed. No attempt was made to further analyze the critical heat flux situation in more detail, since the objective of this analysis was merely to investigate the shutdown capability of the SDS-1. Since shutdown cannot be provided for this accident, SDS-1 does not meet the requirements for a shutdown system regardless of whether the fuel performance criteria are violated or not.

In spite of the fact that ARROTTA seems to underpredict the steady state reactivity insertion caused by voiding the CPS channels ($\Delta\rho=2.8 \beta_{\text{eff}}$) and to overestimate the reactivity worth of the SDS-1 rods ($\Delta\rho=2.5 \beta_{\text{eff}}$) the results of the transient analysis compare quite well with the corresponding STEPAN results.

6.4.2 The loss of coolant in a single CPS channel

For the same initial conditions as above, the analysis was performed under the assumption that a break of a single CPS channel occurs at its upper end and the channel is drained within 44 seconds after the break. Out of the 211 channels of the CPS a channel was selected next to the fuel assemblies with the highest initial channel powers. The analysis was performed for a channel with a fully and a partly withdrawn control rod. No reactor scram was assumed nor was the local protection system and its potential actuation considered.

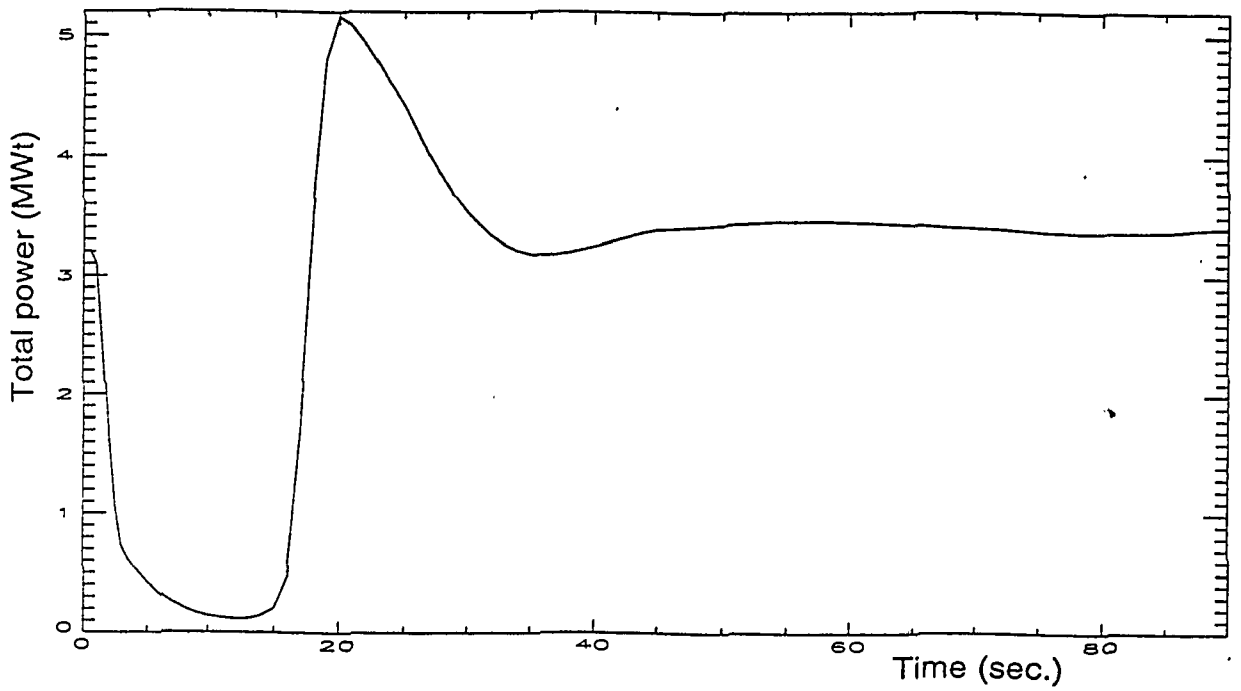
The results are presented in the Figures 95 - 98. The total reactor power increases up to almost 3500 MW for the case of a control rod partly inserted in the broken channel. When the rod was fully withdrawn before the break the maximum power is only 3300 MW. This behavior is explained by the specific design of the manual control rods: if the rod is partly withdrawn, the water column between the absorber and the displacer is located in a core region of high importance e.g. high neutron flux. If the absorbing water column is removed from this region the resulting reactivity increase and consequently power increase will be higher than in the case of the fully withdrawn rod. In this case the displacer will be located in the high importance region of the core and only the gap between the displacer and the channel tube will be filled with water. The amount of water present in the high flux core region before the break is much less and therefore the reactivity effect caused by the loss of this water is less pronounced. For comparison also the loss of water out of a channel housing a short bottom rod partly withdrawn was investigated. In this case there

is no significant effect on reactivity and core power. The impact of the time assumed to empty the channel for the case of the partly inserted manual control rod is shown in Figure 98. Since the total power increase in each case investigated is less than 10% the reactor shutdown system actually will not be actuated under the conditions investigated.

Conclusions

It has to be realized that the analyses presented above are best-estimate and preliminary in nature. Yet the results of the loss of coolant in single CPS channels appear to have surfaced a new safety issue which needs proper attention. The lack of SDS-1 to be able to cope with the CPS -LOCA already has been identified as a concern previously by PSI and IAEA.

In view of the fact that occurrences involving voiding of individual CPS channels already have happened in several RBMK and considering the safety significance of such events it appears absolutely mandatory that further detailed analyses be performed in a systematic way to cover all potential reactivity initiated accidents related to failures in the CPS circuit including air ingress into the system.



Peak nodal power density versus time

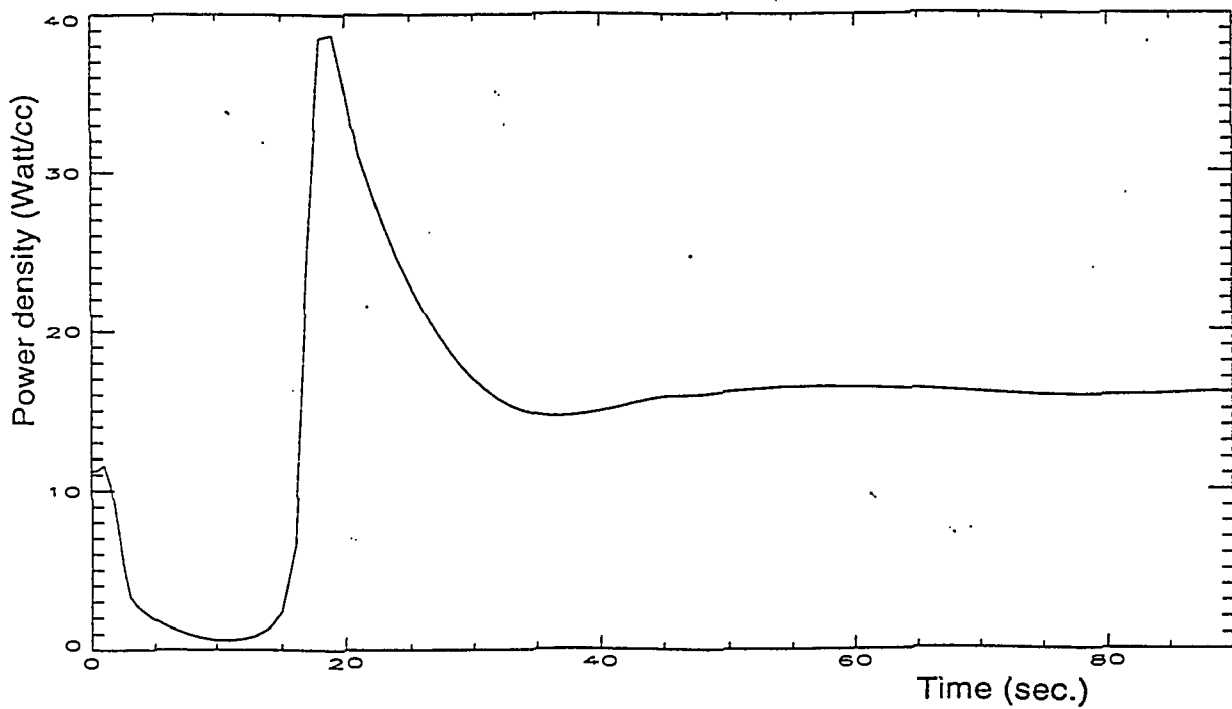


Fig. 93 Total and peak nodal neutron power vs. time during CPS-LOCA. 3D ARROTTA analyses

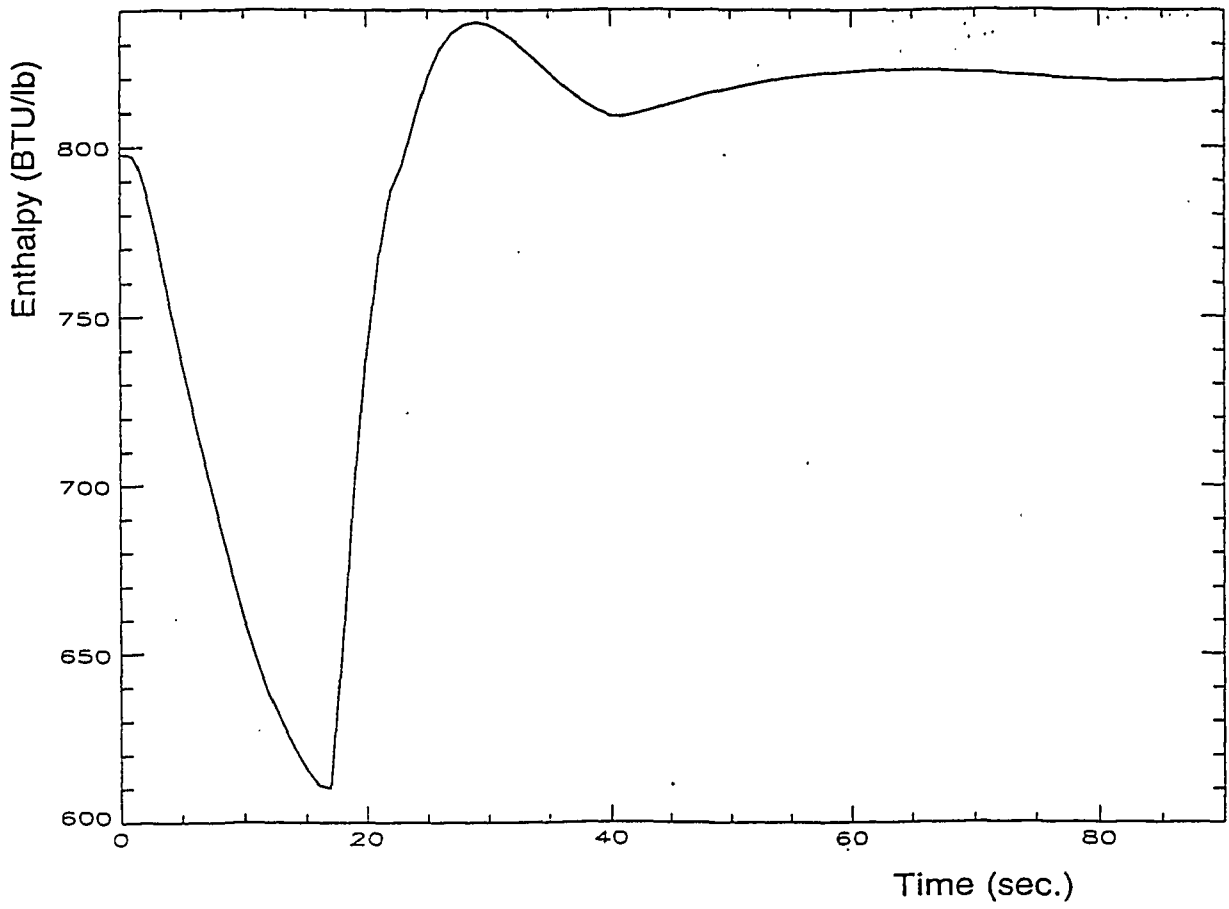


Fig. 94 Peak average coolant enthalpy vs. time during CPS-LOCA. 3-D ARROTTA analysis.

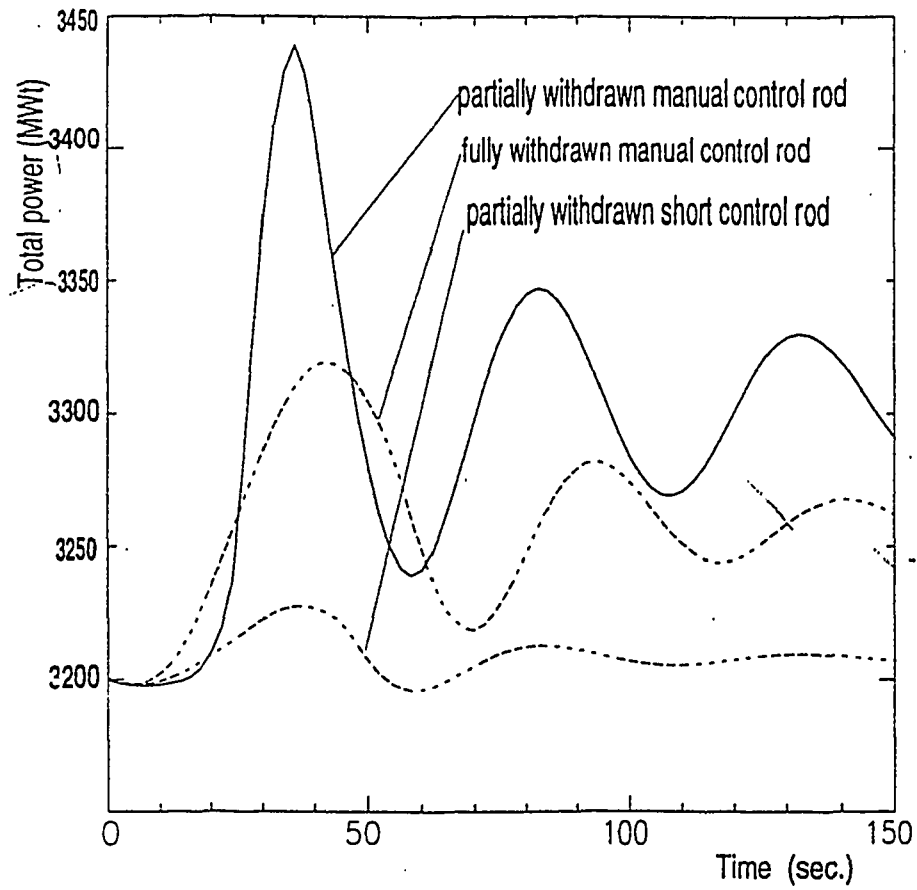


Fig. 95

Total neutron power vs. time during LOCA in single CPS channel. 3D ARROTTA analysis, control rod position as parameter

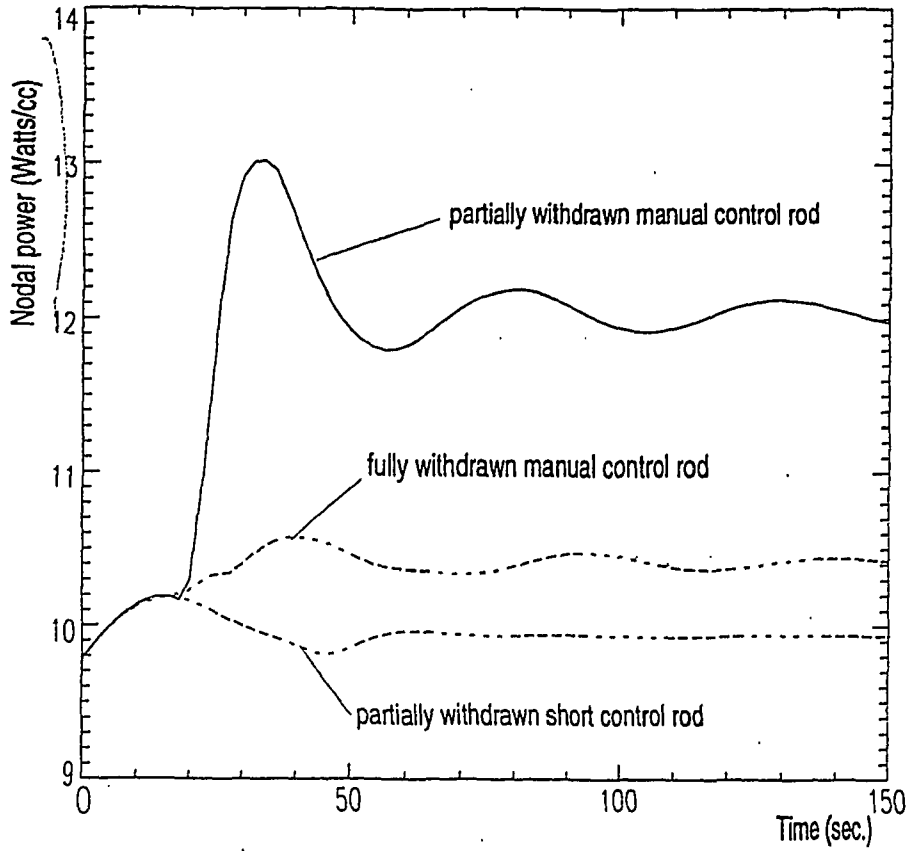


Fig. 96 Peak nodal power vs. time during LOCA in single CPS channel. 3-D ARROTTA analysis, control rod position as parameter.

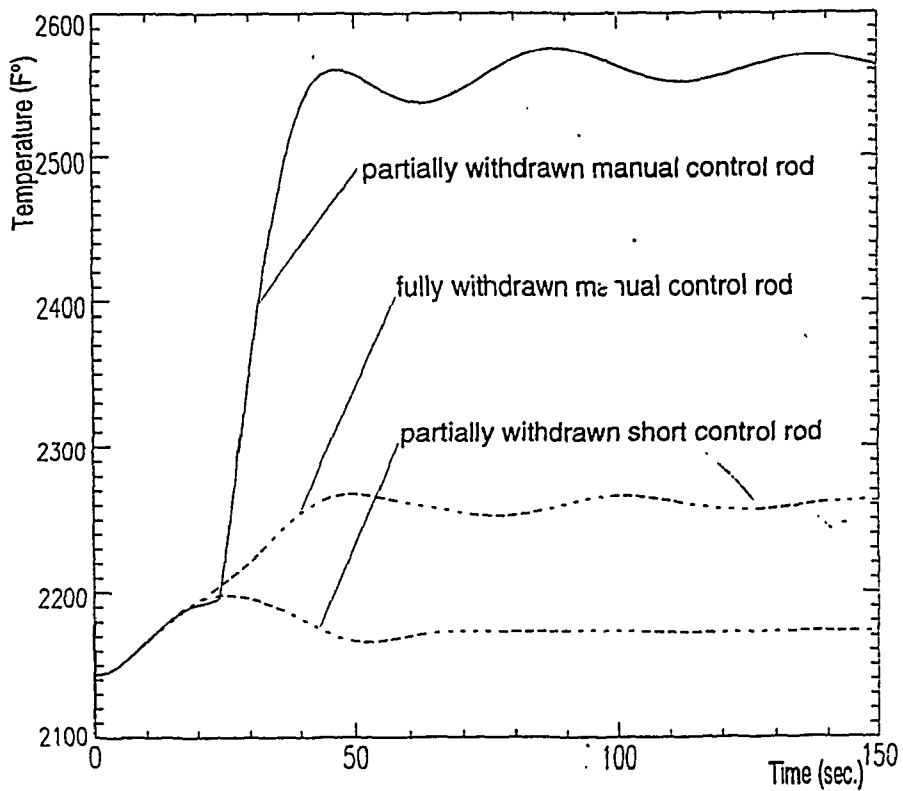


Fig. 97 Peak average fuel temperature vs. time during LOCA in single CPS channel. 3-D ARROTTA analysis, control rod position as parameter.

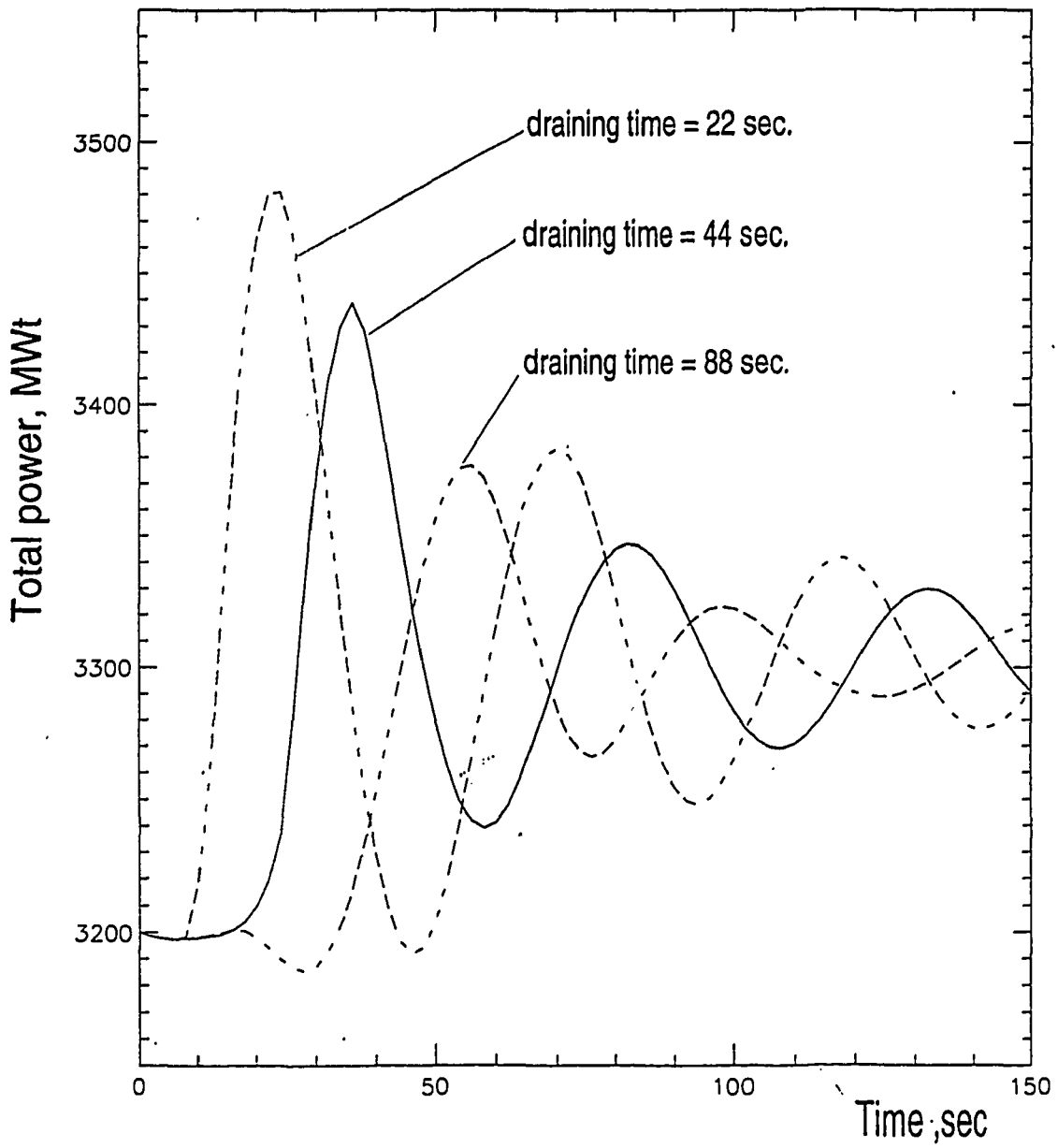


Fig. 98 Total neutron power vs. time during LOCA in single CPS channel.
3-D ARROTTA analysis, partly withdrawn control rod, run-dry time as parameter.

References

- [1] "RBMK shutdown systems", Report of a consultants meeting held in Switzerland in December 1993. IAEA-report RBMK-SC-013, Limited distribution, 1995-2-1.
- [2] L. D. Eisenhart: "ARROTTA-01-An advanced Rapid Reactor Operational Transient Computer Code", Computer Code Manual, NP-7375-CCML, Vol. 2, June 1991
- [3] E. Knoglinger, D. Saphier, D. Hennig: "Evaluation of the SMOLENSK-3 NPP Shut Down System", Phase 1: Code Implementation and Testing, PSI Bericht Nr. 94-17, Oktober 1994, ISSN 1019-0643
- [4] Langenbuch S., Maurer W.: "Quabox-Hyca-01, Ein dreidimensionales Kernmodell mit parallelen Kühlkanälen für Leichtwasser Reaktoren - Programmbeschreibung", GRS - A-445 (April 1980)
- [5] "Investigations of physical characteristics of the SMOLENSK-NPP Unit 3 Reactor during physical start up", Physical Start Up Commission, Deznogorsk 1989.
- [6] "Code on the Safety of Nuclear Power Plants: Design", IAEA Safety Series No. 50-C-D (Rev.1) IAEA, Vienna 1988.

Appendix 1

A1. Verification of the full-scale neutronic thermohydraulic code

This paper presents the description of the full-scale neutronic-thermohydraulic code STEPAN + KOBRA. This code is used for static and transient calculation of the RBMK-reactor including accident analysis. The neutronic part of the code describes the core in the 3-D-geometry in two group diffusion approximation. This code includes the description of the LAR and LPS system logic. The code uses the cross section library which allows to describe all (regular and accident) situation without geometry change. The thermohydraulic part of the code is KOBRA. KOBRA uses 4 equations for the description of the two-phase coolant flow. The different velocity of phases is taken into account by slip model correlation. The code KOBRA describes all 1661 channels of the reactor and main equipment of the circulation circuit. This paper presents the results of the code verification STEPAN and KOBRA and verification results of the joint STEPAN + KOBRA work.

A 1.1. Introduction

The code STEPAN is used for neutron reactor calculation of RBMK. The following tasks are solved by STEPAN:

- the static calculation of the reactor (k_{eff} -task);
- the adjoint fluxes determination;
- the calculations of neutron fields for subcritical reactor with internal neutron source (spontaneous fission);
- quasi-static calculations of xenon build up and decay;
- optimization of neutron fields by control rod movement;
- time-dependent calculations of fast transients;
- fuel reload and burnup management.

Two-energy group diffusion approximation in two or three dimensional geometry is used in the code. The equations are solved by a traditional finite-difference scheme. One point per cell in x-y and 16-32 points in axial direction are used in this scheme.

The task of group cross section calculation has a special meaning for RBMK because of the presence of absorbers in the core. The number of absorbers was increased after the implementation of measures to increase reactor safety. The traditional way to generate the cross sections is to calculate them for a unit cell and to use them in the finite-difference scheme with one point per cell. But this way does not give good results for RBMK. Therefore it is supplemented by a special system of correcting the diffusion coefficient and some cross sections on the basis of experimental data on integral characteristics. After such correction good results may be obtained.

A1.2 The description of methods used and some results of the code

STEPAN verification.

A1.2.1 The equations used.

To describe the neutron transport the diffusion equations are used

$$\frac{\partial \Phi_1}{V_1 \partial t} = \nabla_z D_{1z} \nabla_z \Phi_1 + \nabla_{xy} D_{1xy} \nabla_{xy} \Phi_1 - \Sigma_1 \Phi_1 + \sum_{K=1}^4 (1 - \beta_K) \cdot (v \Sigma \frac{K}{f_1} + v \Sigma \frac{K}{f_2}) + \sum_{l=1}^{24} \lambda_l C_l$$

$$\frac{\partial \Phi_2}{V_2 \partial t} = \nabla_z D_{2z} \nabla_z \Phi_2 + \nabla_{xy} D_{2xy} \nabla_{xy} \Phi_2 - \Sigma_2 \Phi_2 + \Sigma_{12} \Phi_1 \quad (1)$$

$$\frac{\partial C_l}{\partial t} = \beta_l \cdot (v \Sigma \frac{K}{f_2}) - \lambda_l C_l$$

All notations in equation (1) are well-known. As a rule the anisotropy of neutron diffusion in RBMK lattice is not taken into account because it is negligible. But in our case it is considered. The reason is that the corrected diffusion coefficient used are strongly different for radial and axial directions. The equations (1) are solved by transformation in finite-difference form. To discretize the time-dependent part of the task the implicit scheme or quasi-static method is used. For the last case the time derivatives of form-function are not excluded and the point kinetic task to find amplitude factor is solved by the method of Hansen. Neutron cross sections in equations (1) are functions of temperatures of fuel and graphite, the concentration of xenon, burnup and the density of coolant. From all parameters mentioned the calculation of the coolant density is the most complicated problem. It is solved by the thermohydraulic code KOBRA. The KOBRA thermohydraulics code is based on a thermal non-equilibrium and mechanically inhomogeneous model. The model incorporates four basic conservation equations, i.e., conservation of mixture mass, mixture momentum, mixture energy and liquid phase energy. The assumption is used that in two-phase flow the steam is always saturated. The various velocity of phases is taken into account by a slip model.

$$\frac{\partial \rho}{\partial t} + \frac{\partial G}{A \cdot \partial X} = 0$$

$$\frac{\partial G}{\partial t} + \frac{\partial}{\partial X} \left(\frac{G^2 \cdot Z_v}{\rho A} \right) = -A \frac{\partial \rho}{\partial X} + \rho \beta_x A - \xi \frac{G^2}{\rho A^2}$$

$$\frac{\partial \rho \cdot I}{\partial t} + \frac{\partial G I R_v}{A \cdot \partial X} = \frac{\partial \rho}{\partial t} + \frac{\partial P}{\partial X} \cdot \left(\frac{G_g}{\rho A} + \frac{G_f}{\rho_f A} \right) + Q + DISS_f + DISS_g$$

$$\alpha_f \rho_f + \frac{\partial I}{\partial t} + \frac{G_f}{A} \cdot \frac{\partial I_f}{\partial X} = \alpha_f \left(\frac{\partial P}{\partial t} + V_f \frac{\partial P}{\partial X} \right) + Q_{wf} + Q_{if} - \Gamma_{ig} T_f^* - \Gamma_w T \frac{s}{f} + \Gamma_g T_f + DISS_f$$

where

- f - index of liquid phase
- g - index of vapor phase
- s - saturation line
- w - channel wall
- i - the boundary of phase separation
- I - enthalpy
- P - pressure
- G - mass flow
- A - cross-section for the flux
- R_v, Z_v - coefficient taking into account the phase slip

V	- velocity
DISS	- dissipation of energy
Q	- inter-phase or wall-and-fluid energy exchange
T	- temperature
t	- time
x	- distance
Γ	- vapor generation
α	- void fraction
β	- gravitation force
ξ	- wall friction factor
ρ	- density

To complete the equation system constitutive equations for hydraulic resistance and interphase heat exchange and their dependencies on flow regime were implemented. Thermal conductivity was considered for one average fuel pin in each assembly. Similar to the full scale neutronics nodalization, the thermohydraulics configuration has one nodal channel for each coolant tube. Each nodal channel consists of 32 nodes (14 in core and 18 for water and water-steam lines). The total number of channels was 1661, and total number of nodes was about 53152. Boundary conditions may be used on steam drums and group distribution headers. Besides the description of main equipment of the circuit is also possible. If a stationary problem is solved then the stationary thermohydraulic code KOHTYP is employed in connection with STEPAN. The code KOHTYP was written by A.A. Apresov. This code is capable to describe the stationary coolant flow in all 1661 channels. There is a possibility to use the experimental flows from data base of NPP as input data for calculations. To find iodine-135 and xenone-135 concentrations the ordinary equations are used.

A1.2.2. The library of two group cross sections

Two group cross sections are determined by the WIMS-D4 code as functions of temperatures of fuel and graphite, burnup, xenon-135 concentration and the density of coolant. The cell of 25x25 cm is considered and reflector boundary conditions are used. To calculate a cell with an absorber or other non-multiplying cells the configuration consisting of this cell and the surrounding multiplying zone is considered. The reflector conditions are employed at the external boundary of the surrounding zone but cross section weighting is made around the subzones of the cell with non-multiplying channel. So these cells are calculated with boundary conditions similar to ones in the reactor. Two group cross sections are expressed as polynomials of the parameters mentioned above. The application of these cross sections in diffusion code with one point per cell has shown some systematic discrepancies. The worth of the absorbers is lower and the k_{eff} for critical states is larger by 2-3% than one. To exclude these discrepancies more sophisticated new calculation methods for reactor systems like RBMK are worked out. These methods lead to more complicated finite-difference equations and procedures for obtaining cell parameter. This work is not completed now and the efficiency of new methods is not clear understood. So the approach was chosen where one supposes that the discrepancy of the traditional finite-difference scheme with one point per cell can be explained by inaccurate description of neutron leakage between the cells. The diffusion coefficients obtained by Σ_v - average approximation are corrected then on the basis of comparison of calculations of simple systems (supercells, critical assemblies) by finite-difference codes with more precise codes or results of experiments. Special experiments were chosen for this purpose. This correction results in increasing of diffusion coefficient in radial direction by a factor of about 1.5. the exact value depends on the type of the cell. Besides another correction is implemented to $v\Sigma_2$ to increase the void reactivity of infinite lattice. This correction arises from comparison of calculations and experiments on the void reactivity coefficient. The library of two group cross sections made after these corrections is used for reactor calculations.

A1.2.3 Steady-state calculations

Let's consider the results of critical assembly parameters calculated by STEPAN. These critical assemblies were investigated in a special critical facility. Assemblies of various size from 18 to 192 fuel assemblies were studied. The average deviation of k_{eff} calculated for critical state is 0.3%. Maximum deviation of k_{eff} is 0.6%. Average deviation of void reactivity effect (fuel channels were dewatered only) is 0.4%. The average deviation of neutron fluxes calculated from measured one is 6%. Maximum deviation of neutron fluxes calculated from measured one is 10%.

The results of the k_{eff} calculations for RBMK reactors at power are given in Table A1.1. The detailed information about core loading, burnup distribution, the locations of control rods and flow of coolant through the channels from the data base of NPPs was used in these calculations by STEPAN.

Table A1.1: The results of k_{eff} calculation by STEPAN for RBMK on power

N	Reactor, State	Loading		AA**	k_{eff}
		2.0% FA*	2.4% FA		
1	Sm NPP-2,23.03.90	618	960	83***	1.0015
2	Ch NPP-1,22.01.92	707	885	101***	1.0018
3	Ch NPP-3,22.01.92	607	958	96***	1.0024
4	Ig NPP-1,19.07.91	1604	-	57***	1.0043
5	Ig NPP-1,23.01.92	1608	-	53***	1.0058
6	Ig NPP-1,29.01.92	1608	-	53***	1.0055
7	Ig NPP-1,02.04.92	1606	-	55***	1.0023
g	Ig NPP-2,06.06.91	1606	-	55***	1.0066
9	Ig NPP-2,23.01.92	1606	-	55***	1.0063
10	Ig NPP-2,02.04.92	1606	-	55***	1.0069

*FA fuel assembly, 2.0% or 2.4% enrichment.

**AA additional absorbers which were implemented into the core to decrease void reactivity effect.

*** the number of additional absorbers includes the empty channels (water columns) also.

A1.2.4 The neutron field reconstruction according to readings of neutron flux in core detectors.

The small deviations readings of neutron cross sections may result in large deviations of neutron flux in RBMK and other large reactors. Even though k_{eff} is determined accurately, the neutron fluxes calculated and measured by in-core detectors have usually deviations of about 15%. The analysis shows that the deviations have smooth form. So one can conclude that small errors of the calculating model result in exciting of lowest modes of neutron distribution. These small errors may be due to:

- technological parameter deviations which are not taken into account;
- an inadequacy of the mathematical model.

The reason of these errors apparently can not be completely removed. To take it into account and to increase the accuracy of forecast calculations the procedure of the neutron flux distribution reconstruction by correction of macroscopic cross sections on the base of in-core detector readings is used. The value of this correction should be restricted in the sense of their reasonability. So the task of reconstructing the calculated neutron fluxes to improve the agreement with the measurements by cross section correction is a non-linear optimization task.

This task is solved in STEPAN by a special algorithm.

A1.2.5 Calculation of reactivity effects and coefficients

When the reactivity effects for real reactor states are calculated by STEPAN code the usual sequence is:

1. Steady-state calculation
2. The reconstruction of neutron field
3. Calculation of adjoints fluxes
4. Determination of reactivity effects and coefficients

The results of reactivity coefficients calculation are given in Table A1.2. The experimental values are given in brackets for the states where they have been measured $\alpha_\varphi = \frac{\partial K_{eff}}{\partial \varphi}$ -void reactivity

coefficient, where φ is the volumetric steam content, $\varphi = 0$ for the condition without steam and $\varphi = 1$ for the condition when channel is filled by steam only. So φ is expressed in relative units and changed from zero to 1.

Table A1.2: Reactivity coefficients and effects for RBMK reactor calculated by STEPAN

	Reactor State	α_φ	α_w	α_g	α_γ	$\Delta\rho$	$\frac{\partial\rho}{\partial t}$	β_{eff}
		β_{eff}	10^{-4}	10^{-5}	10^{-5}	β_{eff}	β/s	10^{-2}
			β/MW	$1/K$	$1/K$			
1	Sm NPP-2,23.03.90	1.0	-3.0	4.6	-1.5	1.1	-2.3	0.58
2	Ch NPP-1,22.01.90	0.5	-4.8	4.8	-1.5	0.7	-1.9	0.59
3	Ch NPP-2,22.01.92	0.5	-3.4	4.4	-1.5	0.6	-2.2	0.59
4	Ig NPP-1,23.01.92	0.7	-2.2	4.1	-1.5	0.8	-1.9	0.60
5	Ig NPP-1,23.01.92	0.8	-2.0	3.9	-1.5	0.8	-2.1	0.60
6	Ig NPP-1,29.01.92	0.8	-2.0	3.9	-1.4	0.8	-2.0	0.60
7	Ig NPP-1,02.04.92	0.6	-2.6	4.1	-1.4	0.8	-2.0	0.60
8	Ig NPP-2,06.06.91	1.2	-2.8	4.8	-1.5	1.3	-2.2	0.59
9	Ig NPP-2,01.01.92	0.7	-2.0	4.0	-1.4	0.8	-2.2	0.60
10	Ig NPP-2,04.04.92	0.7	-2.0	3.9	-1.4	0.7	-2.1	0.60

α_w - prompt power reactivity coefficient. This value includes the contribution of void reactivity coefficient and Doppler coefficient α_γ .

α_g - graphite temperature reactivity coefficient

$\Delta\rho$ - void reactivity effect when the whole core is dewatered.

$\frac{\partial\rho}{\partial t}$ - the speed of shutdown system.

It is equal to reactivity inserted during the first second after the shutdown start. The value of effective part of delayed neutrons β_{eff} is given in Table too. This value is calculated for these states to take into account the special features of reactor load. One can see that this value is about $0.6 \cdot 10^{-2}$ and is larger than value $0.5 \cdot 10^{-2}$ used earlier/8/. Due to taking into account ^{238}U .

The void reactivity coefficient as a rule is smaller than 1β . The slight larger values for individual states may be explained by the specific distribution of the operative reactivity margin. The speed of the shutdown system for all states is about $2\beta/s$. So the calculations described permit to predict the reactivity effects and coefficients of RBMK by STEPAN.

A1.2.6 The time-dependent calculations

There is special task for PWR three-dimensional space kinetic verification. One group of absorbers is withdrawn and another group begins to insert into the core after the time interval $\Delta t = 7.5s$. The initial state is stationary. The maximum reactivity variation during this process is about 0.1β . The transient has the form of smooth burst. The average power densities over the core calculated by STEPAN and CUBBOX code were compared. A good agreement was obtained. The maximum deviation is about 3%.

One of the design accident in RBMK is the spontaneous withdrawal of control rod (SWCR). To verify the results of calculations of local power density increase near the SWCR the experiments were performed in Smolensk NPP-2. The control rod was withdrawn to the upper position rapidly in one of the experiments. The increase in power density was 1.8 relative to initial value. The calculation by STEPAN gives the value of 1.72. The perturbation which was made by this withdrawal was compensated by the LAC system. This system consists of 12 rods distributed uniformly in the core. The nearest rod in LAC was switched off in this experiment. The calculations show that STEPAN gives quite good prediction of power density burst near the SWCR and fluctuations of neutron distribution over the core.

Table A1.3: The location of control rods of the LAC system in the beginning and at the finish of control rod 34-27 withdrawal

	SLR rod co-ordinates	The initial position (sm)	The final position (sm) (calculation)	The final position (sm) (experiment)
1	62-31	270	250	270
2	62-45	290	310	270
3	46-15	170	230	230
4	46-31	250	430	400
5	46-45	230	230	250
6	46-61	250	250	250
7	32-15	140	460	440
8	32-31	200	200	200
9	32-45	260	380	340
110	32-61	270	270	250
11	16-31	240	360	370
12	16-45	230	230	230

The modelling of the first phase of Chernobyl accident was made by STEPAN/8/. The information about the initial state used included the in-core detector of neutron flux readings, the locations of control rods, the distribution of burnup. The insertion of the control rods began at 1h.23m.40s. according to the signal of reactor shutdown (AZ-5). The positive reactivity inserted by control rods in the initial state of their movement resulted in the neutron power increase. This increase resulted in steam formation and increase of void reactivity due to positive void reactivity effect. The maximum reactivity about 1.5β and the neutron power about 25 nominal values. The disruption of the core is not modelled and the power burst is stopped by Doppler effect.

A feedwater flow perturbation is used in the procedure of void reactivity coefficient measurement. Automatic control rods are moved to compensate perturbation. This process was calculated by

STEPAN + KOBRA code. The state of the Ignalina NPP-2 for 09.04.92 was taken. The reactivity change due to a void fraction change was compensated by AR-2 automatic regulators. The short control rods which are inserted from the bottom are used as AR-2 rods in Ignalina NPP-2. Each rod is managed by separate out of core detector. This procedure of measurements was modelled by three dimensional STEPAN code with thermohydraulic module KOBRA. The real and calculated deviations of each control rod AR-2 are presented in Table A1.4.

Table A1.4: The real and calculated deviations of each control rod AR-2

Control rod coordinates	experiment				calculation			
	16-33	32-33	16-17	32-17	16-33	32-33	16-17	32-17
Deviation, cm	0	-10	-45	-35	0	0	-52	-57

As a result of perturbation of feedwater flow (+508 t/h) control rods changed their position. It may be seen that the main deviations were for control rods 16-17 and 32-17. The same is in calculations. This shows us that the description by the code of the thermohydraulic perturbation and the neutronic reaction is rather good.

A1.2.7 Fuel management

The fuel management is one of the tasks of RBMK neutron calculations. It permits to get the fuel consumption and neutron field changing forecast. So the long time consequences of measures to change reactor load may be analysed. Besides the solution of the fuel management task permits to choose optimal strategy of fuel reloading. RBMK uses the on power reloading. Every fuel assembly when loaded leads to a power density increase. To compensate this increase it is required to move control rods near the place of reloading.

The fuel depletion is a rather slow process so static calculations may be used to model it. The large amount of calculations demands a lot of computer time. This is the reason to take two-dimensional model for the calculations. But the axial direction is important too. So two-dimensional full scale calculation is added by one-dimensional calculation of average axial neutron distribution. Two group cross sections for one-dimensional calculation are made by special procedure which takes into account the axial distribution of control rods.

The linear programming task is solved to find the new the control rods position to compensate each reload operation. The aim of this task is minimisation of fresh fuel assembly power for example. The advantage of this algorithm is the possibility to avoid recalculation of the neutron field in all reactor volume after each reloading operation. The neutron field may be recalculated only in the vicinity of the reloading place. This algorithm of local optimisation permits to model accurately each assembly loading and to decrease the consumption of computer time by about an order.

A1.2.8 Thermohydraulic part of the code verification

A1.2.8.1 Thermohydraulic test calculations

The results given below were obtained by simplified version of KOBRA - KOBRA2. The difference is that KOBRA2 uses three equations instead of four as in KOBRA. The additional equation for liquid phase energy is not considered. But slip model and critical boiling are considered. The code KOBRA was examined by a system of tests for channel type reactor. Results of calculation by code MECA (method of characteristics) or experimental results were used as a bench-mark tests.

The first test describes a case of "instantaneous" switch on the tube heating. In other words, it is similar to the energy release due to reactivity accident. A good agreement with calculation by MECA code was obtained. As any finite-difference scheme, the KOBRA gives more smooth oscillations of pressure at the initial time. The second test (Edwards test) describes behaviour of water near saturation (243 °C) at 7 MPa under condition that the one end of the closed tube is opened to the atmosphere. First the drop of pressure wave occurred, then the choked flow of steam water mixture starts. The behaviour of density and pressure near the rupture is described by KOBRA satisfactory. The pressure drop at the initial time which we have in the experiment and connected with non-equilibrium process is not taken into account.

A1.2.8.2 LNPP-3 single channel flow rate decrease accident calculation

The event description.

The single channel flow-rate decrease event occurred on March 24, 1992 under full power conditions. At 2:34:49s, a "water flow decrease" signal was indicated in the 52-16. The power of this incident channel was 1.96 MW, the average fuel burnup was 20.6 MWday/kgU. The axial distribution over the channel was quite flat, the non-uniformity coefficient was estimated to be 1.13. at 2:34:45s, the reactor was scrammed by "pressure increase" signal from the reactor cavity. The reactor shutdown system was activated when the cavity pressure increased by 0.0017 bar. The cavity pressure increased because the coolant entered the cavity through a breach at the channel wall. The breach was caused by channel overheating under the loss of water flow condition. 14 hours after the incident, an attempt was made to remove the fuel assembly from the core. However, only the hanger and a 0.54m length of the central supporting tube was taken out. The fuel assembly remained in the channel. Further investigations have shown that the channel was ruptured in the upper part of the core approximately 6 m from the bottom. The graphite ring around rupture location was partially destroyed and the graphite block was damaged. A breach appeared at the channel tube and the surrounding graphite. The fuel pin were mechanically bowed at the direction toward the breach.

The event sequence was reconstructed using operational measurement, separate experimental data, and best-estimate code calculation. Actual plan measurements were very limited. First, the location of the breach was found to be at ~ 1 m from the top of the core. Secondly, the time interval between the decrease of flow and channel rupture was estimated as 40 seconds.

The event analysis

The present analysis focused on the calculation of clad temperature, fuel temperature, and tube temperature.

Residual flow rate

For a complete stop of flow at the failed valve, both RELAP5/MOD3 and KOBRA calculations showed that the 920 K temperature level was reached within 34s and 32.5s respectively. The maximum temperature position took place near the center of the core. This result indicated that the channel rupture should have occurred at the core center, which was about 2.5m lower than the observed breach location (~1m from the top). Hence, a certain amount of residual flow rate through the failed valve should exist. The design of the manual control valve allows small leakage flow (0.1 kg/s) through the complete closed valve. This may be different from the value for the failed closed valve. The calculation showed that if a residual flow rate of 0.5 kg/sec was assumed, a longer time was required for the tube wall temperature to reach the 920 K critical value (40 seconds for RELAP5/MOD3 and 39 seconds for KOBRA). The maximum temperature was found at ~0.5 m from the top of the core.

The calculated time span matched the maximum possible value (~40 seconds) obtained from the plant measurement and the calculated maximum temperature location was slightly higher than the location observed at the plant. Hence, the residual flow rate should not be more than 0.5 kg/s. Further calculations indicated that 0.2 kg/s was more reasonable.

Breach flow area

The destruction process of channel tubes and the interactions of the two-phase fluid with the zirconium/graphite structure are rather complicated and the mechanisms are not well-understood still. However, as discussed previously, no significant progressive destruction of graphite structure adjacent to the ruptured channel took place during the first phase. Hence, the analysis assumed that the channel geometry, pin geometry, and the breach flow area remained unchanged. That is, a constant breach flow imposed on the location where the tube wall temperature reached the critical value (920 K). The size of the area was estimated as equal to 6.3 cm². Using this area, both RELAP5/MC3D and KOBRA codes performed the event analyses. For the first 20 seconds, the calculated choked flow rates at the breach were roughly maintained at ~8 kg/s.

Temperature responses

The following analyses used 0.2 kg/s as residual flow rate and 6.3 cm² as breach flow area. Table A1.5 summaries time interval for the channel tube to reach the 920 K critical value, and for the cladding and fuel to reach their respective maximum temperatures.

Table A1.5: Summary of time interval, maximum temperatures of clad and fuel (1.96 MWth channel with 0.2 kg/s residual flow rate and 920 K tube failure temperature)

Code	RELAP5/MOD3	KOBRA
Channel tube wall failure time (s)	30.0	26.5
Maximum Clad Temperature (K)	1380	1350
Maximum Fuel Temperature (K)	1585	1640

Both RELAP5/MOD3 and KOBRA calculations showed similar characteristics. Small differences were also observed. The two code calculations indicated that, after 2-3 seconds of valve flow area closed, dry out of the water film occurred. Subsequently, temperatures of fuel, clad and channel tube swiftly increased. When the tube temperature reached the assumed critical value, channel rupture took place. RELAP5/MOD3 calculation showed that the tube ruptured at 32 seconds, and KOBRA2 at 29 seconds. After the channel rupture occurred, cooling of the channel tube and cladding above the rupture location was greatly enhanced by the substantially large inverse coolant flow originated from steam drum. Thus temperatures of cladding and channel tube above the rupture location decreased rapidly.

Appendix 2

General description of the SADCO code

The SADCO code complex (Safety Analysis and Design Code) is intended to perform coupled neutron and thermohydraulic calculations of RBMK-1000 and RBMK-1500 reactors. Calculation of neutron fluxes at reactor stationary state is made in traditional two-group quasi-critical approximation. 3D calculation model of reactor consists of elementary cells with homogeneous neutron properties which are to be determined at a preliminary stage of neutron macrocross-section preparation.

The two-group diffusion equations system with the present boundary conditions is solved with the use of up-to-date nodal methods. The code can also use the method of finite differences applied to a rectangular finite-difference lattice. In this case an arbitrary (same for all channels) number of calculation nodes is allowed for each reactor channel in the plane: 1×1 , 2×2 , 2×3 , etc. Arbitrary number of nodes can also be set in axial direction (this direction is parallel to channel axis). Total number of nodes is dependent on required accuracy of results and computer capacity. In the overwhelming majority of RBMK reactor actual calculations performed according to SADCO code with the use of nodal methods for calculating neutron flux the total number of nodes amounts to 80 thousands and the time to calculate one state by IBM 486 DX2-66 computer makes 50-60 min.

Nodal methods for neutron calculations of large-size power reactors were found applicable in up-to-date western codes used for BWR and PWR reactors. Application of nodal methods to calculate RBMK reactors enables to considerably increase accuracy of calculations as compared to the method of finite differences while keeping nodalization. The code complex incorporates a library of core cell neutron macro cross-sections. The SADCO code complex uses thermohydraulic calculations to arrange feedback affecting reactivity and spatial distribution of neutron flux. GIDRA code is used to calculate a distribution of boiling coolant density in each fuel channel. A simplified engineering model was developed to calculate fuel element mean temperatures. Empirical correlation used in the model, enable to obtain acceptable agreement with more accurate calculation results and comply with available experimental data.

Calculations of temperature fields in graphite stack according to SADGO code complex is also made with the use of an empirical technique describing not only heat transfer from graphite to coolant, but heat exchange between a cell under consideration and neighbouring cells, both lateral and diagonal ones, too. Interrelated calculations of reactor stationary state at operating power levels are performed by way of interrelated iterations wherein heat fluxes and core hydraulic characteristics are related to spatial neutron distribution. Reactivity effects and efficiency of GPS elements are determined by direct trade-off calculations. Reactivity coefficients are determined as reactivity variation divided by corresponding change in feedback.

A2.1 Neutron cross-sections and reactivity effects

In order to run physical and dynamic calculations and to make assessment of RBMK reactor safety with use the of 3D neutron and thermohydraulic models it is necessary to take into account spatial distribution of neutron cross-sections in the core and their dependence on thermal and physical parameters. Neutron cross-section are, in fact, final relations between neutron fluxes and thermohydraulic characteristics. The problem of developing libraries of neutron cross-sections used in few group diffusion physical and dynamical calculations is one of the principle problems in computer simulation of statical and dynamical neutronics characteristics. To solve this problem first of all it is necessary to achieve required accuracy in neutron cross-sections, their completeness over the whole phase space of core components process parameters, compact and timely presentation in complex codes for reactor physics and dynamics calculations. A wide

variety of different channels in RBMK core including various fuel channels, GPS system channels and other non-multiplying channels is an essential aspect. The problem of developing neutron macro cross-sections for fuel channels containing burnable absorber as well as channels with materials to produce useful radionuclides, is getting vital in recent years. Neutron macro cross-section systems developed at RDIPE for a few-group diffusion equation are based on many-variant calculations with the use of up-to-date neutron codes and computers of high capacity.

To make calculations and corrections of RBMK core cell macro cross-sections there were used well known codes WIMS-D4 and MCU. Macro cross-sections of channels with fuel at hot state are determined depending on initial fuel enrichment and composition, burnup, coolant density in channel, fuel and graphite temperatures, xenon poisoning. Calculations were run with the use of a single cell model (uniform channel lattice with fuel) and multicell model (polylattice consisting of fuel and non-fuel channels).

WIMS-D4 code calculations were performed using the first collision probability method (PIJ option) by simulating fuel channel cluster structure in 30 energy groups with subsequent collapsing the constants into 2 groups (energy cut-off between fast and thermal groups - 2.1 eV). Macro cross-sections for non-breeding channels were obtained from a series of multicell calculations of the 3 x 3 type (CPS channel, additional absorbers, etc., surrounded by 8 fuel channels) according to MCU code by Monte Carlo method which is especially efficient in case of non-multiplying channels having complicated cluster structure. Mean coolant density in surrounding fuel channels and the presence or absence of water in non-multiplying channels are used in this case as parameters.

Calculated macro cross-section values obtained in phase space of process parameter changes are used as bench marks. It became possible to get smooth functional dependence of macro cross-sections within the whole range of process parameters change by applying robust interference-resistant procedure of approximation for each type of macro cross-sections. These dependencies are realised in the form of routines and their totality constitute a library of neutron two-group diffusion macro cross-sections to calculate RBMK-1000 and RBMK1500 reactors.

Testing the developed macro cross-sections library is provided by application of two codes WIMS-D4 and MCU, based on independent macro-cross-section libraries, intended for detailed neutronics calculations. It should also be noted that preparation of macro cross-section library should be made taking into account specific methods and schemes to solve diffusion equation for neutron transport in 3D reactor codes. Thus, the obtained macro cross-section library accumulates all parameters of neutron balance and reactivity effects. The obtained macro cross-section system (library) is used as a constituent part of the SADCO code.

A2.2 Methods to solve neutron diffusion equation

SADCO code complex, used for neutron and thermohydraulic calculations of RBMK reactors, has a block-type code structure. The block intended to calculate 3D neutron distribution in reactor and the most important functional and distributions, determined on the basis of neutron fields, is the most important. A traditional two-group diffusion approximation is applied to calculate 3D neutron flux distribution. SADCO code enables to use different options to solve both steady state and non-stationary transients in reactor. In both cases nodal method is used for solving and a classical procedure is used to homogenise neutron characteristics in elementary volumes of the core, as setting up nodal lattice. The code can use a number of nodal methods to solve diffusion equation with different ways of nodalization (node and polynomial) to solve within the elementary volumes of the model to be calculated. Besides, it is possible to solve the equations by the method of finite differences in rectangular lattice with an arbitrary number of nodes per one channel in core and reflector. Dynamical distribution of memory in the block for neutron

calculations provides a possibility to use arbitrary number of nodes limited by computer capacity only.

Accuracy of calculation performed with the use of nodal methods is very close to the accuracy of finite differences approximation as number of nodes per elementary volume is increased 8-18 times. Application of nodal methods would thus allow to considerably (more than 10 times) reduce calculation time on reaching necessary degree of accuracy. This aspect is very important from viewpoint to carry out multivariate calculations of physical and dynamical characteristics of RBMK-type reactors, as well as during simulation of transient non-stationary modes. As using nodal or finite differences methods they obtain the same type of algebraic equations different in coefficient values only. In 3D case, coefficient matrix of these equations has a strictly seven-diagonal view. Such systems of equations are solved in SADCO code by an incomplete factorisation. The principle advantage of this method is that when calculations are performed with a constant right part (inner iterations), the solution is found out without iterations and the whole task is reduced to iterating the source (outer iterations). This method is more fast acting as compared with widely used method of consecutive upper relaxation.

Since RBMK reactor is large in size the process of the source iteration converges very slowly because the main and the first proper values of the transport operator are very close to each other. To accelerate the convergence the code uses the Chebyshev polynom method. A set of accelerating parameters is determined according to Lebedev-Finogenov scheme. To solve adjoint equation SADCO code uses that very methods which are used for the direct equation of neutron transport. Non-stationary equation of neutron transport is solved taking into account six groups of delayed neutrons, local outer sources (for instance, start-up sources) and distributed sources from various nuclear reactions. As a basis of spatial and temporal discretization of non-stationary neutron diffusion equation they use a completely implicit scheme providing calculation stability practically for any steps in time and very slight dependence of the solution upon the magnitude of these steps. The system of non-stationary transport equations is reduced at each time step to a stationary equation with a modified independent outer source which can be solved by one of nodal or finite differences methods with the help of procedure connecting fission and independent outer sources at each iteration.

SADCO code envisages a possibility to run calculations with automatic choice of a time step. The principle criterion to choose a step is non exceeding a relative change in neutron power during one step of some value set up in advance. To solve non-stationary processes SADCO code was tested with the use of a number of known benchmark tasks: 2D test TWIGL and 3D test LMW. Comparison with the best foreign codes PANTHER and QUABOX/CUBBOX has demonstrated a good agreement of both integral and distributed parameters for the given tests. For the TWIGL test the deviation from the standard value of power did not exceed 0.4%, and for the LMW test all the three codes produce the results which differ by not more than 4-5%.

A2.3 Thermohydraulic model of SADCO code

Calculations and experimental studies of physical characteristics as well as transient and emergency modes of RBMK reactors showed a necessity to use full-scale 3D mathematical models of core static and dynamics for such reactors to justify their reliability and safety. In this case one of the most important tasks is creation of a model describing thermal and hydrodynamical processes in a steam generating channel and satisfying two contradictory requirements:

- the model should be simple enough so that its introduction into a full-scale complex should not result in increased expenses for computer time;
- the model should be able to describe with sufficient accuracy a wide class of non-stationary processes occurring in a fuel channel.

Hydrodynamics model

An experience in simulation of hydrodynamic processes in a steam generating channel and methodical calculations have demonstrated, that the homogeneous model of 1-D 2-phase coolant flow, considering non-uniformity only for phase velocities, meets the listed above conditions. The basic differential equations system employs model of phase gliding velocity and, thus, difference in phase velocities is taken into account. Empirical correlations to calculate actual void fraction are used in the model in order to account surface boiling of subcooled liquid.

Model of heat conductivity in a fuel element

During development of mathematical model, describing fuel element temperature behaviour, it was assumed that temperature field in a fuel pellet was formed only due to heat transfer in radial direction, and uranium dioxide

thermal and physical characteristics depended on temperature. Energy release throughout the pellet volume was assumed to be uniform. Heat conductivity through gas gap is defined by effective heat transfer coefficient, which was calculated using correlation dependence, obtained in more detailed computer codes. Data on the fuel element temperature condition within the whole possible of range parameter variation during operating cycle were processed in order to obtain the required correlation.

Calculation of temperature fields in graphite stack

Heat release in graphite stack can be attributed to two factors: heat release caused by gamma irradiation absorption and heat release caused by neutrons slow down. The mathematical model of temperature fields distribution in graphite substantially depends on conditions of the task to be solved. It is rather significant that typical time period of graphite temperature change in RBMK-reactors varies within the range of 0.5-1 hours and depends upon composition of a gas, used for the graphite stack purging. For studying of comparatively fast processes with typical time periods about several dozens of seconds the description of the graphite average temperature through out the model cell in the form of heat balance equation, which does not account for heat exchange with neighbouring cells, assuming that heat transfer between cells is much less than the transfer to the coolant, is quite satisfactory.

Appendix 3

The TRIADA code.

TRIADA is RBMK 3-D neutronic - thermohydraulic coupled code. It is used to analyse in-pile experiments as well as to perform safety analysis. Neutron flux behaviour in the core is described in diffusion one-group modified approximation. The number of plane nodes can be either 140 or 540 ones, and the number of axial layers -up to 70.

The initial data must contain the information about neutron flux distribution, reactor loading, fuel burn up, control rod arrangement and the main reactor thermo-physical characteristics. The code structure allows for various CPS logic implementation including automatic control system (integral and local) as well as emergency protection and reactor scram system.

In-core detectors and ex-core ion-chambers as well as drive mechanism are completely modelled in RBMK calculations by TRIADA code. The fuel element temperature is defined by heat-balance and heat-conduction equations.

Coolant density distribution over the reactor channels is determined basing on the energy, mass and momentum conservation laws that can be solved using both drift and two-phase models. In order to describe "slow" transients, with typical time periods longer than the time necessary for the coolant to cross the FC heating zone, the 1D distributed model for the thermohydraulics of RBMK boiling channels in the quasi-static approximation is used assuming that the flow rate along fuel channel is constant. The inclusion of the local reactor properties as a function of the coolant parameters the control rod arrangement, the number of additional absorbers, graphite temperature and burnup fraction in the mathematical model permits to verify code basing on the void reactivity coefficient measurement results. In addition TRIADA code was verified by comparison of its results with the experimental data about following transients:

- withdrawal of a control rod group from the core;
- deformation of the power distribution due to control rod movement and actions of the reactor automatic control system;
- measurement of the core physical parameters.

Appendix 4

General Description and Capabilities of ARROTTA

ARROTTA - Advanced Rapid Reactor Operational TransienT Analysis - is a three dimensional XYZ neutronics computer program for both static and transient applications that includes the effects of the thermal hydraulic feedback mechanisms. ARROTTA neutronics are based on the Analytic Nodalization Method as developed for QUANDRY (1) in EPRI RP 1936-1. The thermal hydraulics model in ARROTTA is taken directly from the BEAGL program as developed under EPRI RP 1761-18. ARROTTA can solve steady state simulations, xenon (and samarium) transients, and kinetics transients.

The analytical nodalization method will generate an exact solution to the neutron diffusion equations if a) the node is considered as a homogeneous entity and b) the shape of the transverse leakage function is considered to be of a known quadratic form. The equations in the limit of small mesh revert to the same limit as the standard flux centered finite difference equations. The time derivative term is solved by a standard finite differencing while the time dependent cross section behavior is handled either implicitly or semi-implicitly. Normal zero flux and zero current boundary conditions are allowed independently on all six sides of the problem. ARROTTA uses a full two group model for the diffusion equations and up to six groups of delayed neutron precursors. Initial conditions that may be calculated include a fixed input statepoint, a criticality search based on critical boron concentration, and a search to criticality based on a rod bank position. In all cases these solutions are nonlinear since they are explicit functions of the thermal-hydraulic conditions which are coupled to the nodal cross section values which in turn are coupled to the nodal power. Also, the nonlinear effects of the xenon and iodine poison (as well as the samarium and promethium) may also be handled on a nodal basis. Collectively, all of the above feedback mechanisms (nonlinearities) are handled on the reactor iteration level during eigenvalue problems. In actual transient calculation sequences, the possible feedback mechanisms are delayed by decoupling the nonlinearity between successive timesteps.

The thermal-hydraulic model is comprised of a fluid dynamics model and a heat transfer model. The fluid dynamics is described by an inhomogeneous, nonequilibrium, two phase flow that is based on energy splitting between the phases. One-dimensional (axial) conservation equations are solved by a marching technique for multiple parallel flow channels taking into account six possible flow regimes. Consequently, flow reversal and cross flow phenomenon are outside the scope of this fluid model. The relative flow split amongst the channels may be specified by the user but is time invariant. The system pressure may be specified as time dependent. The inlet coolant temperature, inlet flow rates, and soluble boron poison may all be described by functions that are both time and channel dependent. The heat conduction model is based upon spatially averaged, time-dependent equations for the average pellet temperature. Given the properties of the media, the gap and the inner and outer clad wall temperatures are then determined. In the time-dependent case these heat conduction equations are solved by a semi-implicit formulation.

Notabene Code Characteristics:

- neutron diffusion equations solved in full two group rigor over a rectangular geometry limited to 40 x 40 x 40 nodes (64,000 total);
- ARROTTA will generate initial conditions that include either a control rod group search or a soluble boron search;
- thermal-hydraulic feedback mesh solved at up to 64,000 nodes;
- three separate automatic levels of approximation to the neutron leakage operator;
- time discretization of the neutronics is either fully implicit or semi-implicit;

- fixed or variable time-step size algorithm;
- automatic adaptive computation of acceleration parameters;
- flexible restart procedurs;
- flexible spatial editing routines;
- assembly Discontinuity Factors allow greater accuracy in representing nodes that are not physically homogeneous;
- comprehensive and computationally efficient cross section representation formulation;
- flexible and accurate control rod representation algorithm.

Detailed explanations of the calculational modules of ARROTTA are contained in Volume 1, the Theory and Numerics Manual, of the ARROTTA Computer Code Documentation Package.

Figure 1-1 gives the internal information flow overview as covered in Volume 1. Figure 1-2 details the neutronic iterations levels as covered in Volume 1, Section 2.

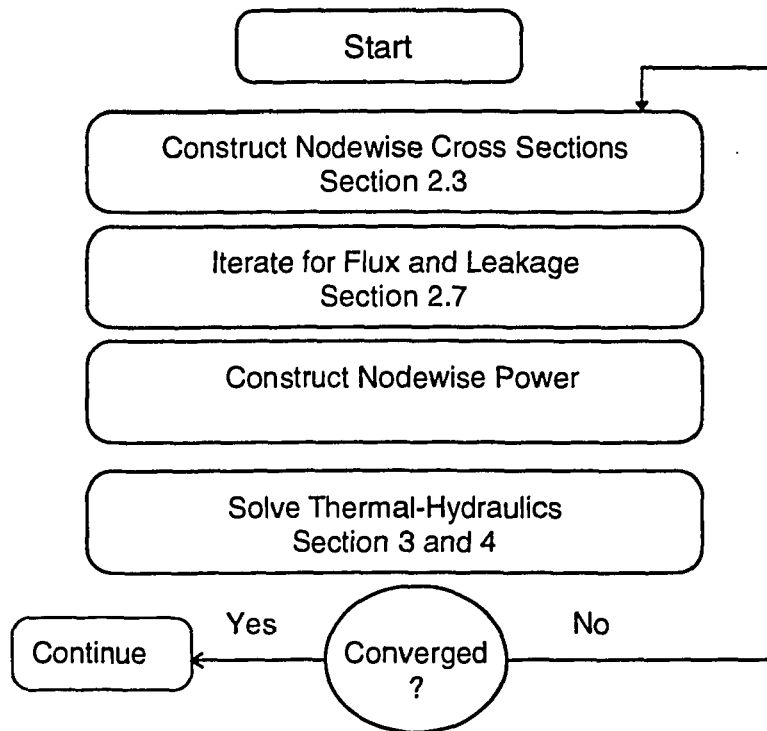


Figure 1-1.: ARROTTA Code Internal Information Flow

ARROTTA is written completely in FORTRAN and is currently available at the Electric Power Software Center. ARROTTA requires the EPRI-LIBRARY (3) set of scratch disk drivers. Even though earlier versions of these routines were machine dependent, EPRI-LIBRARY is now a set of machine independent FORTRAN that is maintained as part of the expected software base. The normal implementation of this code is to use the FORTRAN-4 compiler on the CDC system (4) and the FORTRAN-H EXTENDED and ENHANCED compiler using the Automatic Precision Increase (AUTODBL) feature (AD option 15331) on the IBM system (5). More recently, it has become available on both the SUN SPARC-1 and the IBM RISC/6000 workstations.

The ARROTTA Computer Code Documentation Package consists of four volumens. Volume 1, the Theory and Numerics Manual, discusses the general equations and approximations, geometry representations, constitutive relationships, and numerical analysis (both theoretical and observable) techniques and procedures employed in the various models in ARROTTA. Volume 2, the User's Manual, provides detailed descriptions and examples for using ARROTTA including complete descriptions of the input data that is required and cogent descriptions of the output data possible. Volume 3, the Programmer's Manual, provides the complete implementation procedures for the ARROTTA computer code and describes the general coding of ARROTTA including functional descriptions of all ARROTTA subroutines and functions, FTB scratch file storage, and COMMON variables. Volume 4 is the Applications and Validation and Verification Manual.

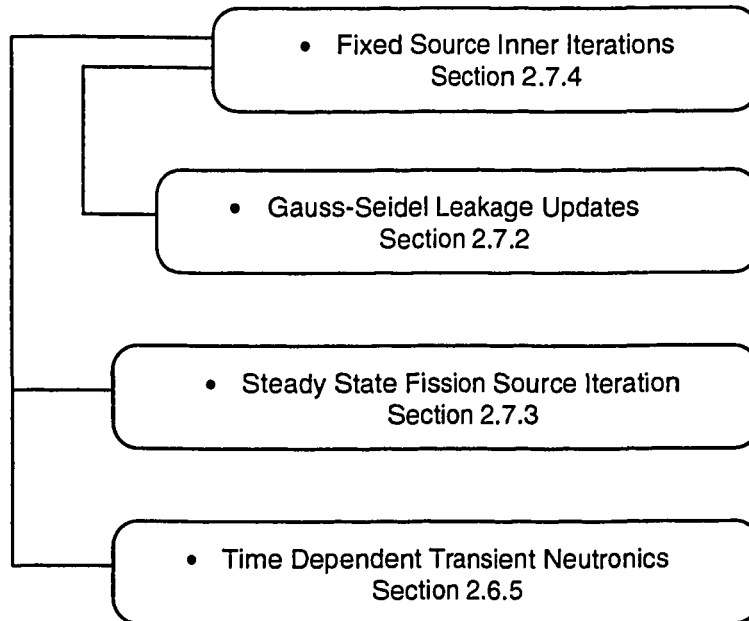


Figure 1-2.: ARROTTA Code Neutronic Iterations

This volume presents the mathematical theory and modeling of both the neutronics and the coupled thermal hydraulics phenomena contained in ARROTTA. In addition, the computational problems of the solution numerical analysis are explored in order that the reader of this volume might have an appreciation of the underlying procedures and techniques that have been used.

Section 2 describes the Analytical Nodal method as implemented in ARROTTA including an overview of the derivation of both the static and transient neutronic equations. Other equations pertinent to the neutron formalism are also documented. Additionally, emphasis is placed on the numerical analysis techniques used, especially the adaptive choosing of estimate for the needed acceleration parameters.

Section 3 provides the fluid dynamics model, an inhomogeneous, non-equilibrium two-phase flow model based on energy splitting between the liquid and vapor phases. One-dimensional conservation equations for the mass and energy are solved in the axial direction under the hypothesis of no cross flow by a marching technique. Each actual reactor channel can be modeled as a separate parallel channel in this formalism.

Section 4 discussed the fuel rod heat conduction equations for the average pellet temperature and the clad inner and outer surface temperatures. Also included is a model that corrects for the nonlinearity in the heat conduction model due to the assumptions of the pellet temperature distribution. These equations are solved semi-implicitly.